Vascular Imaging

19

Harriet J. Paltiel

Abbreviations

AVF	Arteriovenous fistula
BCV	Brachiocephalic vein
CCA	Common carotid artery
CEUS	Contrast-enhanced US
CFA	Common femoral artery
CFV	Common femoral vein
CT	Computed tomography
DVT	Deep vein thrombosis
ECA	External carotid artery
EDV	End-diastolic velocity
FV	Femoral vein
ICA	Internal carotid artery
IJV	Internal jugular vein
IMT	Intima-media thickness
IV	Intravenous
IVC	Inferior vena cava
MIP	Maximum intensity projection
MR	Magnetic resonance
MRA	Magnetic resonance angiography
NF	Neurofibromatosis type 1
PICC	Peripherally inserted central catheter
PRF	Pulse repetition frequency
PSV	Peak systolic velocity
RI	Resistive index
SCA	Subclavian artery
SCV	Subclavian vein
SFA	Superficial femoral artery
SMA	Superior mesenteric artery
SVC	Superior vena cava
US	Ultrasound

Electronic Supplementary Material The online version of this chapter (https://doi.org/10.1007/978-3-030-56802-3_19) contains supplementary material, which is available to authorized users.

H. J. Paltiel (✉)
Division of Ultrasound, Department of Radiology,
Boston Children's Hospital and Harvard Medical School,
Boston, MA, USA
e-mail: harriet.paltiel@childrens.harvard.edu

Introduction

Abnormalities of the neck vessels and peripheral and retroperitoneal vasculature in children are relatively rare. Nonetheless, increasing numbers of hospitalized children and those with chronic conditions routinely require ultrasound evaluation of these vessels prior to diagnostic procedures and following therapeutic intervention. In this chapter, ultrasound techniques used in evaluation of the pediatric vasculature, pertinent embryology, and normal anatomy are reviewed, and the ultrasound findings, associated clinical features, and management approach to vascular disorders in children are discussed.

Neck Vessels

Indications for ultrasound evaluation of the carotid artery in children include assessment for stenosis or thrombosis. The internal jugular vein (IJV) is usually imaged to determine patency prior to central line insertion, to diagnose thrombosis, and to evaluate venous ectasia.

Technique

Patient Positioning

Ultrasound studies of the carotid artery and IJV are performed with the patient supine, the neck hyperextended, and the head rotated to the opposite side. Exposure of the anterior neck can be facilitated by placing a pillow under the upper back.

Ultrasound Transducer Selection

High-frequency linear transducers are used to optimize image resolution. Occasionally, a curvilinear transducer or use of an extended field of view will be helpful in delineating a large

H. J. Paltiel, E. Y. Lee (eds.), *Pediatric Ultrasound*, https://doi.org/10.1007/978-3-030-56802-3_19

abnormality. A small footprint vector transducer may be useful when imaging the medial subclavian vein (SCV), lower IJV, and the brachiocephalic vein, particularly in young children with limited ability to cooperate with the examination or in patients with decreased mobility of the neck.

Imaging Approaches

Transverse, longitudinal, and oblique ultrasound images of the neck are obtained with grayscale, color, and spectral Doppler imaging. Color and power Doppler imaging outline the course of the patent vessel lumen and facilitate placement of a Doppler cursor when performing velocity measurements.

Initial grayscale evaluation is performed in the transverse plane. Images are obtained from the supraclavicular notch to the angle of the mandible. Inferior angulation of the transducer in the supraclavicular notch is used to image the inferior portions of the common carotid artery (CCA) and brachiocephalic vein. Color Doppler studies should be performed with sensitivity and gain settings that anticipate vessel flow velocities and optimize the color display. Pulse repetition frequency (PRF) and frame rate must be set to permit accurate characterization of vascular hemodynamics. Use of a large color image area will slow down the frame rate, and the deeper a vessel is located from the transducer face the slower the required PRF. The whole vessel lumen should be filled with color flow without leakage of color signal into the adjacent stationary soft tissues.

When imaging the CCA, the carotid bulb appears as a widening of the artery close to its bifurcation. Transverse images of the carotid bifurcation will depict the orientation of the internal and external carotid arteries and help determine the optimal longitudinal or oblique planes in which to perform color and spectral Doppler imaging (Fig. 19.1).

The IJV is readily imaged in both transverse and longitudinal planes. Venous pulsations are seen with grayscale and Doppler imaging that are related to right heart contraction (Fig. 19.2). Changes in diameter of the IJV reflect changes in intrathoracic pressure. Inspiration causes negative intrathoracic pressure that results in flow to the heart and a decrease in jugular venous diameter. Expiration and the Valsalva

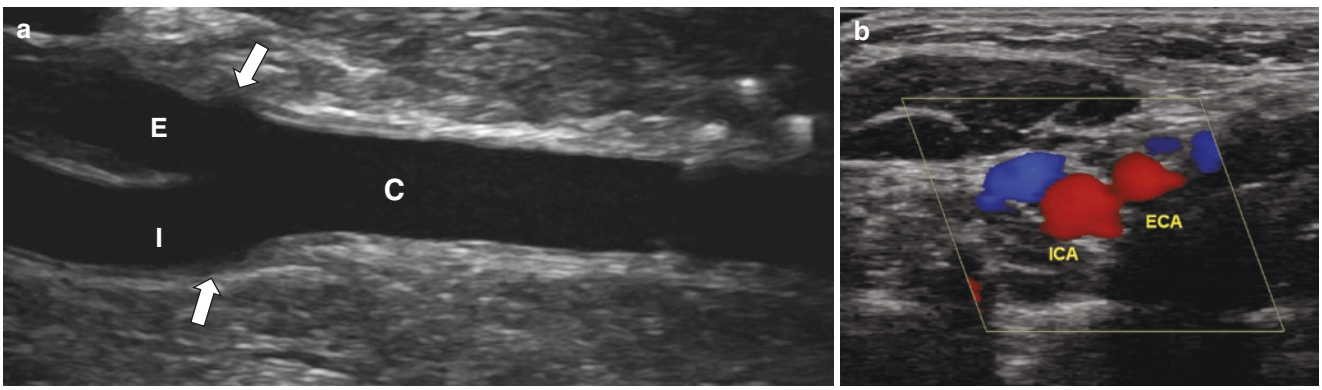

Fig. 19.1 Common carotid artery (CCA) bifurcation in a 2-year-old female. (**a**) Sagittal grayscale ultrasound image of the right CCA (C) shows mild widening at the bulb (arrows) just proximal to its bifurcation into the external (E) and internal (I) carotid arteries. (**b**) Transverse color Doppler ultrasound image depicts the bifurcation into the external carotid artery (ECA) and internal carotid artery (ICA)

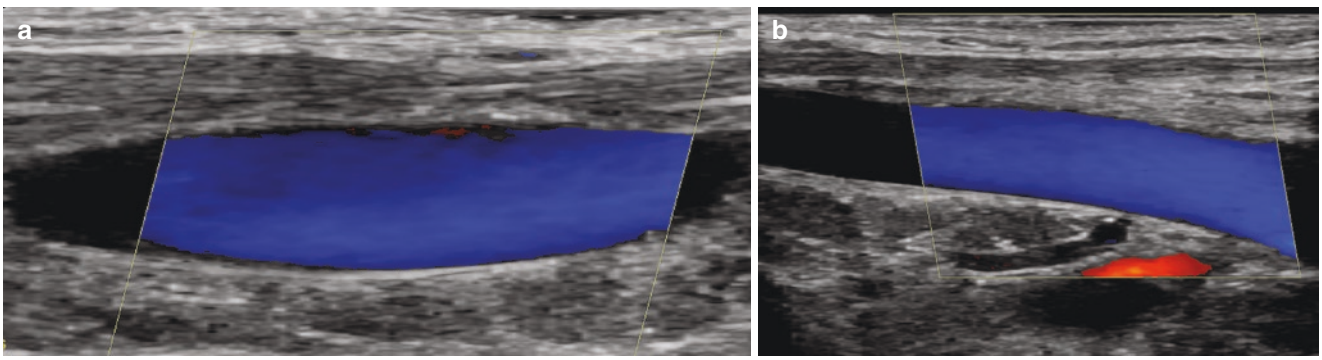

Fig. 19.2 Normal pulsatility of the internal jugular vein (IJV) in a 12-year-old female. (**a**) Sagittal color Doppler ultrasound image shows the IJV at its widest during a normal cardiac cycle. (**b**) Sagittal color Doppler ultrasound image shows the IJV in a relatively collapsed state during the same cardiac cycle

maneuver will cause increased intrathoracic pressure with decreased blood flow to the heart and venous enlargement.

Coronal scanning through the supraclavicular fossa is performed to evaluate the confluence of the medial SCV and lower IJV, as well as the superior portions of the brachiocephalic vein (Fig. 19.3). Images are obtained with light transducer pressure to minimize compression of the IJV (Fig. 19.4). Comparison views of the opposite side are helpful to highlight asymmetry. Cine clips can be used to demonstrate venous compressibility and to determine the extent of an abnormality that exceeds the ultrasound field of view.

Carotid Artery

Normal Development and Anatomy

Normal Development

In embryonic life, the paired primitive right and left dorsal aortas connect ventrally with paired pharyngeal arch arteries. The third pharyngeal arch artery gives rise to the CCA and the proximal part of the internal carotid artery (ICA). The external carotid artery arises as a bud from this arch [1].

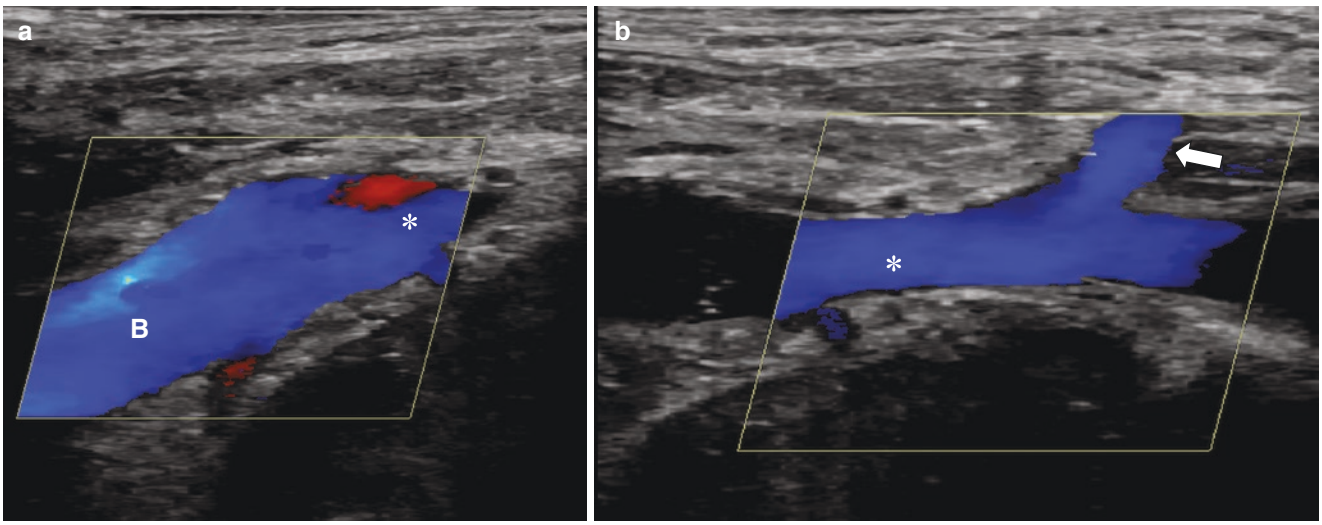

Fig. 19.3 Confluence of IJV, subclavian vein (SCV), and brachiocephalic vein (BCV) in a 12-year-old female. (**a**) Coronal color Doppler ultrasound image of the confluence of the left SCV (asterisk) and brachiocephalic vein (B). (**b**). Transverse color Doppler ultrasound image shows the confluence of the left IJV (arrow) with the medial left SCV (asterisk)

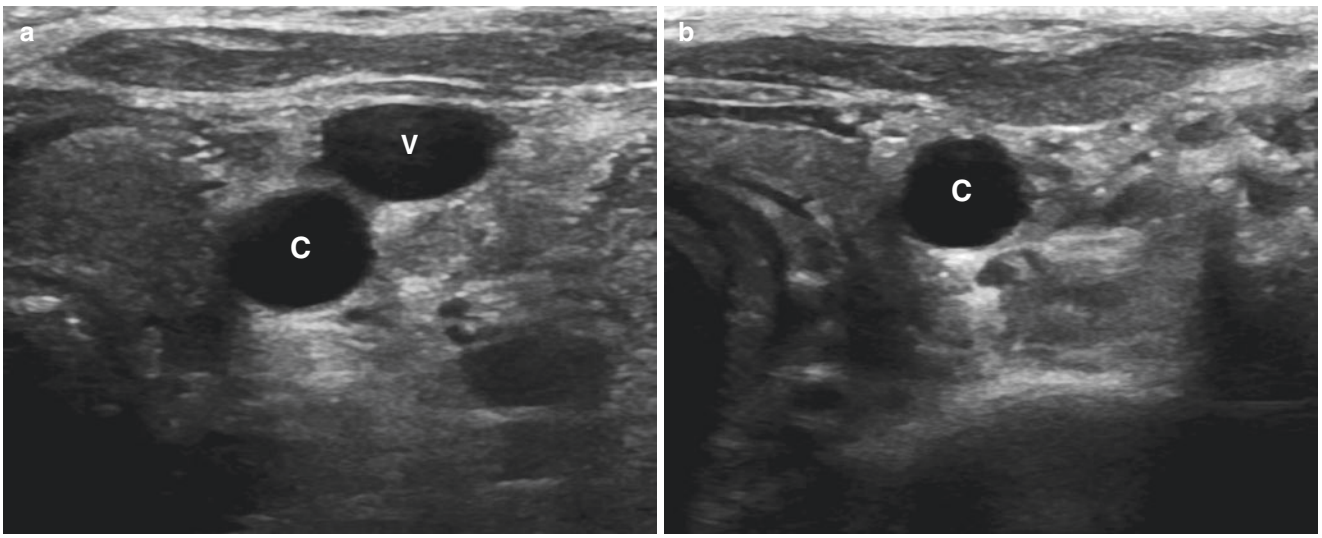

Fig. 19.4 Normal compressibility of the IJV in a 12-year-old female. (**a**) Transverse grayscale ultrasound image of the left neck obtained with light transducer pressure shows a normal IJV (V) and CCA (C). (**b**) Transverse grayscale ultrasound image of the left IJV obtained with firm transducer pressure shows normal collapsibility of the vein. *C*, CCA

Normal Anatomy

In about 75% of the population, the first branch of the aortic arch is the brachiocephalic artery which divides into the right common carotid and subclavian arteries. The second branch of the aortic arch is the left CCA which has a separate origin from the left subclavian artery (SCA) (Fig. 19.5).

Both common carotid arteries ascend into the neck deep to the IJV and the sternocleidomastoid muscle and posterolateral to the thyroid gland. The CCA usually gives off no branches in the neck. At its bifurcation it divides into the ICA and external carotid artery (ECA). The ICA usually gives off no cervical branches. The ECA has multiple cervical branches that supply the muscles of the face (Fig. 19.6).

Longitudinal ultrasound images of the CCA depict the layers of the wall as two parallel, echogenic lines separated by a hypoechoic zone. The distance between these layers represents the thickness of the intima and media or intima-media thickness (IMT) (Fig. 19.7). IMT and carotid distensibility do not appear to increase significantly with age or differ between males and females [2].

Doppler imaging of the CCA reveals a narrow frequency spectrum in systole and a somewhat wider spectrum in diastole with a clear spectral window (Fig. 19.8) [3]. Since approximately 80% of CCA flow extends into the ICA, its frequency spectrum resembles that of ICA, and forward flow occurs throughout the cardiac cycle. CCA velocity measurements have not been described in children. In adults, peak systolic velocities (PSVs) of 78–118 cm/sec, end-diastolic velocities (EDVs) of 20–32 cm/sec, and resistive indices (RIs) of 0.72–0.84 have been reported [4].

The ICA supplies the low-resistance cerebral vessels and demonstrates forward flow throughout systole and diastole (Fig. 19.9). In neonates, PSVs that range between 60 and 68 cm/sec, EDVs of 14–17 cm/sec, and arterial RIs of 0.72–0.78 have been reported [5]. Normal velocity measurements for these vessels in older children have not been established. In adults, these measurements are increased, with PSV of 62–90 cm/sec, EDV of 23–37 cm/sec, and RIs of 0.54–0.66 [4].

Since the ECA supplies the high-resistance vascular bed of the facial muscles, flow in the ECA resembles that of other peripheral arteries, with a sharp systolic peak and a rapid decline during diastole that may approach zero or briefly reverse direction (Fig. 19.10) [3]. Normal velocity measurements have not been reported in children. In adults, normal values include PSV of 57–87 cm/sec, EDV of 11–21 cm/sec, and RIs of 0.72–0.84 [4].

Anatomic Variants

In approximately 15% of individuals, there is a common origin of the brachiocephalic and left common carotid arteries, the so-called "bovine arch" configuration. In the remaining 10%, the left CCA arises from the brachiocephalic artery proper, rather than from a common trunk.

Thrombosis and Stenosis

Carotid artery thrombosis and stenosis are unusual in children. ICA thrombosis can occur as a rare complication of an impalement injury of the oral cavity, or secondary to vasculitis, as in the setting of Takayasu arteritis.

Penetrating palatal wounds are caused by objects in the mouth such as pencils, toothbrushes, pieces of wood, or plastic [6]. ICA thrombosis in this setting occurs in fewer than 1% of patients. It is thought to result from compression of the ICA against a cervical vertebra leading to an intimal tear that serves as the nidus for thrombosis [7]. Signs of ICA injury include a hematoma in the lateral neck and Horner's

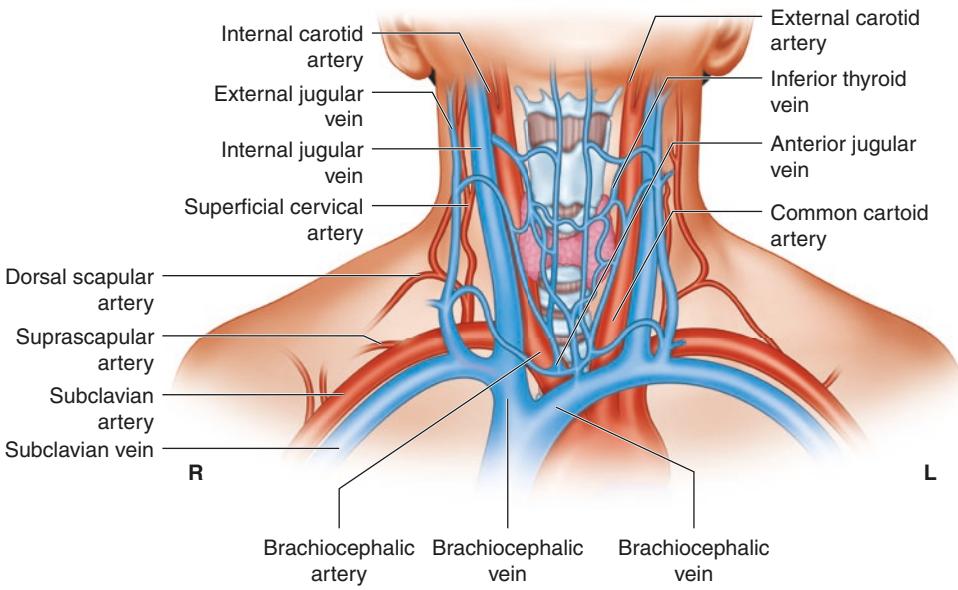

Fig. 19.5 Diagram of normal vessels to the neck and upper extremities

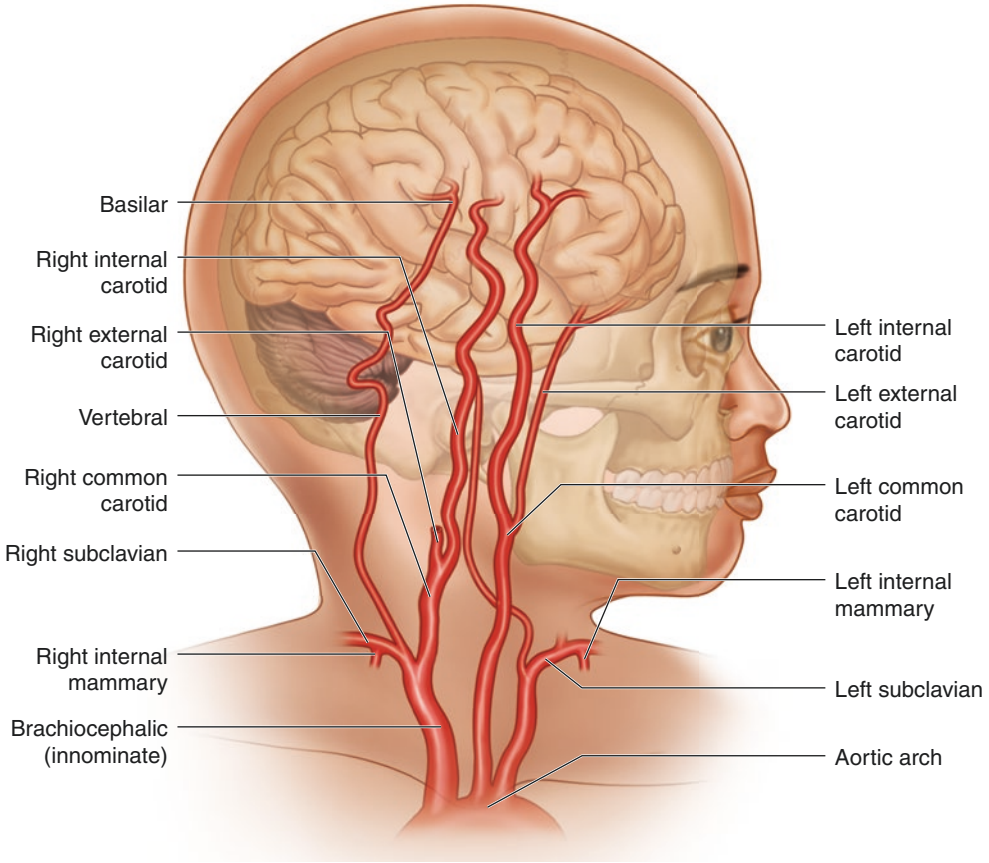

Fig. 19.6 Diagram of normal arterial supply to the neck, face, and brain

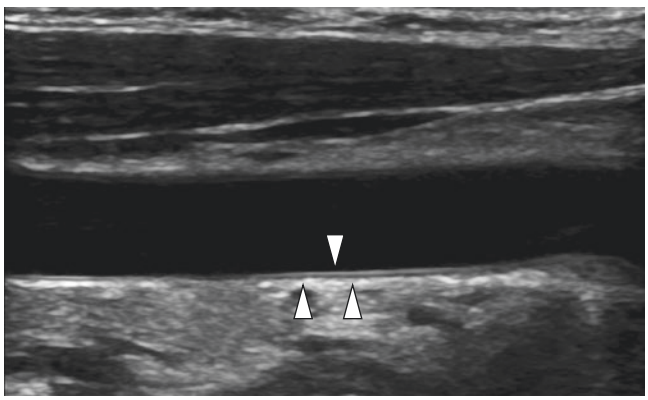

Fig. 19.7 Normal intima-media thickness (IMT) of the right CCA in a 17-year-old female. Sagittal ultrasound image shows the IMT between arrowheads

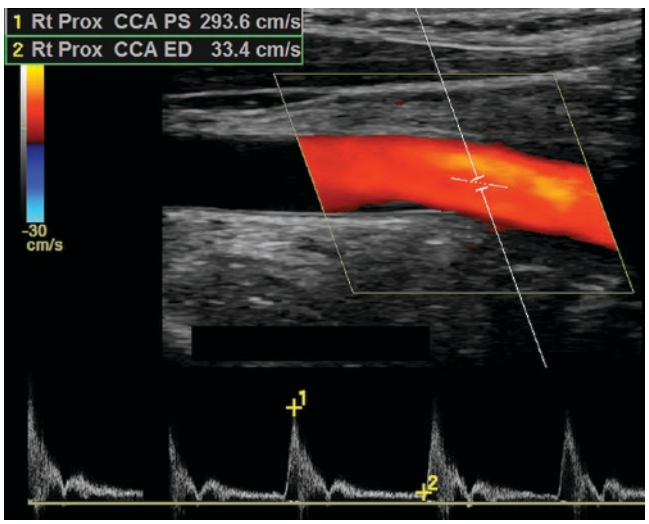

Fig. 19.8 Normal CCA in a 15-year-old female. Longitudinal color Doppler ultrasound image with spectral analysis shows normal flow with relatively low-resistance spectral Doppler waveforms

syndrome (ipsilateral ptosis, meiosis, and anhidrosis) [8]. These signs can develop up to 3 days after injury [7]. Doppler ultrasound evaluation of the neck can be performed to diagnose a cervical hematoma and to evaluate flow in the ICA in selected patients.

Takayasu arteritis is an idiopathic, granulomatous vasculitis of the aorta and its major branches and is one of the most common vasculitides in children. Inflammation and intimal proliferation result in wall thickening, stenosis, and thrombosis. Aneurysms and dissection result from destruction of the muscular and elastic layers of the vessel wall. Children typically present with hypertension, vascular bruits, asymmetric blood pressure between limbs, or asymmetric arterial pulses in

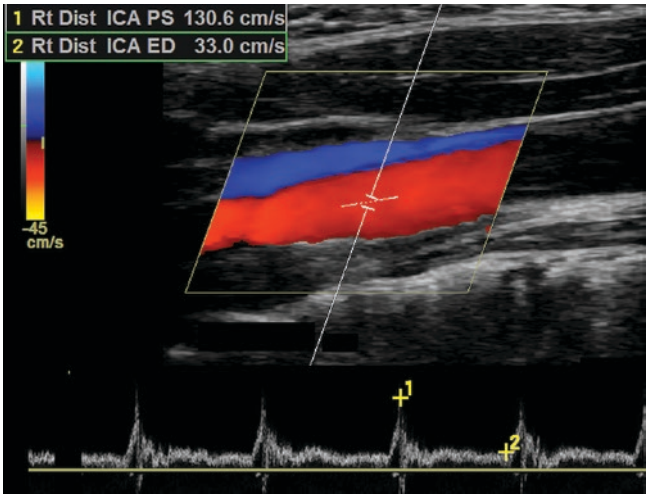

Fig. 19.9 Normal internal carotid artery (ICA) in a 15-year-old female. Longitudinal color Doppler ultrasound image with spectral analysis shows normal flow with low-resistance spectral Doppler waveforms

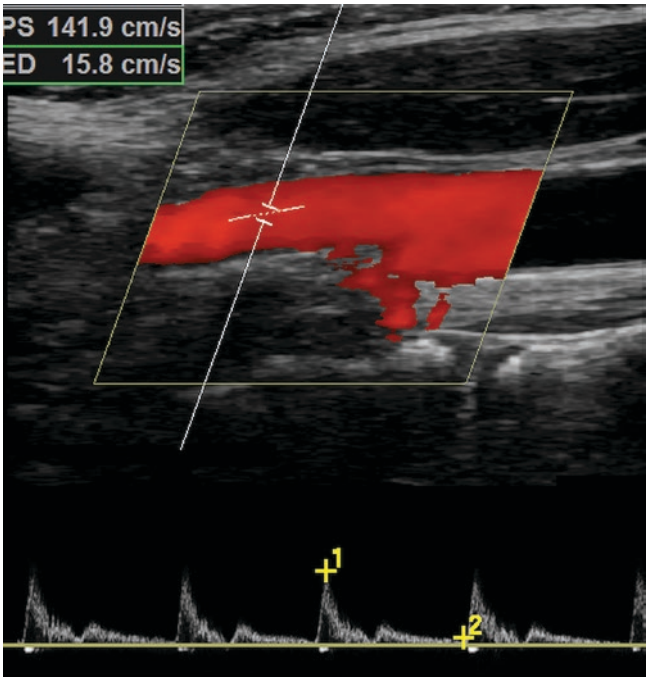

Fig. 19.10 Normal external carotid artery (ECA) in a 15-year-old female. Longitudinal color Doppler ultrasound image with spectral analysis shows normal flow with relatively high-resistance spectral Doppler waveforms

the extremities, sometimes accompanied by fever, malaise, or musculoskeletal symptoms. The absence of specific symptoms and laboratory biomarkers and difficulties in determining disease activity and progression often lead to delayed diagnosis and underestimation of disease activity [9].

The diagnosis is confirmed by imaging documentation of large vessel wall abnormalities, including stenosis, occlusion, aneurysms, and collateral circulation on computed tomography angiography (CTA), magnetic resonance angiography (MRA), or conventional catheter angiography. Ultrasound with color Doppler can detect vascular stenosis, thrombosis, and aneurysms (Fig. 19.11). Diffuse thickening of the IMT has been described, the so-called "Macaroni" sign.

Non-invasive means of monitoring disease activity include documentation of an abnormally hypoechoic appearance of the vessel wall that precedes the development of stenosis or occlusion [10], as well as contrast-enhanced ultrasound (CEUS) assessment of wall vascularity [11].

Carotid artery thrombosis is diagnosed when no intraluminal flow is detectable. Slow-flow color Doppler sensitivity settings should be used or power Doppler, with its increased sensitivity to slow-velocity and low-amplitude signals. The pulsed Doppler cursor should be located centrally within the vessel lumen to avoid transmitted pulsations from an adjacent vessel.

Most penetrating palatal injuries heal without sequelae. Optimal treatment of ICA thrombosis after penetrating palatal trauma has not been determined. Some authors advocate anticoagulation, while others recommend thrombolytic agents. The benefits of surgical intervention are currently unproven [7]. The goal in treatment of Takayasu arteritis is to induce and maintain disease remission. Medical treatment with glucocorticoids combined with antihypertensive and antiplatelet drugs works well in most patients. Additional immunosuppressant drugs and biological agents are necessary in some children. Endovascular or surgical revascularization therapy is an option in patients with cerebrovascular disease [12].

Extracranial ICA stenosis can also occur in patients with sickle cell anemia which is associated with an increased risk of stroke. There are currently no velocity criteria for children comparable to those used in adults with atherosclerosis to determine a clinically significant degree of arterial stenosis. Some authors advocate use of a time-averaged mean of maximal velocity technique adapted from the transcranial Doppler ultrasound method commonly used for screening children with sickle cell anemia. A velocity $\geq$ 160 cm/sec is predictive of extracranial ICA stenosis with 80% sensitivity and 100% specificity [13].

Treatment of cervical carotid artery disease in patients with sickle cell anemia consists of acute anticoagulation and exchange transfusion, with maintenance on a long-term transfusion program [14].

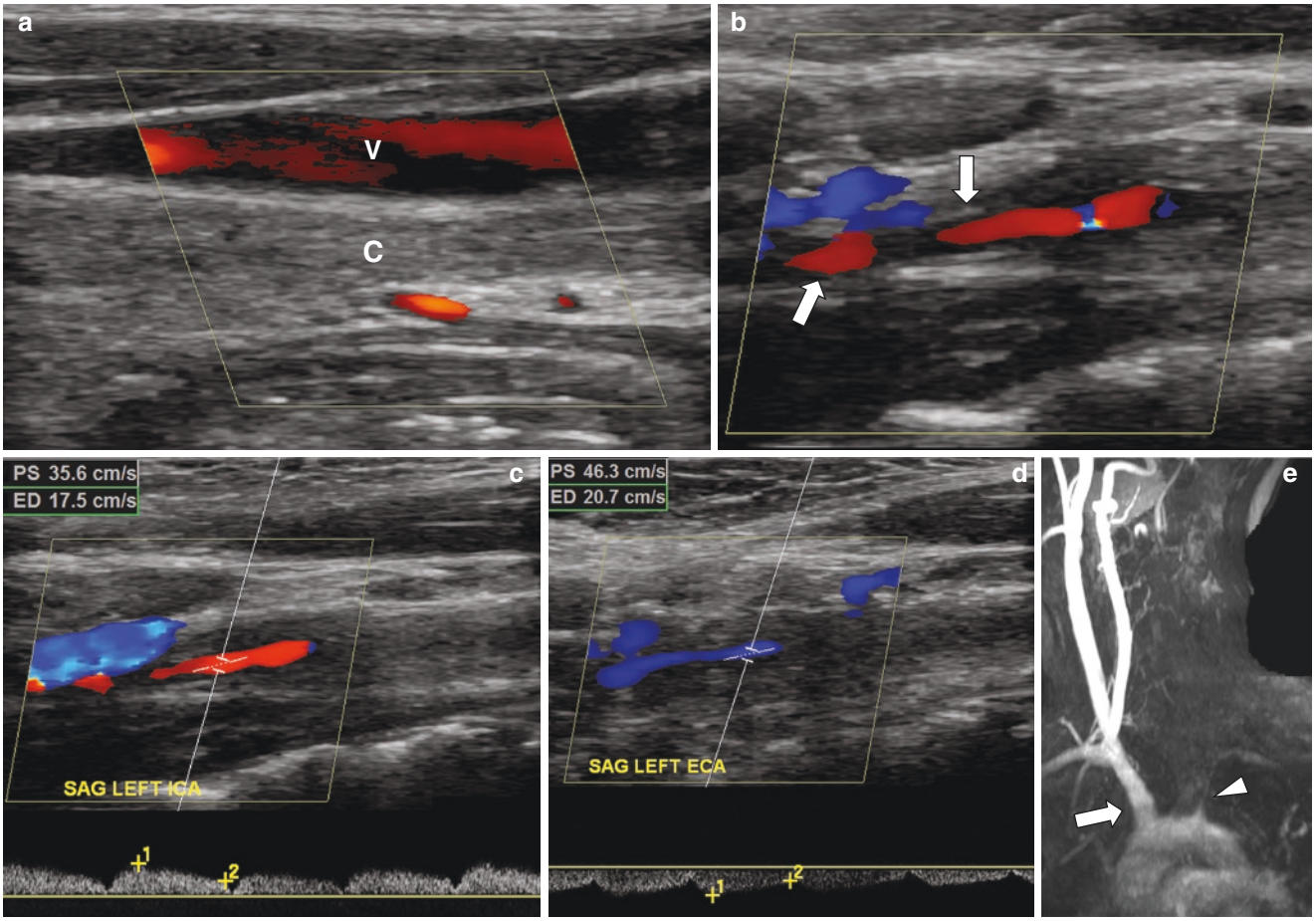

Fig. 19.11 Carotid artery occlusion in a 15-year-old female with Takayasu arteritis. (**a**) Sagittal power Doppler ultrasound image reveals complete occlusion of the left CCA (C). Flow is identified in the IJV (V). (**b**) Sagittal color Doppler ultrasound image shows a thick-walled, narrow left ICA (arrows) with antegrade flow. (**c**) Sagittal color Doppler ultrasound image of the left ICA. Spectral Doppler analysis shows a delayed and blunted systolic upstroke related to more proximal stenosis and occlusion. (**d**) Sagittal color Doppler ultrasound image of the left ECA. The vessel is narrowed and thick-walled. Spectral Doppler analysis demonstrates reversed flow direction with a delayed and blunted systolic peak. (**e**) Coronal oblique magnetic resonance angiography (MRA) image confirms complete occlusion (arrowhead) of the left CCA just beyond its origin. The right brachiocephalic artery (arrow) and its branches appear normal

Aneurysm

An aneurysm can be defined as a localized increase in the diameter of an artery of at least 50% compared to the normal diameter of that artery [15, 16].

Extracranial carotid artery aneurysms in children are extremely rare but are associated with a high mortality and morbidity. They can be congenital or inflammatory in etiology or may develop as a complication of pharyngeal infection or trauma. Extracranial carotid aneurysms occur most often in the ICA, followed by the CCA, and ECA. There is a nearly 2:1 male predominance in children. Clinical presentation ranges from an asymptomatic mass to rapidly fatal hemorrhage [17, 18].

Although angiography is considered the reference standard imaging technique, Doppler ultrasound evaluation is usually initially performed and can provide useful information regarding aneurysm size, extent, flow characteristics, presence of mural thrombus, and dissection.

Because the natural history of asymptomatic aneurysms is unknown and the risk of central nervous system complications is high, early operative intervention is advised whether or not the child is symptomatic [17, 19].

Dissection

Craniocervical arterial dissection in childhood occurs in 2.5 children per 100,000 per year and usually presents with symptoms of acute ischemic stroke or as a transient ischemic attack [20]. Risk factors for dissection in children include head and neck injury, connective tissue disorders, and male gender. Extracranial dissections account for 5–25% of childhood-onset acute ischemic stroke and are often preceded by trauma [21]. Post-traumatic dissection is associated with cervical

spine injuries, deformities, and/or instability and the presence of basilar skull fractures, facial and/or chest injuries, and focal neurological deficits. Children are at particular risk for dissection because of a lower craniocervical stability related to immature neck musculature, higher dependency on ligamentous rather than bony structures, large head to neck proportion, and less well-developed protective reflexes [22].

Symptoms of post-traumatic cerebrovascular injuries are nonspecific and often lead to misdiagnosis. When unrecognized and untreated, hemorrhage and/or acute ischemic stroke can lead to neurological sequelae, frequently with a devastating outcome. The extracranial ICA is usually affected more than 2 cm above its origin in contrast to atherosclerotic disease, where the ICA is more often involved at its origin or in the region of the siphon. Patients typically present with headache associated with anterior neck pain or ischemic symptoms. Symptoms may develop suddenly or progress slowly over more than a week [23].

Magnetic resonance (MR) imaging is the reference imaging technique for diagnosis of ICA dissection. Doppler ultrasound findings include decreased or absent flow velocities in the injured vessel and in some cases can directly visualize the intimal flap. Ultrasound can be useful in follow-up by documenting a return to normal flow velocities and directionality [23, 24].

There is no current consensus on the best treatment for extracranial carotid artery dissection. Recently published childhood stroke guidelines recommend anticoagulation. Endovascular or surgical procedures are recommended for those children with ongoing symptoms despite aggressive medical therapy [21].

Internal Jugular Vein

Normal Development and Anatomy

Normal Development

The earliest vessels of the cranium form a primordial hindbrain channel which drains into the precardinal vein. The cranial portion of the precardinal vein eventually forms the internal jugular vein (IJV).

Normal Anatomy

The IJV is formed by the union of inferior petrosal and sigmoid dural venous sinuses in or just distal to the jugular foramen. It descends in the carotid sheath along with the ICA with the vagus nerve located between them.

The IJV receives tributaries from the face and neck and descends into the thorax behind the two heads of the sternocleidomastoid muscle. It unites with the SCV to form the brachiocephalic vein (Fig. 19.12).

The IJV transports venous blood from the brain to the heart. A normal IJV will show complete collapse with moderate transducer pressure. Patient sniffing will reduce intrathoracic pressure with brief collapse of the vein and increased venous flow toward the heart that can be documented with spectral Doppler (Fig. 19.4) [25, 26].

Anatomic Variants

An asymmetry in size of the right and left IJVs is very common, with the left usually larger than the right (Fig. 19.13) [27, 28]. IJV caliber can vary markedly as a reflection of hydration status, heart rate and function, rate and amplitude of respiration, postural changes, and compression from adjacent structures [28]. Other variants, such as duplication and fenestration, are rare and usually discovered incidentally [29].

Congenital Anomalies

Jugular Vein Phlebectasia

Jugular vein phlebectasia is a rare abnormality of the IJV in children that consists of fusiform dilation of a segment of the IJV. Clinically it presents as a transient soft, painless mass in the lateral aspect of the neck when intrathoracic pressure is increased, as when coughing, sneezing, crying, bending over, or performing a Valsalva maneuver [30]. It is believed to occur as a result of focal mural weakness in the wall (Fig. 19.14, Cineclip 19.1 and 19.2). It affects males more than females and is usually unilateral and right-sided, although both IJVs can be affected.

Dynamic ultrasound of the neck with and without a Valsalva maneuver is useful in confirming the diagnosis of phlebectasia when the affected vein dilates to a diameter approximately twice its resting diameter [31]. Color Doppler ultrasound will depict blood flow and can exclude the presence of thrombosis.

Treatment of jugular vein phlebectasia is generally conservative. However, surgery can be performed if the patient develops progressive enlargement or thrombosis of the ectatic vein. Surgical options described in the literature include ligation, venoplasty, and resection [32].

Thrombosis

The most frequent indication for venous Doppler ultrasound in children is to diagnose deep vein thrombosis (DVT). Undetected and untreated DVT can lead to fatal pulmonary embolism. Although the incidence of venous thromboembolism in childhood is significantly lower than that in adults, it is increasingly recognized in the pediatric population as a complication of present-day health care. Central venous catheters are mandatory for the management of critically ill children, and the most common cause of jugular vein thrombosis is the presence of a central venous catheter [33, 34].

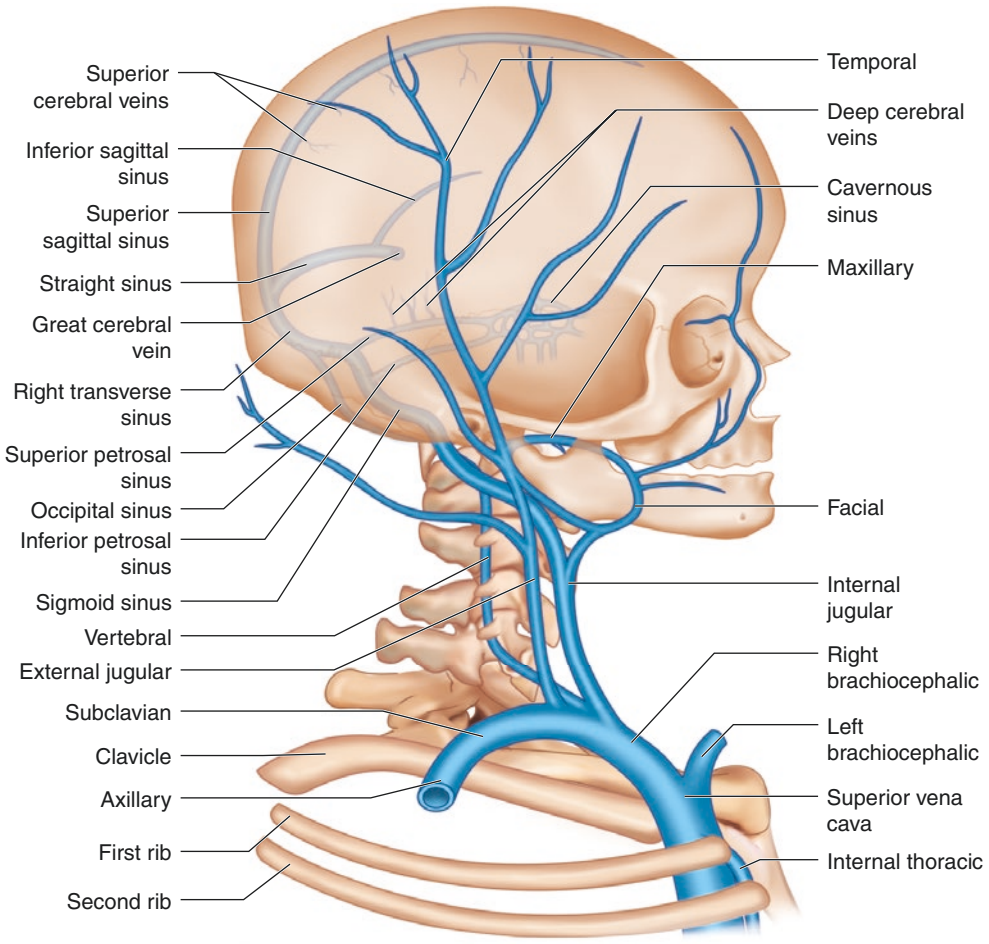

Fig. 19.12 Diagram of normal anatomy of the veins of the head and neck

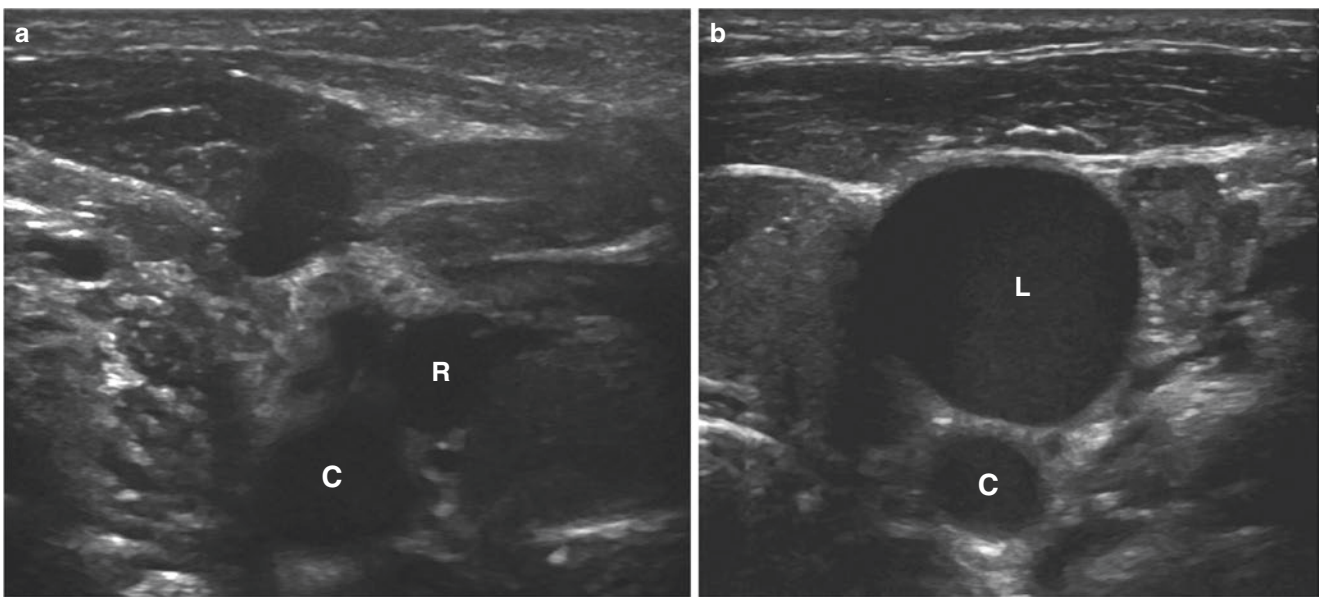

Fig. 19.13 Asymmetric IJVs in a 7-month-old female. Transverse grayscale ultrasound images of the right (**a**) and left (**b**) IJVs. The right (R) IJV is significantly smaller than the left (L) IJV. *C*, CCA

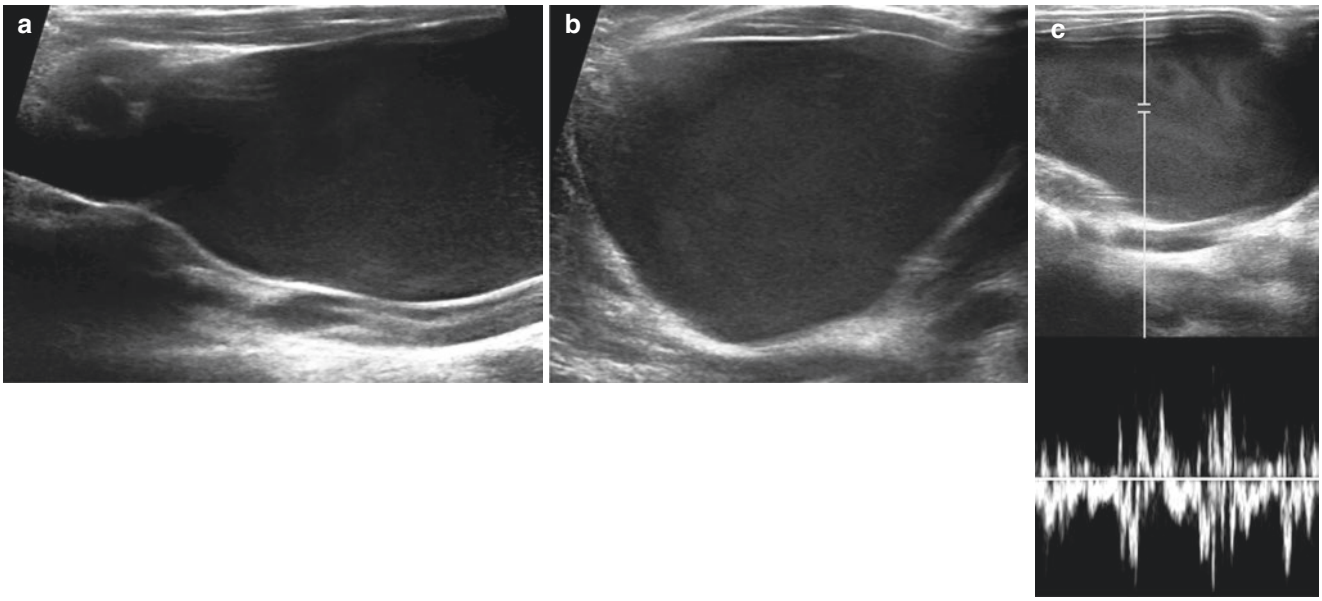

Fig. 19.14 Jugular vein phlebectasia in a 2-year-old male. (**a**) Sagittal and (**b**) transverse grayscale ultrasound images of the left IJV show a markedly ectatic vessel. (**c**) Spectral Doppler analysis depicts normal venous flow

Additional risk factors include the hypercoagulability associated with malignancy, polycythemia, deep neck infections, immobilization, trauma, head and neck surgery, and intravenous (IV) drug abuse.

Central venous catheter-related IJV thromboembolism is usually asymptomatic or manifests with chronic symptoms, including repeated loss of catheter patency, catheter-related sepsis, and prominent collateral circulation in the skin over the chest, back, neck, and face [35–37]. Symptomatic thromboembolism manifests acutely with swelling of the face, pulmonary embolism, chylothorax, and/or superior vena cava (SVC) syndrome (characterized by a sensation of fullness in the head, dilated neck veins, dyspnea, and mediastinal widening on chest radiography).

Lemierre syndrome is a rare and potentially lethal oropharyngeal infection that develops in immunocompetent adolescents and young adults and is mainly caused by *Fusobacterium necrophorum*. It usually manifests as a septic thrombophlebitis of the IJV although other veins of the head and neck may be affected and can lead to septic pulmonary emboli. Patients present with fever, neck pain, and tonsillopharyngitis [38].

Ultrasound is the preferred initial imaging modality for the diagnosis of venous thromboembolism. Abnormalities include a dilated, non-compressible vein, intraluminal echoes, lack of color flow, and abnormal spectral Doppler venous waveforms (Fig. 19.15) [39]. Serial ultrasound examinations are useful for monitoring the response to therapy. A normally compressible vein will be seen after complete resolution of thrombosis. Features of chronic thrombosis include wall thickening, intraluminal webs, and phleboliths (Fig. 19.16). Collateral vessels can also be readily imaged.

Ultrasound is also a useful screening modality for Lemierre syndrome, but it is limited in showing the full extent of thrombosis and may not allow adequate assessment of the associated inflammatory findings which are better depicted at CT [40].

Stenosis

Stenosis in the upper third of the IJV is common and occurs as a result of compression of the vessel between the transverse process of C1 or C2 and the occipital bone [41].

Aneurysm

A venous aneurysm is defined as an isolated region of dilation that communicates with a normal sized venous segment and is not associated with prior trauma. Most venous aneurysms arise from the superficial veins in the head, neck, or extremities. Venous aneurysms differ from phlebectasia in that they are usually acquired, not congenital lesions, and are typically diagnosed in adults.

A venous aneurysm differs from a varicose vein in that it is an isolated lesion, and there is no associated venous elongation as occurs with a varicosity. Aneurysms of the IJV are rare. Two types have been described, fusiform (more common) and saccular [42]. Patients present with neck swelling that is compressible and accentuated with the Valsalva maneuver.

Doppler ultrasound imaging depicts a focal enlargement of the internal jugular vein that increases with straining. Images of both sides of the neck should be obtained because the lesions can be bilateral.

Congenital jugular vein aneurysms should be excised only if they are symptomatic, enlarging, or disfiguring [43]. A unilateral aneurysm can be safely treated by ligation, with a low complication rate.

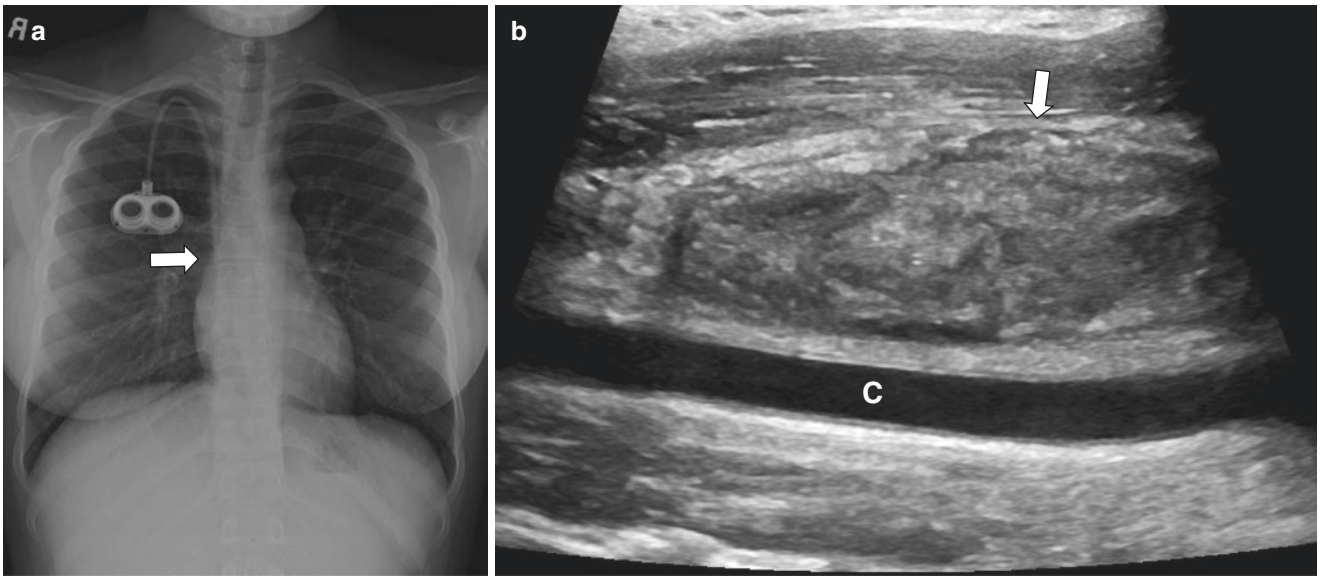

Fig. 19.15 Right IJV thrombosis in a 19-year-old female with sickle cell disease and a central venous port catheter. (**a**) Chest radiograph shows the central venous port catheter with tip (arrow) at the junction of the superior vena cava (SVC) and right atrium. (**b**) Sagittal grayscale ultrasound image of the right neck demonstrates a thrombus-filled, distended right IJV (arrow). *C*, CCA

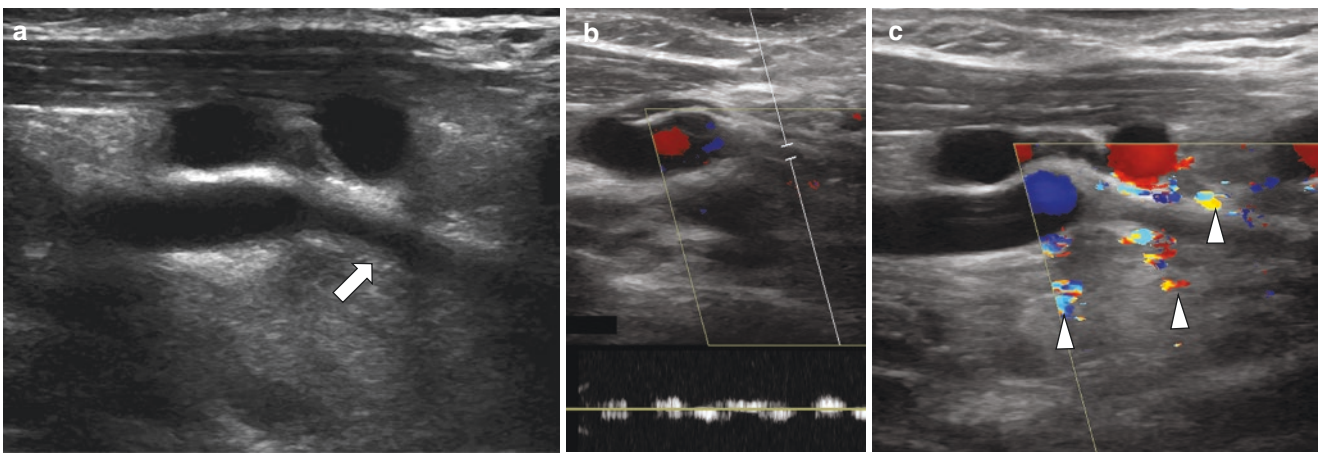

Fig. 19.16 Chronic right IJV thrombosis in a 7-month-old female with congenital heart disease and a right upper extremity peripherally inserted central catheter (PICC). (**a**) Sagittal grayscale ultrasound image reveals marked mural thickening (arrow) of the lower right IJV with significant luminal narrowing. (**b**) Sagittal color Doppler ultrasound image with spectral analysis depicts an abnormal, dampened venous waveform in the residual lumen. (**c**) Sagittal color Doppler ultrasound image demonstrates multiple collateral vessels (arrowheads) adjacent to the narrowed portion of the lower right IJV

Extremity Arteries

Arterial diseases that affect the extremities in childhood are uncommon and are usually due to acute or remote iatrogenic injury related to arterial cannulation, penetrating trauma, or vasculitis.

Technique

Patient Positioning

When imaging the upper extremity arteries, the patient's head is turned away from the transducer to help visualize the more proximal parts of the subclavian and brachiocephalic arteries. The axillary arteries are examined with the transducer in the axilla and the patient's arm elevated. The rest of the arterial system is examined with the arm slightly abducted and rotated externally. The position of the transducer for examination of the SCA varies depending on whether the distal portion or medial portion of the artery is studied. A supraclavicular approach is used to evaluate the medial segment of the SCA, and an infraclavicular approach to study the lateral portion of the SCA.

Imaging of the lower extremity arteries is performed with the patient supine or in a semi-erect position with the head elevated about 30°. The leg should be mildly abducted and

externally rotated, and the knee slightly flexed. Each arterial segment is scanned in the longitudinal plane with grayscale and Doppler imaging. Transverse images may also be useful. Representative longitudinal color Doppler and/or grayscale images as well as angle-corrected spectral Doppler waveforms with velocity measurements should be documented for each arterial segment. Cine clips can be used to document any flow abnormality [44]. When evaluating the popliteal artery, a decubitus position may be useful.

Ultrasound Transducer Selection

The highest-frequency transducer that permits adequate penetration and visualization should be used, generally a 5–12 MHz linear array transducer, with a higher-frequency transducer used in areas where the arteries are more superficial. Occasionally, a 3–5 MHz sector or curved linear array probe may be necessary in large patients or in individuals with substantial edema.

Imaging Approaches

Grayscale imaging is initially performed to determine the presence of echogenic thrombus or an extravascular mass. Color Doppler imaging permits a preliminary overview of the area of interest, and spectral Doppler ultrasound is then used to determine the blood flow patterns. The spectral Doppler gate is adjusted within the arterial lumen to optimize flow signal. A medium or high wall filter is generally used in evaluating the arteries. A low wall filter can be used to improve detection of slow flow. Power Doppler may be more sensitive than color Doppler in the detection of slow flow. CEUS can also be used to evaluate patients with peripheral arterial occlusive disease [45].

For upper extremity examinations, the subclavian, axillary, and brachial arteries are evaluated down to the elbow, with other vessels studied as clinically indicated, including the innominate, radial, and ulnar arteries and the palmar arches. Angle-corrected spectral Doppler measurements of arterial velocity should be obtained proximal to, at, and beyond any suspected stenosis.

For lower extremity examinations, evaluation begins in the groin and includes the common femoral artery (CFA); proximal deep femoral artery; proximal, mid, and distal superficial femoral artery (SFA); and popliteal artery (above and below the knee). When clinically indicated, imaging of the common and external iliac arteries, tibioperoneal trunk, and anterior tibial, posterior tibial, peroneal, and dorsalis pedis arteries should be performed [44].

The posterior tibial artery is identified on longitudinal imaging of the mid-calf using a posteromedial approach. The artery can then be traced both proximally and distally. Another method is to identify the artery at the medial malleolus of the ankle and then follow it cranially. On anterior imaging of the leg, the anterior tibial artery is identified along the interosseous membrane near the fibula. The peroneal artery can also be seen from an anterior approach where it appears posterior to the interosseous membrane. A posterolateral approach is used to identify the peroneal artery.

On grayscale imaging, normal extremity arteries have a smooth wall and an anechoic lumen. Their walls are thicker than those of the adjacent veins and do not collapse when light pressure is applied with the transducer. In normal upper and lower extremity arteries, laminar flow is present without turbulence or aliasing on color Doppler. At rest, a high-resistance triphasic waveform is typically noted, with a sharp systolic upstroke, transient flow reversal in early diastole and a short phase of low-velocity, antegrade flow in late diastole (Figs. 19.17, 19.18, and 19.19). Following exercise, there is a relative increase in antegrade diastolic flow that results in a lower-resistance waveform.

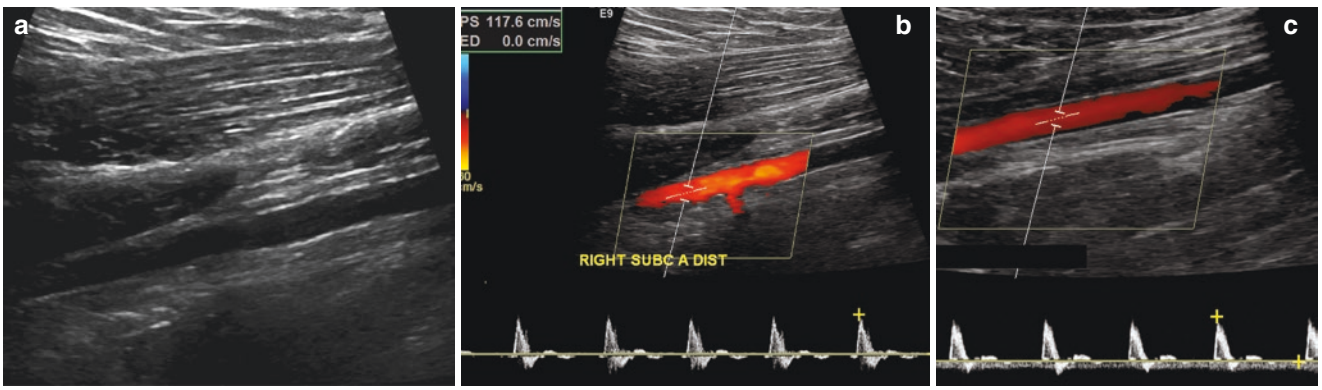

Fig. 19.17 Normal right upper extremity arteries in a 17-year-old female. (**a**) Sagittal grayscale ultrasound image shows the subclavian artery (SCA) with a smooth, mildly echogenic wall. (**b**) Sagittal color Doppler ultrasound image with spectral analysis reveals normal color flow and a triphasic waveform. Similar triphasic waveforms are depicted within the (**c**) axillary artery *(Fig. 19.17 continues)*

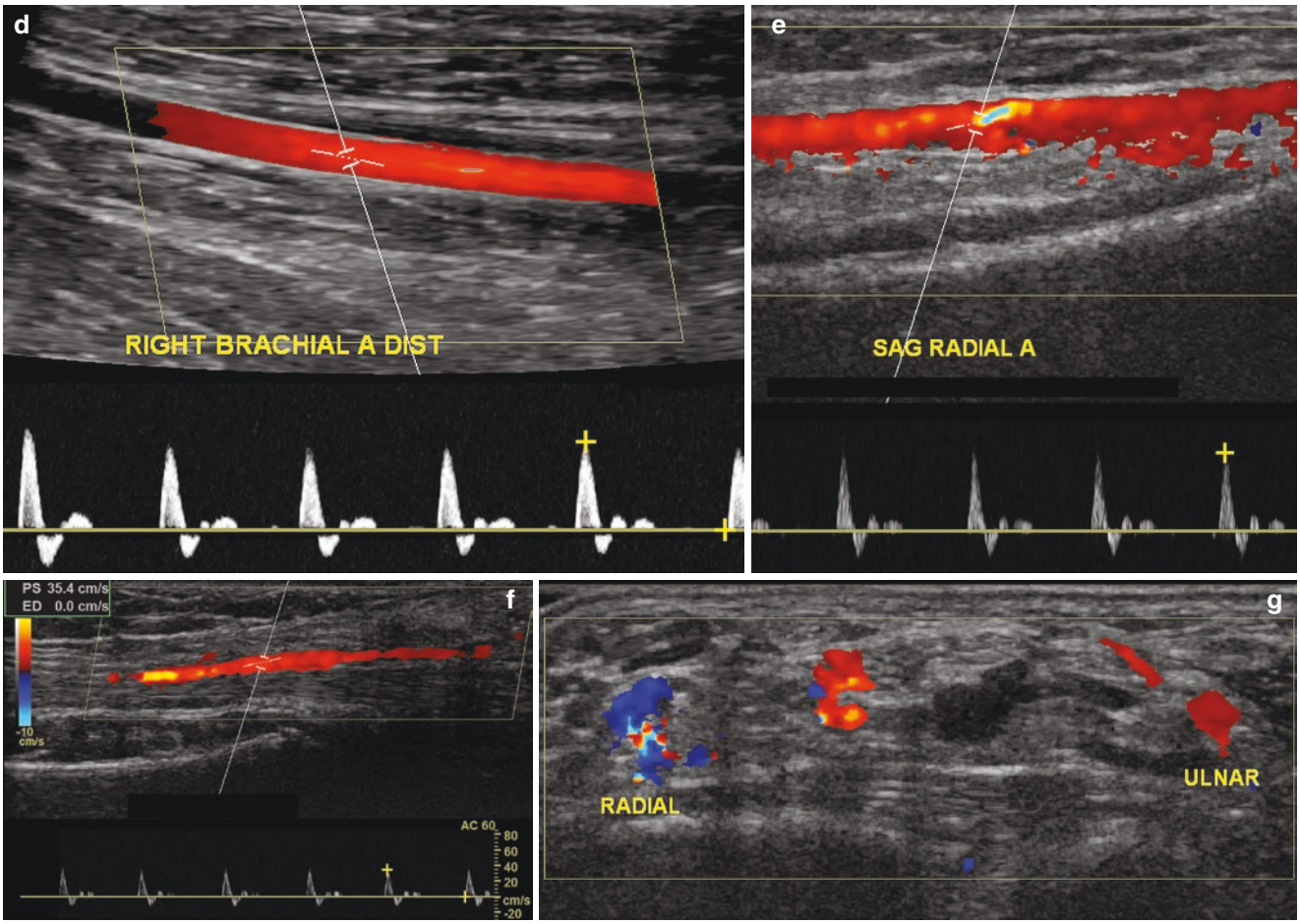

Fig. 19.17 (*continued*) (**d**) brachial artery, (**e**) radial artery, and (**f**) ulnar artery. (**g**) Transverse color Doppler ultrasound image shows the normal relationship of the right radial and ulnar arteries

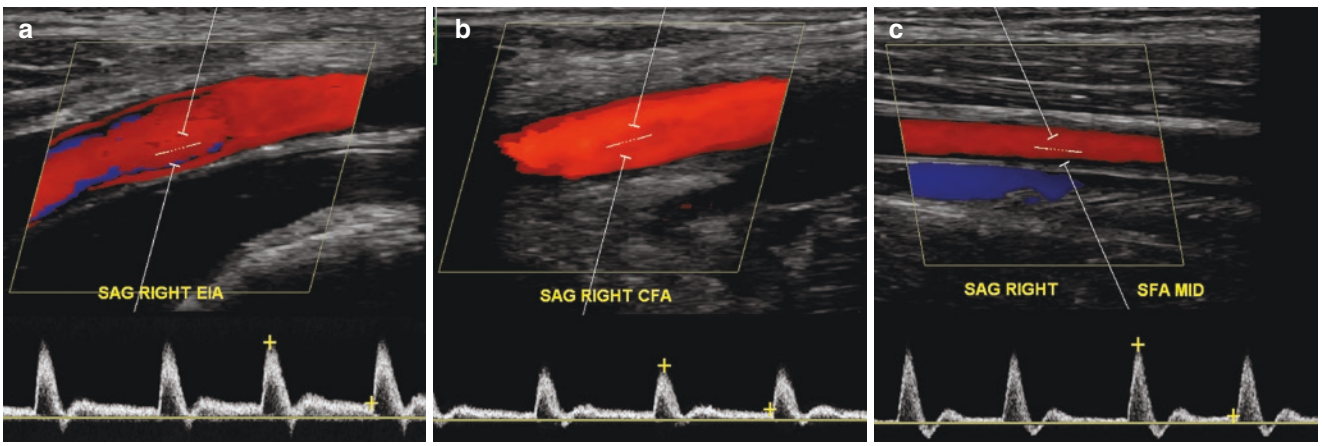

Fig. 19.18 Normal right lower extremity arteries in a 15-year-old female. Sagittal color Doppler ultrasound images with spectral analysis reveal normal color flow and triphasic waveforms in the (**a**) external iliac, (**b**) common femoral, (**c**) superficial femoral *(Fig. 19.18 continues)*

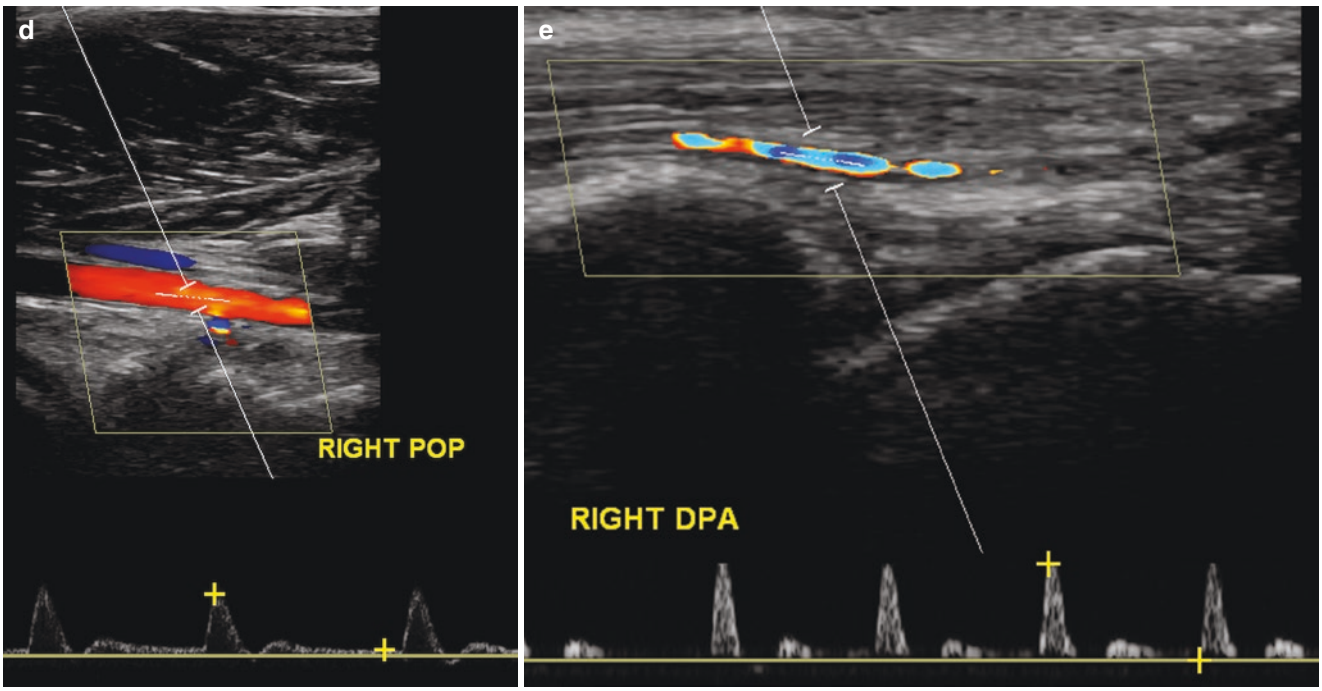

Fig. 19.18 (*continued*) (**d**) popliteal, and (**e**) dorsalis pedis arteries

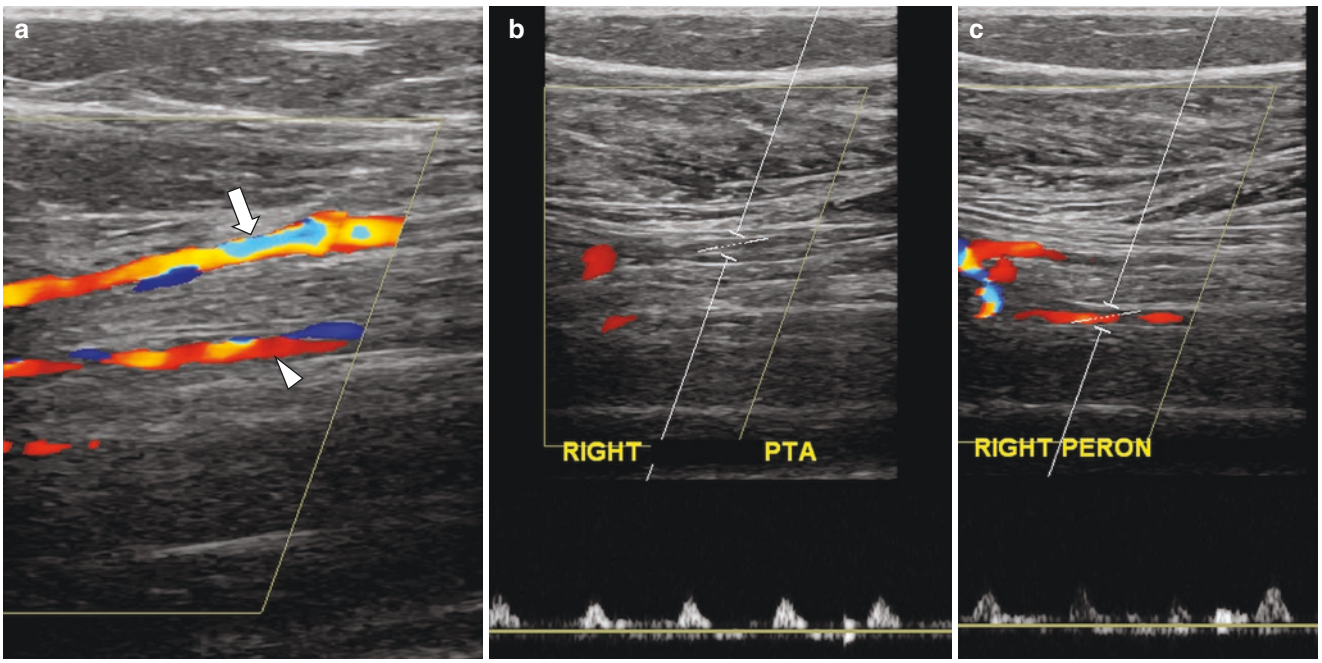

Fig. 19.19 Normal right calf arteries in a 14-year-old female. (**a**) Sagittal color Doppler ultrasound image shows the posterior tibial artery (arrow) and the peroneal artery (arrowhead) located more deeply. Spectral Doppler analysis of the posterior tibial artery (**b**) and peroneal artery (**c**) reveals low-velocity triphasic waveforms

Normal Development and Anatomy

Upper Extremity

The upper extremity receives its arterial supply from the SCA.

Normal Development

In the embryo, the right fourth pharyngeal arch artery becomes the proximal part of the right SCA. The distal part of the right SCA arises from the right dorsal aorta and the right seventh intersegmental artery. The left SCA is not derived from a pharyngeal arch artery; it forms instead from the left seventh intersegmental artery [46]. The subclavian arteries grow into the early upper limb buds and form the subclavian-axillary-brachial trunk.

The distal portion of the trunk becomes the interosseous artery that initially supplies the plexus of arteries in the primitive hand. A branch of the trunk artery, the median artery, temporarily replaces the interosseous artery in feeding the hand.

Subsequently, the ulnar and radial arteries develop and supply the forearm as well as the superficial and deep palmar arches of hand. The deep branch of the brachial artery as well as the arteries around the shoulder and elbow arise later as branches of the primary axial vessel.

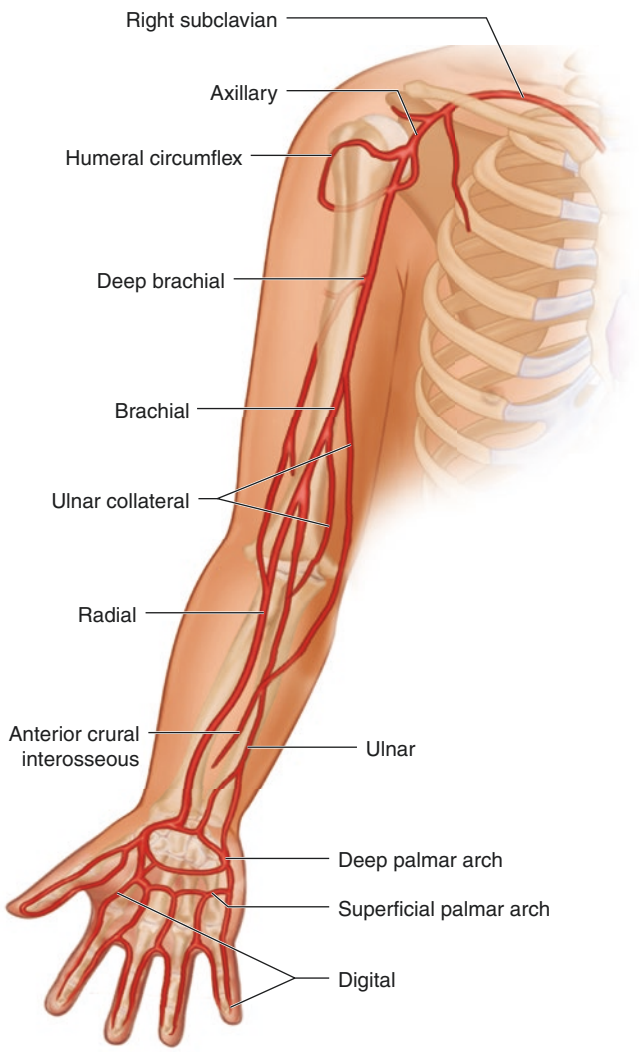

Fig. 19.20 Diagram of the upper extremity arteries

Normal Anatomy

The vertebral artery, internal mammary artery, thyrocervical and costocervical trunks, and dorsal scapular artery arise from the SCA which extends laterally across the upper chest. The SCA lies anterior to the SCV when evaluated from the supraclavicular fossa. It continues as the axillary artery at the level of the first rib. Below the margin of the teres major muscle, it continues as the brachial artery to the antecubital fossa where it divides into the radial and ulnar arteries.

The radial and ulnar arteries extend to the wrist where they anastomose with each other. The radial artery gives rise to the deep palmar arch which supplies the metacarpals of the hand, and the ulnar artery gives rise to the superficial palmar arch, which supplies the digits of the hand (Fig. 19.20).

Lower Extremity

The lower extremities receive their arterial blood supply from the CFA (Fig. 19.21).

Normal Development

In the embryo, the umbilical artery gives off a small branch, the ischiadic artery, that temporarily supplies the growing limb. The external iliac artery arises from the umbilical artery slightly proximal to the ischiadic artery and soon provides most of the blood supply to the limb. The external iliac artery gives rise to the femoral, popliteal, and posterior tibial arteries. The popliteal artery anastomoses with the ischiadic artery, and the lower ischiadic artery eventually develops into the peroneal and inferior geniculate arteries. The ischiadic artery also supplies the early vascular plexus of the foot.

Normal Anatomy

The CFA arises from the external iliac artery at the level of the inguinal ligament. It extends caudally for several centimeters where it divides into the superficial femoral artery

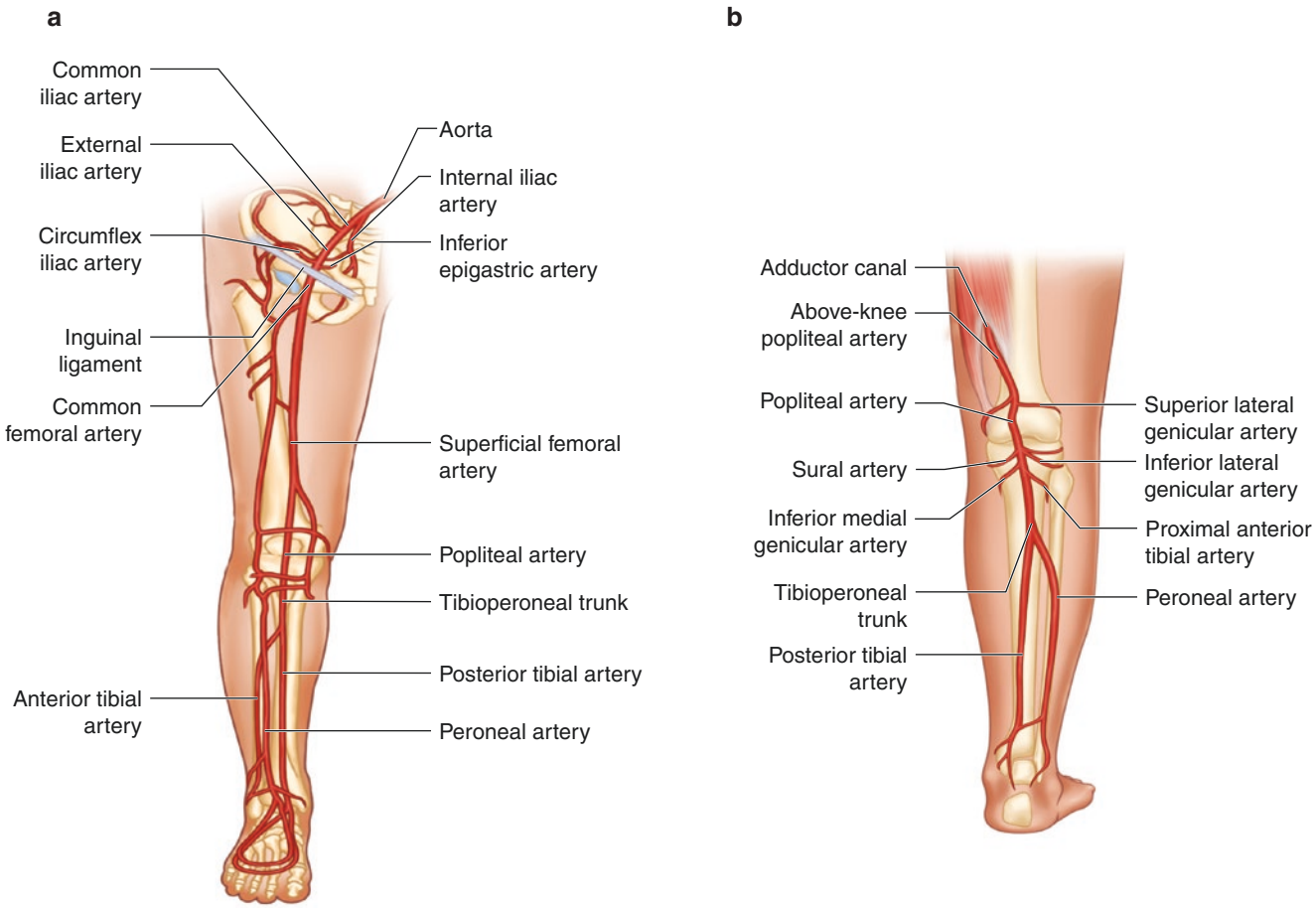

Fig. 19.21 Diagrams of lower extremity arteries. (**a**) Anterior view of the right lower extremity arteries. (**b**) Posterior view of the right lower extremity arteries

(SFA) and the deep femoral (profunda femoris) artery. The SFA extends along the medial aspect of the thigh in parallel with the femoral vein (FV) to the adductor canal. Below the adductor canal, the popliteal artery runs posterior to the knee, supplying branches to the calf. The deep femoral artery gives off perforating branches, as well as the medial and lateral circumflex arteries that supply the femoral head and the deep muscles of the thigh.

The popliteal artery divides into the tibioperoneal trunk and the anterior tibial artery. The tibioperoneal trunk branches into the posterior tibial and peroneal arteries. At the level of the ankle, the posterior tibial artery divides into the medial and lateral plantar arteries.

The anterior tibial artery courses laterally, extending through the interosseous membrane between the tibia and fibula, and into the anterior compartment of the lower leg. The anterior tibial artery continues as the dorsalis pedis artery. The dorsalis pedis artery joins the lateral plantar artery to form the plantar arch. The peroneal artery passes through the interosseous membrane above the ankle to supply small arterial branches to the lateral ankle and foot.

Anatomic Variants

Upper limb arterial variants are relatively rare. The most common is a high origin of the radial artery. Other variations include a superficial position of the brachial, ulnar, and radial arteries, and accessory brachial arteries [47].

The foot usually receives most of its arterial supply from branches of the anterior and posterior tibial arteries. A frequent variation of this pattern consists of a dominant peroneal artery with a hypoplastic or aplastic posterior tibial artery or a hypoplastic anterior tibial artery. Peronea arteria magna is a variant where both the anterior and posterior tibial arteries are hypoplastic and a large, dominant peroneal artery supplies the entire leg and foot [48].

Stenosis and Thrombosis

Symptoms of acute ischemia include limb cyanosis and pulselessness, while patients with chronic disorders may present with exercise-induced discomfort, claudication, excessive

exertional fatigue, and weakness. In long-standing cases, there may be a limb-length discrepancy, loss of extremity muscle mass, and a small foot [49, 50].

Evaluation for stenosis is performed with color and spectral Doppler imaging to document peak systolic and end-diastolic flow velocity and Doppler waveform morphology. Any zones of focal narrowing identified on grayscale imaging require confirmation with color Doppler. The presence of turbulent color Doppler signal should be further characterized with spectral Doppler.

When a change in spectral waveform morphology is noted in an arterial segment, additional proximal and distal evaluation with color and spectral Doppler should be performed to identify the transition points.

Arterial stenosis is diagnosed by analyzing waveform morphology, PSV, and EDV. Both absolute PSV values and the peak velocity ratio (defined as peak velocity at or in the downstream jet divided by peak velocity of the artery 2 cm upstream) are assessed. A focal increase in the PSV ratio at the stenosis relative to the adjacent non-stenotic artery exceeding 2.0 along with spectral broadening and loss of transient flow reversal in the artery is consistent with at least 50% diameter stenosis [51].

The spectral Doppler waveform distal to a stenosis of greater than 50% will be abnormal with a tardus-parvus pattern [49]. For the femoral and popliteal arteries, a combination of a peak systolic velocity over 200 cm/sec and a peak velocity ratio greater than 2:1 has identified focal stenoses greater than 70% with a sensitivity of 79% and a specificity of 99% (Fig. 19.22) [52].

Peripheral arterial thrombosis is rare in children. Most cases are due to complications related to arterial catheterization. Non-catheter-related cases are unusual. Early diagnosis and rapid institution of appropriate treatment are vital in order to avoid limb loss [53].

On grayscale imaging, the thrombosed arterial lumen is usually filled with echogenic thrombus. External pressure on the vessel by the transducer can be used to show non-compressibility. On color and spectral Doppler of an occluded artery, no flow signal should be detectable. The presence of collateral vessels suggests chronic occlusion (Table 19.1).

Acute thrombosis superimposed on chronic thrombosis can also occur. Use of color and spectral Doppler is highly sensitive and specific for demonstrating the absence of flow and can distinguish stenosis from occlusion in the lower extremity with close to 100% accuracy [54]. The sensitivity for detecting occlusion of the SFA and popliteal artery is also high [55].

Detection of occlusion in the lower leg is better for the anterior and posterior tibial arteries than for the peroneal artery. A recent study in a group of adult patients revealed a sensitivity of 93% for patency of the tibial artery. However, there were many false positives as documented at angiography [56]. Similar data is not currently available for children.

Infants and children with acute limb ischemia are usually treated with anticoagulation. Patients who do not respond to anticoagulation may require systemic thrombolysis or surgical thrombectomy and arterial repair [50, 57, 58]. Management strategies for pediatric patients with chronic ischemia are not

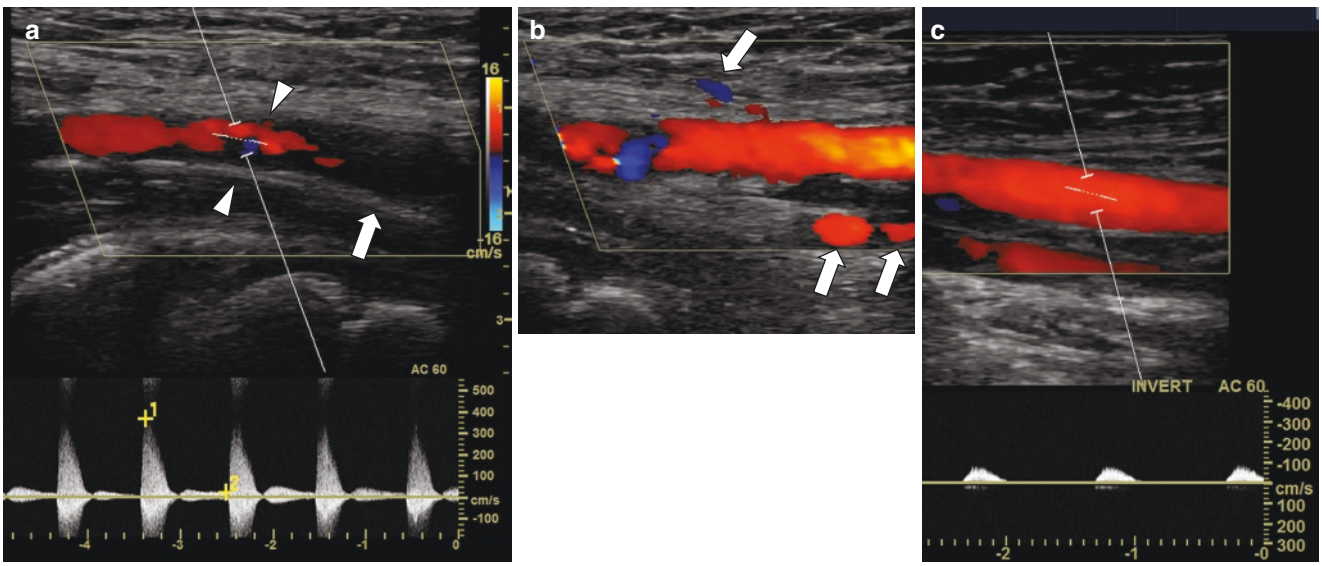

Fig. 19.22 Stenosis with focal occlusion of the right common femoral artery (CFA) in a 10-year-old male with remote history of right groin catheterization. (**a**) Sagittal color Doppler ultrasound image of the CFA with spectral analysis shows irregular mural thickening (arrowheads) with luminal narrowing. Peak systolic velocity measures 370 cm/sec. More distally the artery is occluded (arrow). (**b**) Sagittal color Doppler ultrasound image of the CFA distal to the stenosis shows adjacent collateral vessels (arrows). (**c**) Spectral analysis reveals an abnormal parvus-tardus waveform distally in the SFA with peak systolic velocity less than 100 cm/sec

Table 19.1 Ultrasound imaging features of arterial thrombosis

Technique	Ultrasound findings
Grayscale imaging	Arterial lumen contains echogenic thrombus
Doppler imaging	No flow at site of thrombosis
	Abnormal flow distal to thrombus
	Flow in collateral vessels with chronic occlusion

well-established. Extremity revascularization procedures have been successfully performed in symptomatic children [49].

Aneurysm

Aneurysms of the peripheral arteries are extremely rare in children. An underlying condition is often present, such as infection, trauma, connective tissue disorder, noninfectious arteritis, and congenital vascular malformation [59]. Infected (mycotic) aneurysms can develop by direct inoculation of bacteria into the arterial wall at the time of vascular injury. They are frequently seen in IV drug abusers who inadvertently inoculate themselves with contaminated needles that enter an arterial wall when they are aiming for an adjacent vein.

Peripheral arterial aneurysms can thrombose and lead to distal emboli and associated soft tissue ischemia or necrosis. Children with upper extremity aneurysms may present with a mass at the site of the involved artery or with paresthesias [59].

As previously described, the appearance of an aneurysm on grayscale and color Doppler imaging will vary according to the size of the aneurysmal neck, the presence of intraluminal clot, and mural calcification.

Larger and symptomatic aneurysms should be repaired. Treatment of upper extremity aneurysms usually includes resection with arterial reconstruction using reversed saphenous vein interposition grafts [59]. Lower extremity aneurysms are treated on a case-by-case basis and may require excision, endovascular embolization, or bypass grafting [59, 60]. Doppler US can be used to monitor the vessel after treatment.

Infected aneurysms have significant morbidity and mortality. Treatment consists of a combination of antibiotic therapy, aggressive surgical debridement of infected tissue, and vascular reconstruction, as needed. Endovascular therapies can be used for the treatment of ruptured infected aneurysm and in patients at great risk for open surgery [61, 62].

Pseudoaneurysm

A pseudoaneurysm is a focal disruption of the wall of an artery that develops as a result of direct trauma or erosion by inflammation or tumor. Blood flows beyond the confines of the vessel wall, and a hematoma develops next to the artery at the site of injury that is contained by the surrounding tissues. Once clot lysis has occurred, a pseudoaneurysm remains. A pseudoaneurysm differs from an aneurysm in that the arterial wall is disrupted. Blood within the pseudoaneurysm flows back into the feeding artery through a narrow opening. The outer wall of the pseudoaneurysm consists of compressed thrombus and the surrounding soft tissues.

Pseudoaneurysms typically present as a painful, pulsatile mass. They may exert pressure on the overlying skin that results in ischemia, necrosis, and hemorrhage. Clot that forms within the pseudoaneurysm can lead to distal embolization.

Grayscale ultrasound will show a round or oval bulge along the course of the artery that may contain thrombus. Color Doppler evaluation is performed to detect flow within the lumen of the pseudoaneurysm. When flow is identified, it often has a swirling, "yin-yang" pattern. Flow through the neck of the pseudoaneurysm is typically biphasic with a "to-and-fro" pattern on spectral Doppler (Figs. 19.23, 19.24**;** Cineclip 19.3) [63].

Surgical repair is indicated in patients with pseudoaneurysm due to prior vascular surgical intervention with suture line disruption, infection, or non-iatrogenic trauma. Other indications include skin or soft tissue ischemia, associated arteriovenous fistula (AVF), and injury to the vessel above the inguinal ligament. Urgent repair is recommended for any patient with rupture, an expanding pulsatile mass, or compression of surrounding structures causing claudication, neuropathy, or critical limb ischemia.

Femoral artery pseudoaneurysm can be managed with ultrasound-guided compression, ultrasound-guided thrombin injection, or surgery. Endovascular treatments, including coils, fibrin glue, and stent graft exclusion, have met with varying degrees of success [64].

Arteriovenous Fistula

An AVF is an abnormal vascular communication between a high-pressure artery and a low-pressure vein that bypasses the capillary bed. It can be congenital or acquired as a result of a traumatic injury. Pain commonly occurs when the AVF is located on a weight-bearing surface or when a large lesion ulcerates. Increased blood flow through an extremity fistula can increase oxygen delivery to the tissues that leads to a growth discrepancy between the normal and affected limbs. Cardiac output can also be increased and congestive heart failure may occur; this happens more often with acquired fistulae than with congenital lesions [65].

Femoral AVFs can develop when a femoral venous puncture is performed below the CFA, where several superficial branches of the femoral artery overlie the femoral vein or

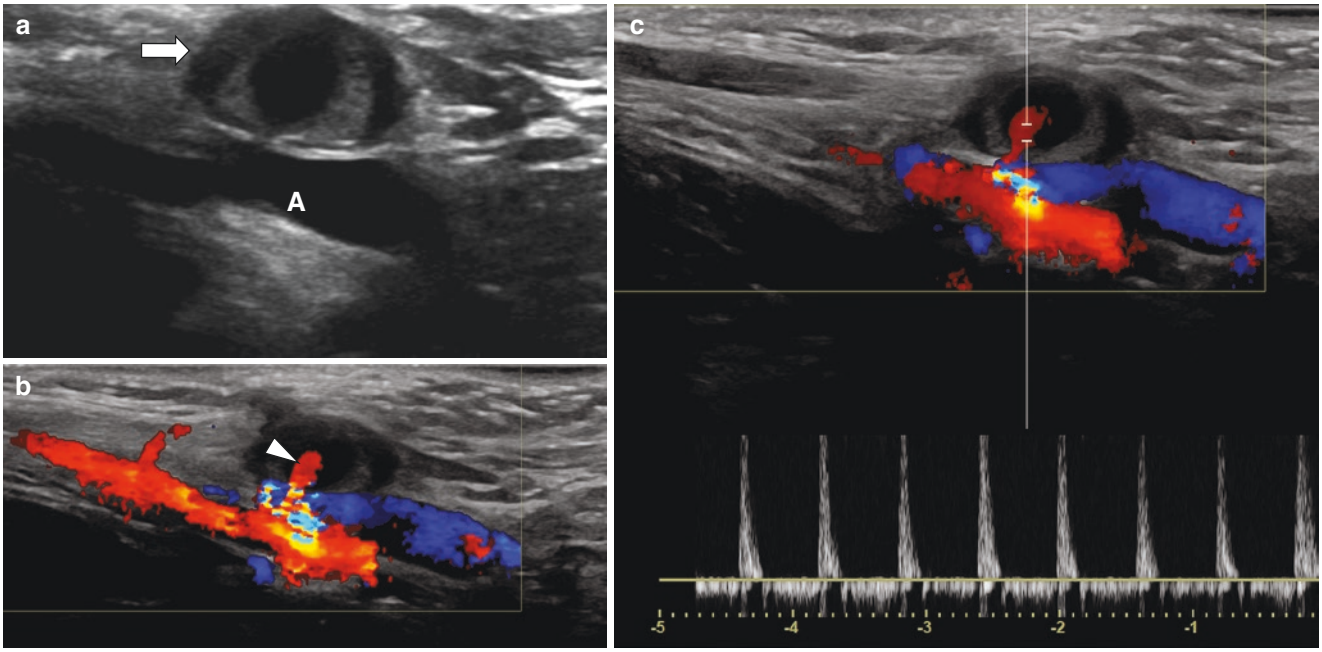

Fig. 19.23 Pseudoaneurysm of the right axillary artery in a 3-year-old male that developed as a complication of catheterization. (**a**) Sagittal grayscale ultrasound image of the right axillary artery shows a rounded heterogeneous collection (arrow) adjacent to the axillary artery (A). (**b**) Sagittal color Doppler ultrasound image shows a neck (arrowhead) extending from the axillary artery into the collection. (**c**) Spectral Doppler analysis of the aneurysmal neck shows to-and-fro flow

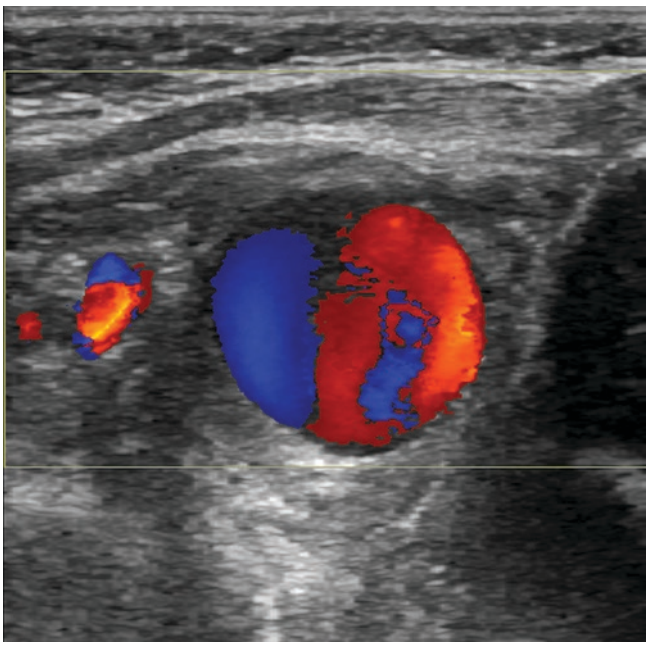

Fig. 19.24 Pseudoaneurysm of the left axillary artery in a 10-month-old male with a history of prior catheterization shows a typical "yin-yang" color Doppler pattern within the lumen of the pseudoaneurysm

when arterial and venous punctures are performed on the same side. A diagnosis of an AVF is made on physical examination with a finding of a continuous "to-and-fro" bruit that can be confirmed by ultrasound.

AVFs are rarely evident on grayscale imaging and are best depicted on color Doppler imaging (Fig. 19.25). Color Doppler demonstrates a direct communication between an artery and vein, turbulent flow in the region of the fistula, and perivascular soft tissue vibrations. Spectral Doppler analysis of the artery at the site of the fistulous connection shows a low-resistance pattern with high diastolic flow that contrasts with the typically high-resistance pattern of normal peripheral arteries. The draining vein can show an arterialized waveform [66].

Many of the iatrogenic AVFs are small and close spontaneously within 1 year. Ultrasound-guided compression or surgical repair can occasionally be necessary. Because cardiac volume overload and limb damage do not often develop with persistent AVFs, conservative management for at least 1 year is usual. Arterial embolization is the most effective treatment for high-flow lesions, with subsequent surgical resection occasionally being necessary [67]. The distinguishing clinical and ultrasound features of arterial aneurysm, pseudoaneurysm, and AVF are described in Table 19.2.

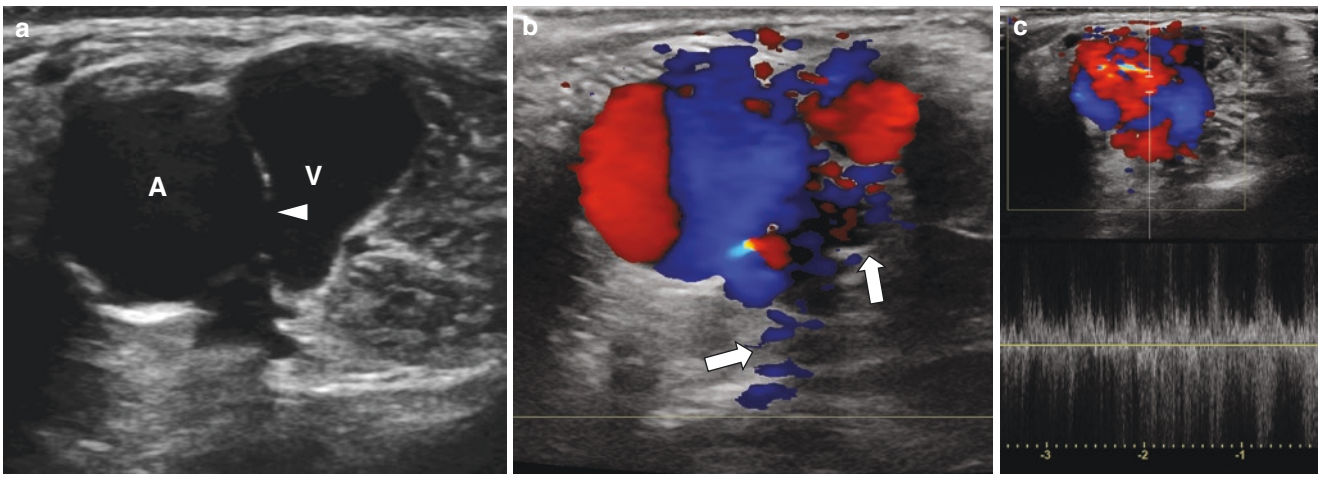

Fig. 19.25 Post-traumatic arteriovenous fistula (AVF) in a 3-year-old male with a history of inadvertent placement of a PICC in the left popliteal artery. (**a**) Transverse grayscale ultrasound image of the left popliteal vessels shows marked dilation of both the artery (A) and vein (V). A direct connection (arrowhead) is visible between the two vessels. (**b**) Color Doppler ultrasound image shows flow through the AFV with prominent soft tissue vibration artifact (arrows). (**c**) Disordered flow is depicted at the site of the fistula with spectral Doppler

Table 19.2 **Clinical and ultrasound features of arterial aneurysm, pseudoaneurysm, and arteriovenous fistula**

	Aneurysm	Pseudoaneurysm	Arteriovenous (AV) fistula
Clinical features	Underlying condition often present (e.g., infection, trauma, connective tissue disorder, IV drug abuse)	Develops after trauma or erosion by inflammation or tumor	Congenital or acquired, usually from trauma
	Popliteal artery common site		Iatrogenic lesions may resolve spontaneously
Pathology	Congenital or acquired weakness or destruction of medial layer of vessel wall	Focal disruption of arterial wall with hematoma at injury site contained by surrounding tissues	Communication between normal artery and vein in post-traumatic lesions
			Intrinsically abnormal vessels in setting of arteriovenous malformations
Ultrasound findings	Focal or diffuse arterial dilation best seen on transverse images	Round or oval anechoic structure with or without central thrombus	Traumatic fistulas have few grayscale findings. AV malformations may show dilated vessels
	Variable color/spectral Doppler signal depends on amount of thrombus, size of aneurysmal neck, and presence of calcification	Color/spectral Doppler shows disorganized internal flow with "yin-yang" pattern	Color/spectral Doppler demonstrates low-resistance arterial flow, arterialized venous flow, and soft tissue vibration artifact
		"To-and-fro" flow in neck communicating with adjacent artery	

Extremity Veins

Technique

Patient Positioning

Patient positioning for examination of the upper and lower extremity veins is generally the same as that previously described for the upper and lower extremity arteries. The popliteal vein is examined with the patient prone and a pillow placed under the ankle to slightly flex the knee or with the patient in a decubitus position (with the side to be evaluated positioned uppermost). The posterior tibial and peroneal veins are imaged using a medial or posteromedial approach. The anterior tibial veins are imaged from an anterolateral approach.

Ultrasound Transducer Selection

The highest-frequency transducer that permits adequate penetration and visualization should be used, as described above for the upper and lower extremity arteries, typically a 5–10 MHz linear array transducer.

When imaging the upper extremities, a small footprint, high-frequency transducer can be placed in the suprasternal notch to visualize the junction of the brachiocephalic veins (BCVs) with the SVC (Fig. 19.26), although in practice imaging of this confluence is often difficult to achieve because of overlying lung tissue.

In the lower extremities, the superficial great saphenous veins are easily visualized by ultrasound in most patients. The deep veins in the proximal and mid-thigh are more difficult to image because of the thickness of the overlying muscles. Use

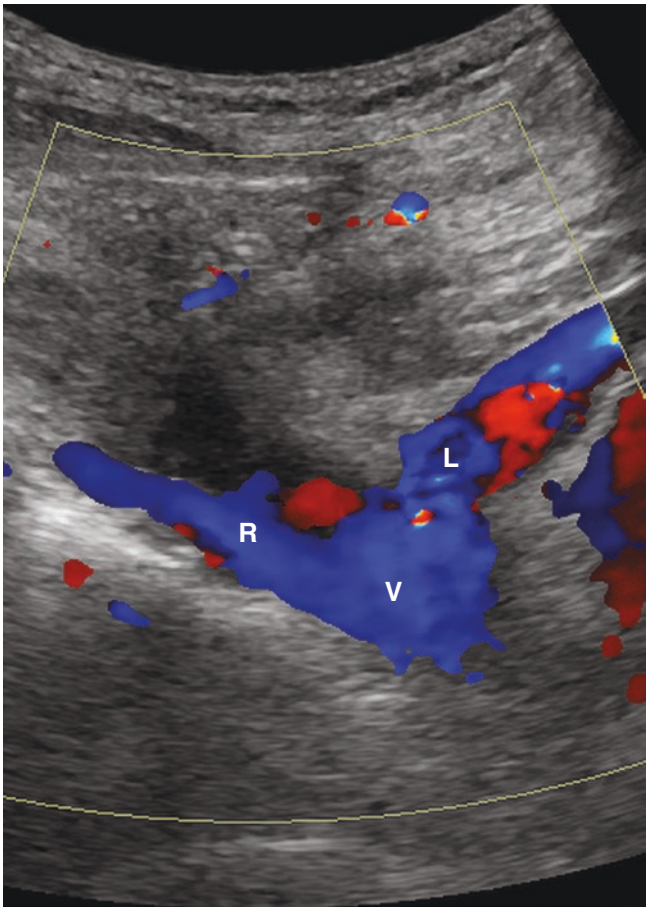

Fig. 19.26 Normal confluence of the brachiocephalic veins (BCVs) with the SVC in a 16-year-old female. Coronal color Doppler ultrasound image. *R*, Right brachiocephalic vein; *L*, left brachiocephalic vein; *V*, SVC

of a lower-frequency curved array or sector transducer may improve visualization of the deep venous system.

Imaging Approaches

Assessment of the upper extremity veins includes grayscale compression and color and spectral Doppler imaging of the visualized portions of the IJV; subclavian, axillary, and BCVs and any focal symptomatic areas (Fig. 19.27).

All veins are evaluated with compression at 1–2 cm intervals in the transverse plane. Venous compression should be applied to accessible veins in the transverse plane with sufficient pressure to completely collapse the vessel lumen. An attempt should be made to visualize the brachial, cephalic, and basilic veins in the upper arm to the elbow with color Doppler, and any focal symptomatic areas should be evaluated further with compression [44].

Grayscale images with and without compression or cine clips obtained with compression should be acquired from the superior aspect of the IJV in the neck to the thoracic inlet. The SCV is evaluated from its medial to lateral aspect with longitudinal color and spectral Doppler images and reviewed for evidence of luminal patency, transmitted cardiac pulsations, and respiratory variation. An inferiorly angled, supraclavicular approach is used to document the superior BCV and the medial portion of the SCV. An infraclavicular, superiorly angled approach can be used to demonstrate the lateral aspect of the SCV. In many cases the SCV can be compressed. The midportion of the SCV is often incompletely imaged as it is located deep to the clavicle.

Spectral Doppler images are obtained from longitudinal images of the vessel with an insonation angle of 60°or less. A normal Doppler waveform will always return to the baseline. The absence of pulsatility raises concern for more central stenosis or obstruction [68].

Evaluation of the lower extremity veins includes the following images for each deep venous segment as recommended by the 2019 American College of Radiology (ACR)-American Institute of Ultrasound in Medicine (AIUM)-Society for Pediatric Radiology (SPR)-Society of Radiologists in Ultrasound (SRU) practice parameter for the performance of peripheral venous ultrasound examinations [44]: imaging is performed from the inguinal ligament to the ankle whenever possible. Venous compression is applied every 2 cm or less in the transverse plane with sufficient pressure on the skin to completely obliterate the normal venous lumen [69].

The common femoral, femoral (formerly known as the superficial femoral) [70], popliteal, posterior tibial, and peroneal veins are evaluated. The deep (profunda) femoral vein (FV) should also be examined at its confluence with the FV. The great saphenous vein is imaged at the saphenofemoral junction. Focal symptoms may require additional imaging (Fig. 19.28).

All studies, whether unilateral or bilateral, should include right and left common femoral or right and left external iliac venous spectral Doppler waveforms. All spectral Doppler waveforms should be obtained from the long axis of the vessel. Tracings should be compared for asymmetry and/or loss of respiratory phasicity [71]. Both sides should be assessed with similar patient positioning and similar phase of respiration so that symmetry can be assessed.

Popliteal venous spectral Doppler waveforms of the symptomatic leg should also be obtained. Routine spectral Doppler distal augmentation is not necessary for the diagnosis of DVT [72]. However, in challenging situations, color Doppler imaging with distal augmentation can aid in identification of vessels and in differentiating complete from incomplete occlusion [73].

When studies are normal, static images or cine loops are recorded at selected sites as a representative subset of the images acquired during a comprehensive study as described below:

1. Grayscale images (or cine loops) should be recorded without and with compression at each of the following levels whenever possible: common femoral vein (CFV); confluence of the CFV with the great saphenous vein; deep (profunda) FV at the confluence with the FV; FV in the upper, mid, and distal portions of the thigh; and popliteal vein.

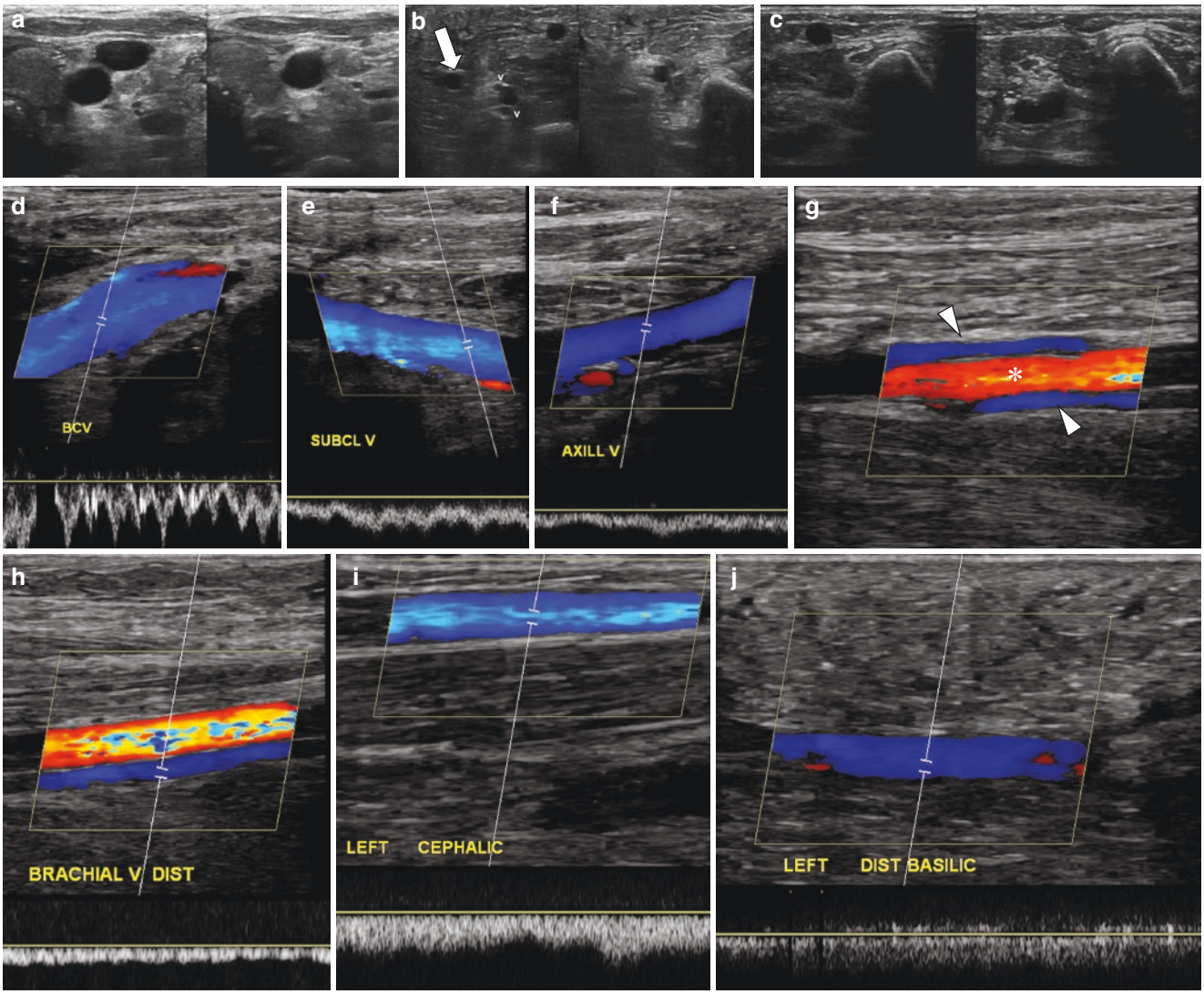

Fig. 19.27 Normal left upper extremity veins in an 11-year-old female. Transverse grayscale ultrasound images of the (**a**) IJV, (**b**) basilic vein (arrow) and paired brachial veins (v) and (**c**) cephalic vein imaged with light transducer pressure (left panels) and with firm transducer pressure (right panels). Sagittal color Doppler ultrasound images with normal spectral waveforms are shown for the BCV, SCV, and axillary veins (**d–f**). (**g**) Sagittal color Doppler ultrasound image of normal paired brachial veins (arrowheads) on either side of the brachial artery (asterisk). (**h**) Sagittal color Doppler ultrasound image of a brachial vein with a normal spectral waveform. Sagittal color Doppler ultrasound images with spectral analysis of the cephalic (**i**) and basilic (**j**) veins depict normal waveforms

2. Representative images or cine loops without and with compression of the posterior tibial and peroneal veins.
3. Color and spectral Doppler waveforms should be obtained from the long axis of each of the following vessels: right common femoral or external iliac vein; left common femoral or external iliac vein; and popliteal vein on the symptomatic side or on both sides if the examination is bilateral.

Abnormal symptoms or findings generally require additional images for complete documentation. Protocol adjustments may be necessary depending on patient presentation, clinical indication, or anticipated treatment options (e.g., a bilateral study or more detailed assessment of the superficial venous system) [74–76].

When a thrombus is identified in the CFV, its most proximal extent should be demonstrated by including the external

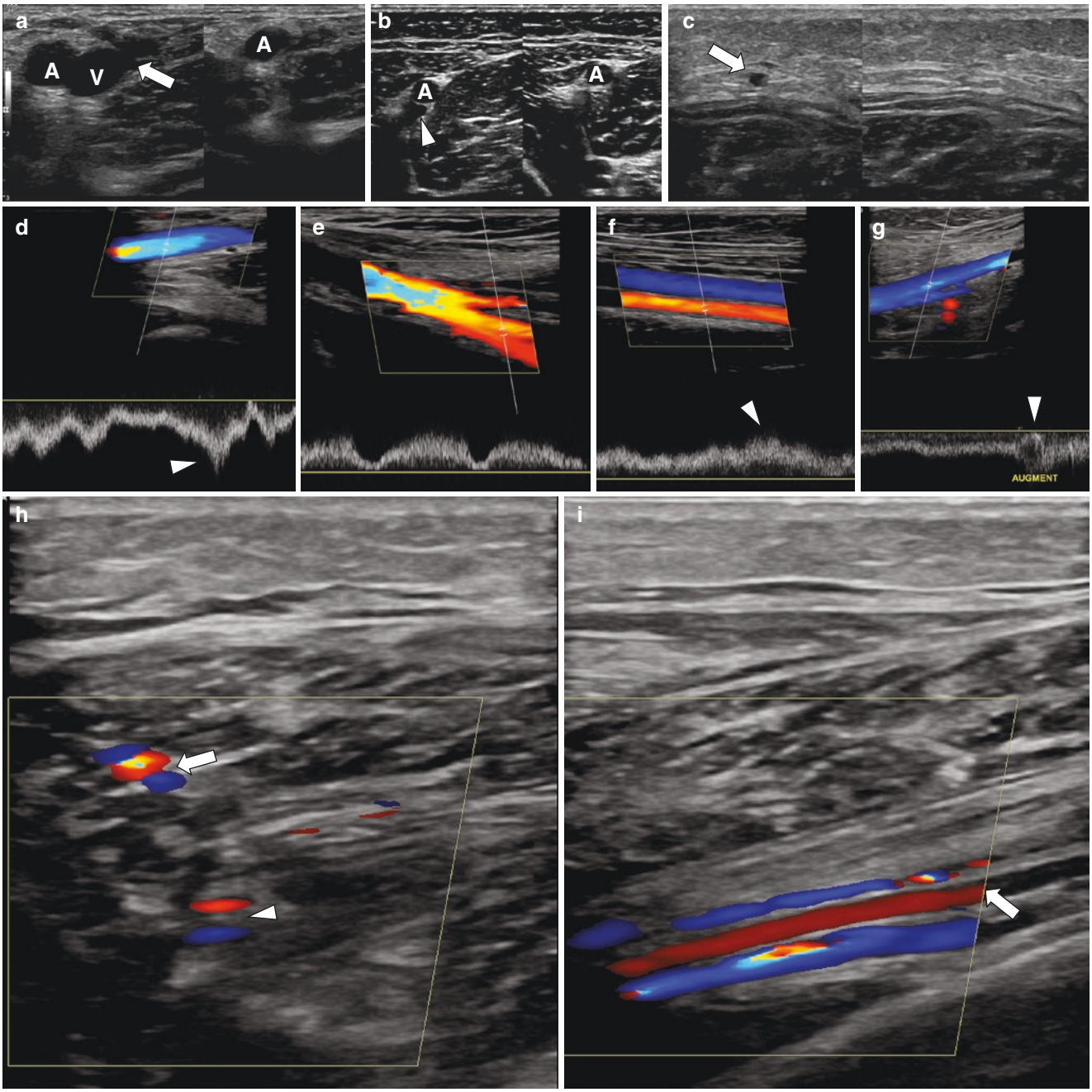

Fig. 19.28 Normal right lower right extremity veins in an 11-year-old female. Transverse grayscale ultrasound images obtained with light transducer pressure (left panels) and firm transducer pressure (right panels) depict (**a**) the confluence of the common femoral vein (CFV) and great saphenous vein (arrow); *V*, CFV; *A*, CFA; (**b**) FV (arrowhead); *A*, Superficial femoral artery; and (**c**) calf veins (arrow). Sagittal color Doppler ultrasound images with spectral analysis of the CFV (**d**), deep FV (**e**), FV (**f**), and popliteal vein (**g**). There is increased flow with augmentation maneuvers (arrowheads) on images (**d**), (**f**), and (**g**). (**h**) Sagittal color Doppler ultrasound image of the posterior tibial (arrow) and peroneal (arrowhead) calf vessels. (**i**) Sagittal color Doppler ultrasound image shows the paired peroneal veins on either side of the peroneal artery (arrow)

Table 19.3 Ultrasound imaging features of deep vein thrombosis (DVT)

Category	Ultrasound findings
Acute DVT	Enlarged vein
	Lack of compressibility
	Thrombus in vessel lumen
	No Doppler flow at site of thrombus
	Loss of flow pulsatility distal to thrombus
	No flow augmentation
	No response to Valsalva maneuver
Chronic (residual) DVT	Thick or irregular vessel wall
	Narrow or irregular lumen
	Thrombus broadly attached to vessel wall
	Web-like filaments in vessel lumen

iliac veins and inferior vena cava (IVC) in the evaluation. Any additional musculoskeletal findings in the imaging field should be documented, such as a hematoma, knee joint effusion, or popliteal cyst. The ultrasound imaging features of acute and chronic DVT are summarized in Table 19.3.

Normal Development and Anatomy

Upper Extremity

Normal Development

In the embryo, the upper limb buds are drained by marginal veins. The pre-axial (i.e., radial) and post-axial (i.e., ulnar) portions of the marginal vein develop into the superficial cephalic and basilic veins, respectively. The deep veins develop alongside the corresponding upper limb arteries.

Normal Anatomy

The venous drainage of the upper extremity is comprised of a deep and superficial system, both of which ultimately drain into the axillary vein (Fig. 19.29) [77].

The deep veins of the hand drain to the paired ulnar and radial veins of the forearm that join distal to the elbow to form the paired brachial veins. The brachial veins extend superiorly along the medial aspect of the arm to join the basilic vein and form the axillary vein, usually at the level of the teres major muscle.

The axillary vein courses through the axilla to the level of the first rib. As it extends beneath the first rib, it becomes the SCV. The medial portion of the SCV joins with the internal and external jugular veins to form the brachiocephalic (innominate) vein.

The superficial veins arise on the dorsum of the hand. They drain into the ulnar, radial, and median forearm veins at variable levels. These veins unite to form the medially located basilic vein and the laterally located cephalic vein. The basilic vein usually drains into the brachial veins in the upper arm. The cephalic vein extends along the superficial soft tissues of the shoulder and drains into the axillary vein in the lateral aspect of the upper chest.

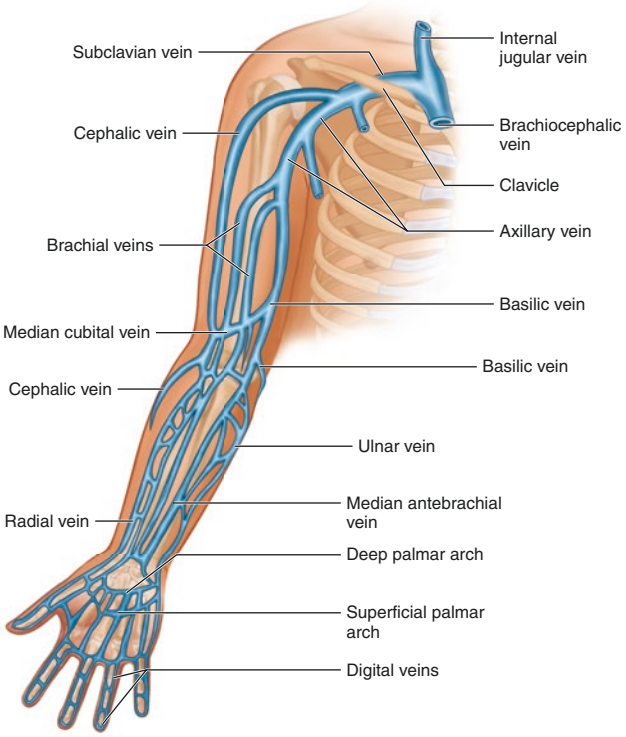

Fig. 19.29 Diagram of normal upper extremity venous anatomy

Lower Extremity

The venous drainage of the lower extremity is comprised of deep and superficial systems, both of which drain into the CFV (Fig. 19.30) [78, 79].

Normal Development

In the embryo, the lower extremity venous system appears between weeks 5 and 6 of life. The superficial veins develop first and include a primitive marginal vein and the small saphenous vein. Between weeks 7 and 8, three venous plexuses mature, including the posterior tibial veins, the great saphenous vein, and the FV.

Early venous outflow from the primitive lower limb occurs through a lateral/posterior fibular (peroneal) vein. The primitive fibular vein develops two branches: the anterior tibial vein and a connecting vessel. The anterior tibial vein becomes the main deep draining vein of the calf. The anterior tibial vein and primitive fibular veins together constitute the sciatic vein.

A portion of the primitive fibular vein distal to the anterior tibial vein branch develops into the short or lesser saphenous vein. The connecting vessel grows medially from the middle of the sciatic vein and connects to a proximal medial vessel that will become the FV and the deep venous system, while the sciatic vein regresses. The FV extends down the leg as the posterior tibial vein [80].

Normal Anatomy

The deep veins of the foot drain into the anterior and posterior tibial veins. The posterior tibial vein joins the pero-

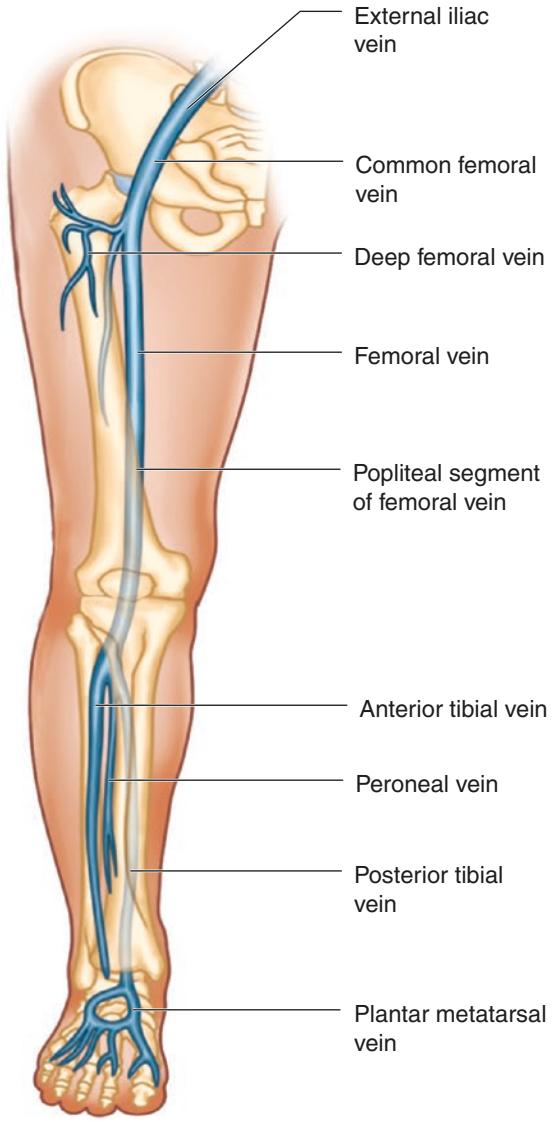

Fig. 19.30 Diagram of normal lower extremity venous anatomy

neal vein(s) (which are usually paired) before anastomosing with the anterior tibial vein to form the popliteal vein. The popliteal vein continues superiorly as the FV after it leaves the adductor canal in the distal thigh. The FV ascends to join the deep (profunda) FV just below the inguinal ligament, where it becomes the CFV. The CFV becomes the external iliac vein above the inguinal ligament.

The superficial venous system includes the small (short) and great saphenous veins (Fig. 19.31). The small saphenous vein drains the soft tissues overlying the medial malleolus and then ascends posteriorly to anastomose with the popliteal vein. The great saphenous vein drains the medial calf and then ascends to join the CFV in the proximal thigh below the inguinal ligament. The deep and superficial veins are connected at different levels in the calf by perforating veins that drain from the skin to the deep veins.

Anatomic Variants

FV duplication is identified in approximately 30% of patients and can be complete or segmental [81]. In about 40% of patients where multiple vessels are identified in the popliteal fossa, the cause is a high confluence of the posterior tibial and peroneal veins, rather than a true duplication of the popliteal vein [82, 83]. It is important to be aware of the possibility of venous duplication when evaluating patients for deep vein thrombosis in order to avoid a false negative interpretation (Fig. 19.32) [84].

Thrombosis

DVTs in children usually occurs as a complication of an underlying disease, such as sepsis, cancer, and congenital heart disease, or as a complication of medical, surgical, or therapeutic intervention. Other common causes include immobilization, hypercoagulability, and oral contraceptives [85–87]. Patients with peripheral DVT will present with pain, swelling, and erythema of the affected limb. DVT of the lower extremities is much more common in children than upper extremity DVT. Apart from central venous catheter-associated venous thrombosis, upper extremity DVT is rare in children.

Clinical evaluation of the peripheral venous system is often difficult and frequently inaccurate. Clinical decision rules to improve pretest probability have been recommended by the American College of Physicians and the American Academy of Family Physicians [88–90]. The Wells criteria generate a score for certain physical examination findings and pertinent clinical history [91].

Clinical factors associated with increased probability of DVT include immobilization, active cancer, a swollen extremity, localized tenderness along the course of the deep venous system, pitting edema localized to the symptomatic extremity, collateral superficial veins, and previously documented DVT. The modified Wells score separates patients into two groups: DVT unlikely and DVT likely [92].

Current guidelines recommend a D-dimer test for low-risk patients [93, 94]. The D-dimer test measures a degradation product of fibrin and has a high negative predictive value for DVT that is sensitive but not specific. A positive test may be caused by low levels of fibrin associated with inflammation, infection, vasculitis, or trauma [95]. When the D-dimer test result is positive, the patient should undergo a venous Doppler examination of the symptomatic limb. A negative D-dimer test effectively rules out the possibility of DVT.

Acute Deep Vein Thrombosis

The ultrasound features of acute DVT include an enlarged vein with lack of compressibility, visualization of thrombus

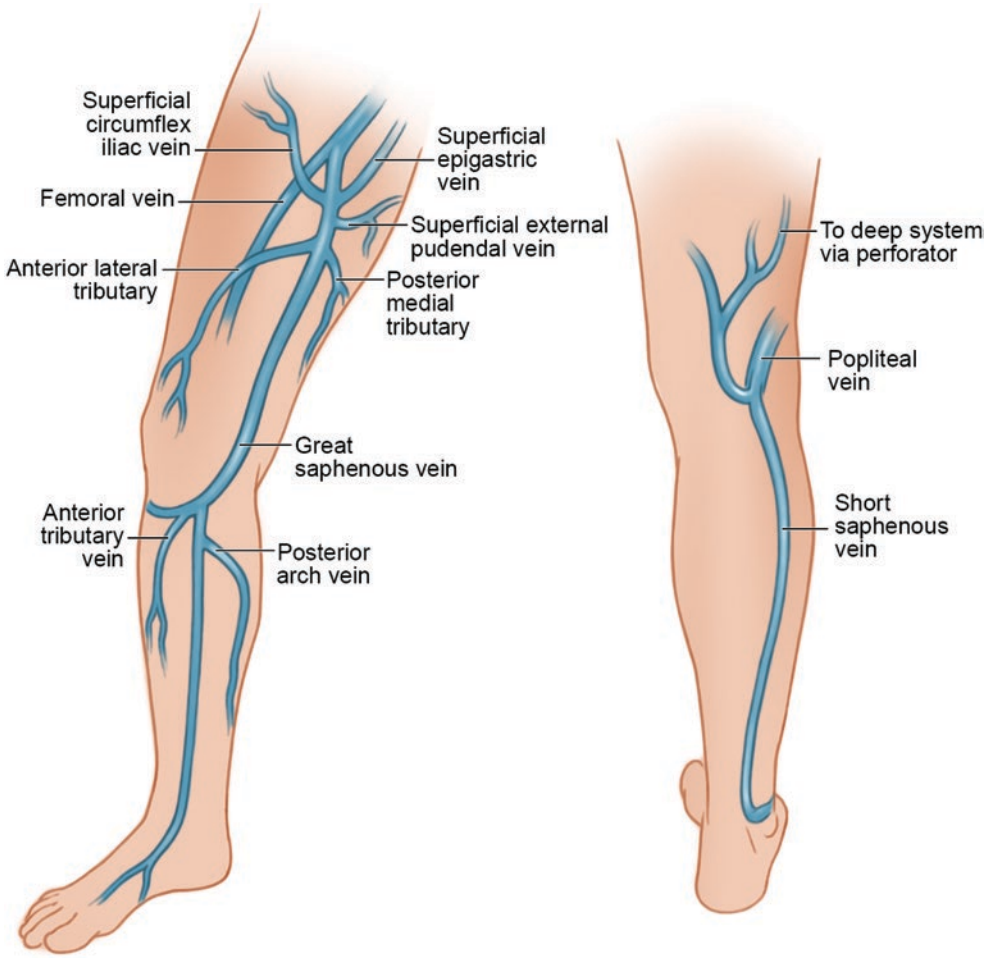

Fig. 19.31 Diagram of lower extremity superficial venous drainage. (© Catherine Delphia 2020)

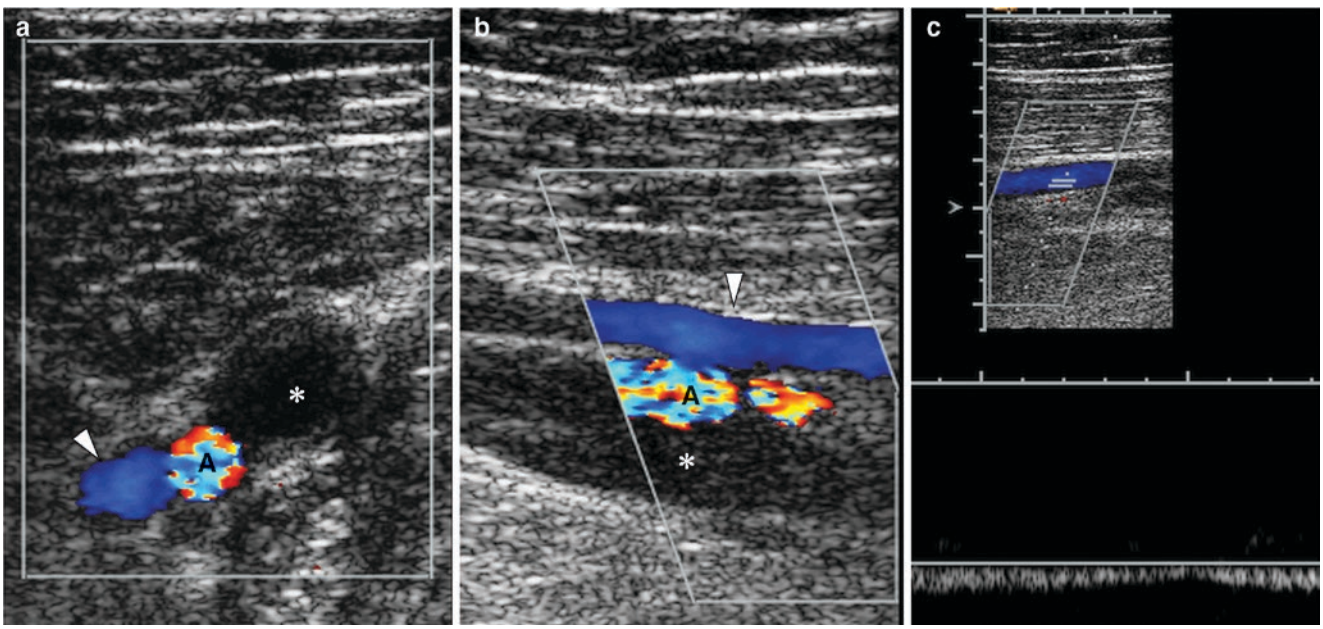

Fig. 19.32 Acute deep vein thrombosis (DVT) in a 14-year-old male carrier for factor V Leiden deficiency with FV duplication. (**a**) Transverse and (**b**) sagittal color Doppler ultrasound images of the right FV reveal duplication with the medial vein (asterisks) distended by thrombus and patency (arrowheads) of the lateral vein. *A*, femoral artery. (**c**) Spectral Doppler analysis shows normal flow in the patent lateral FV

within the vessel lumen, absence of flow on Doppler imaging at the site of thrombosis, loss of the normal cardiac- and respiratory-related pulsations distal to the site of thrombosis, and lack of flow augmentation or response to the Valsalva maneuver [78, 79].

On grayscale imaging, an intraluminal thrombus can sometimes appear anechoic. Flow will be present in veins with nonocclusive thrombi, and compression and augmentation maneuvers may be normal. Despite these potential pitfalls, grayscale imaging combined with compression maneuvers and color Doppler evaluation should permit a diagnosis of thrombosis in most cases (Fig. 19.33).

In the upper extremities, the sensitivity and specificity of color flow Doppler imaging for diagnosing DVT range from 78% to 100% and 82% to 100%, respectively [96]. The accuracy of compression ultrasound for lower extremity DVT has been shown to reach 95% with 98% specificity, while studies of color Doppler imaging report a sensitivity of 95%, specificity of 99%, and accuracy of 98% [79]. Detection rates of lower extremity acute venous

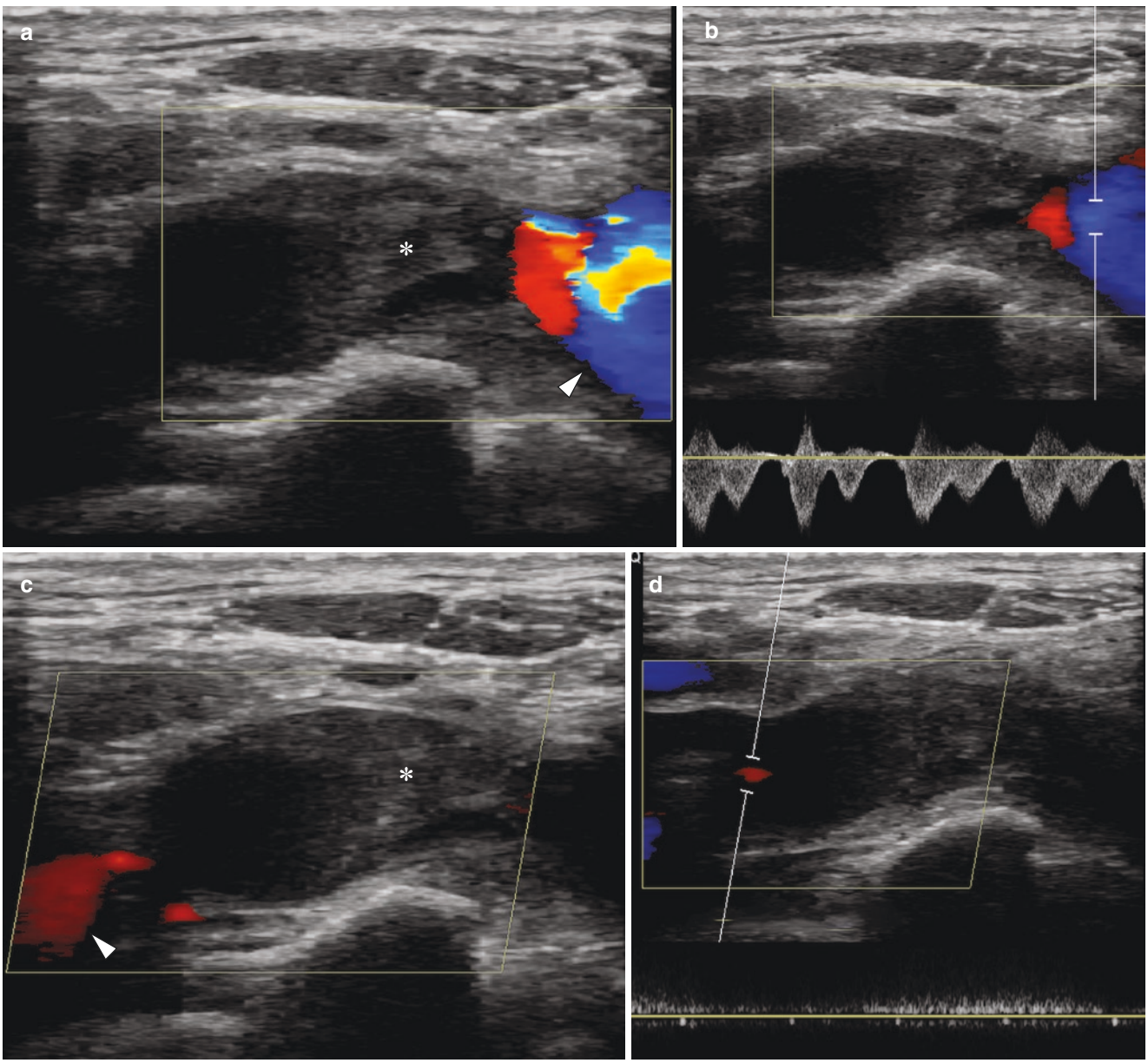

Fig. 19.33 Acute near-occlusive right upper extremity DVT in a 14-year-old male. (**a**) Coronal color Doppler ultrasound image shows an echogenic thrombus (asterisk) in the medial SCV with flow identified in the BCV (arrowhead). (**b**) A normal spectral Doppler ultrasound waveform is depicted within the upper BCV. (**c**) Coronal color Doppler ultrasound image shows a small amount of flow (arrowhead) in the SCV lateral to the thrombus (asterisk). (**d**) Spectral Doppler ultrasound evaluation reveals sluggish, dampened flow in the SCV lateral to the thrombus

thrombosis are greater for thrombosis above the knee than for thrombosis in the calf since the calf veins are significantly smaller and it is difficult to be certain that all of the calf vessels (some of which may be duplicated) are free of thrombus [79].

Treatment goals for venous thromboembolism include resolution of the existing thrombus, prevention of local thrombus extension, embolization, recurrence, and minimization of long-term complications such as post-thrombotic syndrome. The most common treatments for venous thromboembolism in children include unfractionated heparin, low molecular weight heparin, and warfarin. Other options include fondaparinux, a factor Xa inhibitor, and the direct thrombin inhibitors [97].

For infants and children with major vessel occlusion causing compromise of organs or limbs, systemic or catheter-directed thrombolytic therapy may be warranted. Data on the efficacy, dose, and safety of thrombolytic agents in this setting are limited, and indications for thrombolytic therapy are highly individualized [98].

Chronic (Residual) Deep Vein Thrombosis

Distinguishing acute from residual or chronic DVT by both clinical and imaging criteria may be challenging. Both acute and chronic DVT may show non-compressibility of the involved vessel. Chronic venous thrombosis is characterized by thickened or irregular walls, a narrowed or irregular lumen, and collateral vessel formation (Fig. 19.34). The clot is usually

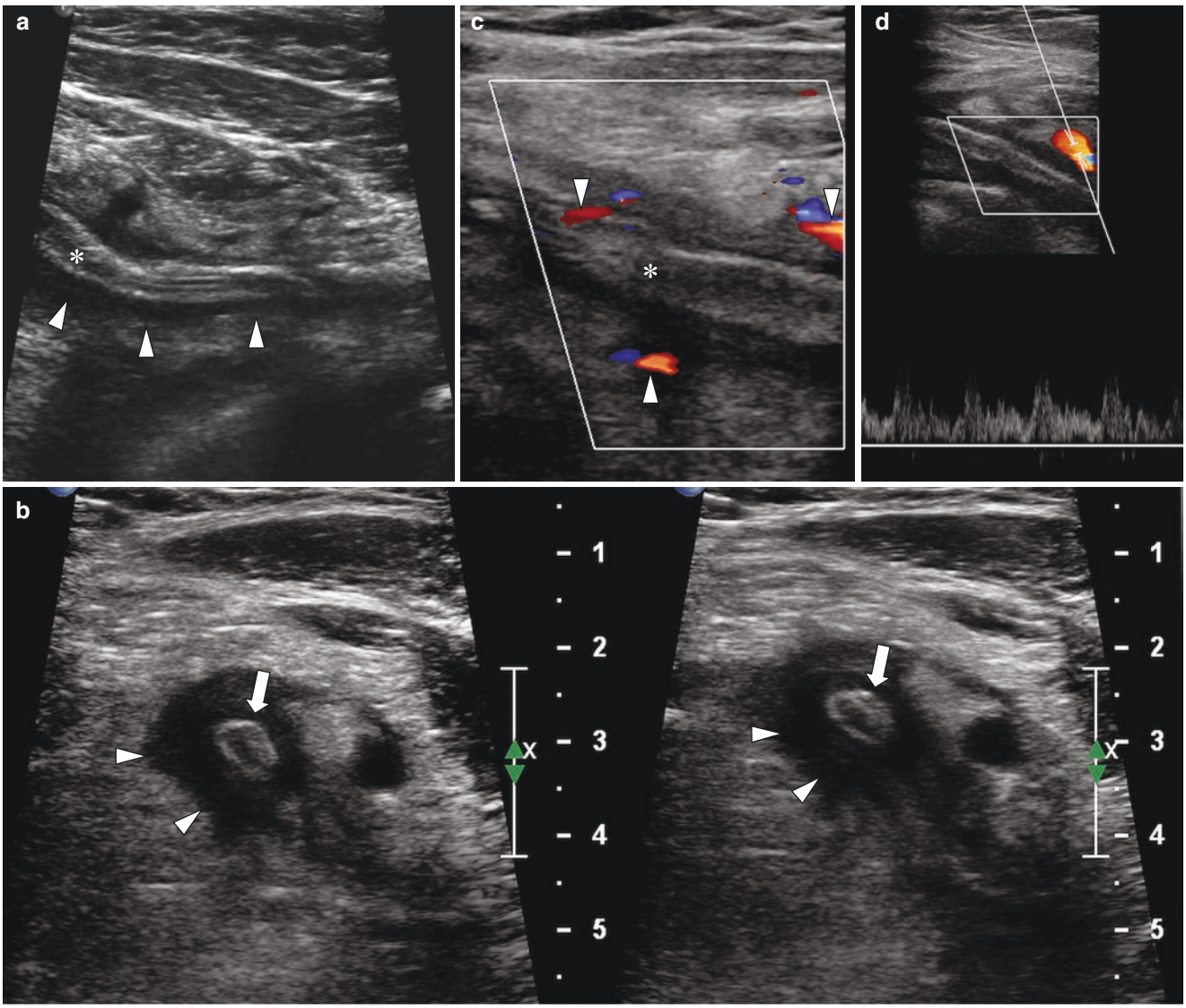

Fig. 19.34 Chronic left upper extremity DVT in a 16-year-old female with a PICC line. (**a**) Sagittal grayscale ultrasound image of the left SCV-axillary venous confluence shows a thickened, echogenic PICC (asterisk) surrounded by hypoechoic thrombus (arrowheads). (**b**) Transverse grayscale ultrasound images of the axillary vein without (left panel) and with (right panel) compression reveal no collapsibility. The centrally located PICC (arrows) is surrounded by hypoechoic thrombus (arrowheads). (**c**) Sagittal color Doppler ultrasound image of the lateral subclavian vein demonstrates multiple collateral vessels (arrowheads). *Asterisk*, Thrombus. (**d**) Spectral Doppler evaluation of a collateral vessel depicts venous-type flow

hypoechoic. Residual thrombus will become broadly adherent to the vessel wall. There may be intraluminal echogenic, web-like filaments within the vein [79]. Differentiation between hypoechoic thrombus and normal-flowing blood often requires further evaluation with color and spectral Doppler imaging.

There are limited data regarding the management of chronic DVT. However, there are reports of aggressive treatment in some patients to encourage symptom resolution [99]. Recanalization of occluded veins and venous stenting have been able to re-establish deep vein flow and decrease venous hypertension.

Retroperitoneal Vessels

Technique

Patient Positioning

Ultrasound imaging of the retroperitoneal vessels is performed with the patient supine as well as in the right and left decubitus positions to optimize visualization of the inferior portions of the abdominal aorta and IVC.

Ultrasound Transducer Selection

The highest-frequency transducer that permits adequate penetration of the abdomen should be used.

Imaging Approaches

Ultrasound imaging is optimally performed after patient fasting so that air in the bowel is minimized. Grayscale images of the upper portions of the abdominal aorta and IVC are best obtained via an anterior midline approach. The inferior portions of these vessels as well as their bifurcation are often better depicted via a coronal approach through the flanks. Images should be obtained in both transverse and longitudinal planes. Color and spectral Doppler images are ideally acquired from an oblique or coronal scan plane. Angle-corrected velocity measurements should be obtained from the center of a longitudinal image of the aorta or IVC.

Aorta

Normal Development and Anatomy

Normal Development

The development of the aorta begins in the third week of life when two strands of cells migrate dorsally from the endocardial mesenchyme and extend caudally along the neural groove to form the dorsal aortas. After about 1 week, the two aortas fuse into a single aortic trunk that descends caudally. The right dorsal aorta will become the right subclavian artery. The left aorta develops into the descending thoracic aorta. Multiple segmental arteries arise from the dorsal aortas that join together to form successive segments. As the embryo develops, most of these segmental arteries will regress, except for the precursors to the three major mesenteric vessels. The 10th segmental artery will become the celiac artery that supplies the foregut, the 13th segmental artery will develop into the superior mesenteric artery (SMA) that supplies the midgut, and the 22nd segmental artery will form the inferior mesenteric artery (IMA) that supplies the hindgut [100].

Normal Anatomy

The mature abdominal aorta extends inferiorly from the diaphragmatic hiatus, anterior and slightly to the left of the lumbar vertebral bodies (Figs. 19.35 and 19.36). It divides into the right and left common iliac arteries at the level of the fourth lumbar vertebra. On grayscale imaging, the aorta has echogenic walls and an anechoic lumen and is pulsatile on real-time imaging. Spectral Doppler analysis shows a high-resistance, triphasic waveform with a rapid systolic upstroke, a prompt decline in velocity, and brief flow reversal in early diastole followed by low-velocity antegrade flow in late systole (Fig. 19.37) [8, 101]. The arterial branches of the aorta supplying the solid abdominal viscera have a biphasic, low-resistance arterial waveform with a rapid systolic upstroke followed by continuous antegrade flow through systole and diastole.

Thrombosis

Aortic thrombosis occurs most often in the neonatal period as a complication of umbilical artery catheterization [102]. Other predisposing causes include cardiac and pulmonary abnormalities, sepsis, peripartum asphyxia, fetal meconium aspiration, extreme prematurity, hypertension, and the presence of a prothrombotic condition such as factor V Leiden mutation. Aortic thrombosis is frequently asymptomatic and detected incidentally by US. Patients may present with signs of lower extremity ischemia, hematuria, or hypertension if thrombosis involves the renal arteries. Long-term complications include impaired lower extremity growth and renovascular hypertension.

Ultrasound imaging of infants with suspected aortic thrombosis should assess the entire abdominal aorta and both kidneys with grayscale, color, and spectral Doppler. Ultrasound can reliably localize the position of an intra-abdominal umbilical arterial catheter. When an umbilical catheter is present, it is depicted as an echogenic linear structure in the lumen of the aorta (Fig. 19.38). The optimal position of the catheter tip is either in the abdominal aorta below the origin of the renal arteries or in the thoracic aorta below the vessels of the aortic arch.

An acute thrombus will manifest as an echogenic mass within the aortic lumen. Color Doppler is useful in determining whether the thrombus is partially or completely occlusive

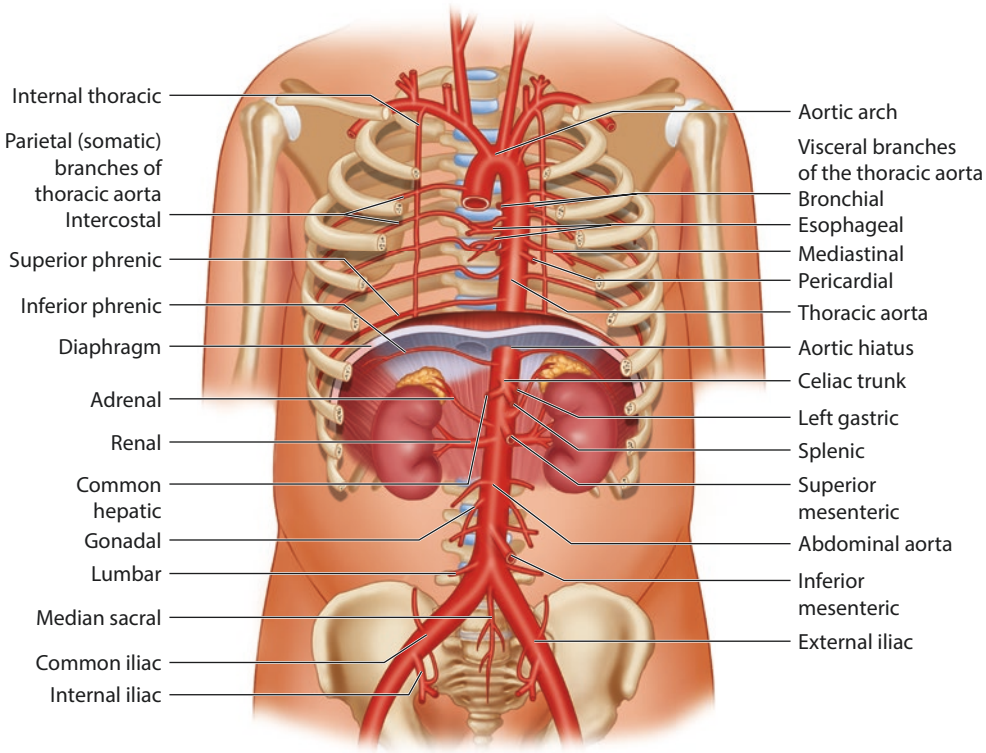

Fig. 19.35 Diagram of the aorta and its major intrathoracic and abdominal branches

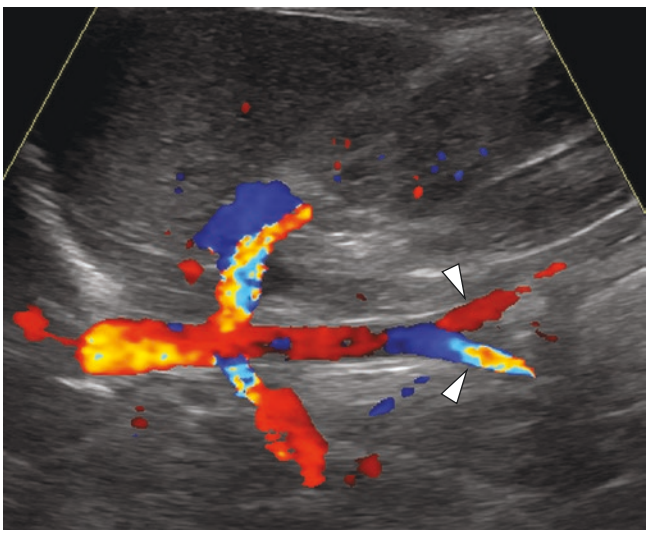

Fig. 19.36 Normal abdominal aorta in a 9-day-old male. Sagittal color Doppler ultrasound image of the abdominal aorta from the level of the diaphragm to the bifurcation into the common iliac arteries (arrowheads)

and aids in the detection of collateral vessels. In contrast to the sharp systolic upstroke and triphasic high-resistance flow of the normal aorta, spectral Doppler evaluation of the vessels distal to the thrombus as well as collateral vessels often reveals low-velocity waveforms with increased diastolic flow due to downstream arterial dilation (Fig. 19.38). Over time, a resolving thrombus will decrease in size and ultimately appear as a thin, linear intraluminal structure.

Treatment for neonatal aortic thrombosis consists of removal of the umbilical artery catheter (if present) and therapeutic anticoagulation. In patients with clinical evidence of ischemia but without imminent tissue loss or visceral injury, therapeutic anticoagulation with or without systemic thrombolysis is recommended, based on anatomic imaging findings and clinical concern for clot propagation. Constant reassessment is mandatory in order to avoid delays in intervention for those with clinical progression. Patients with clinical evidence of ischemia with imminent tissue loss or end-organ dysfunction require immediate therapeutic anticoagulation and surgical thrombectomy [103]. Doppler sonography can be used to document resolution of the thrombus.

Stenosis

Aortic stenosis in children usually occurs in the setting of mid-aortic syndrome, a term used for obstructive lesions of the mid-aorta, regardless of etiology [104]. Approximately 64% of cases are idiopathic. The remainder have been described in association with a variety of genetic and acquired diseases, including Takayasu arteritis, neurofibromatosis, and Williams syndrome [105]. Mid-aortic syndrome usually involves the renal (> 80%) and splanchnic (50–70%) branches of the aorta. In most patients there is diffuse or segmental narrowing of the abdominal and/or distal descending

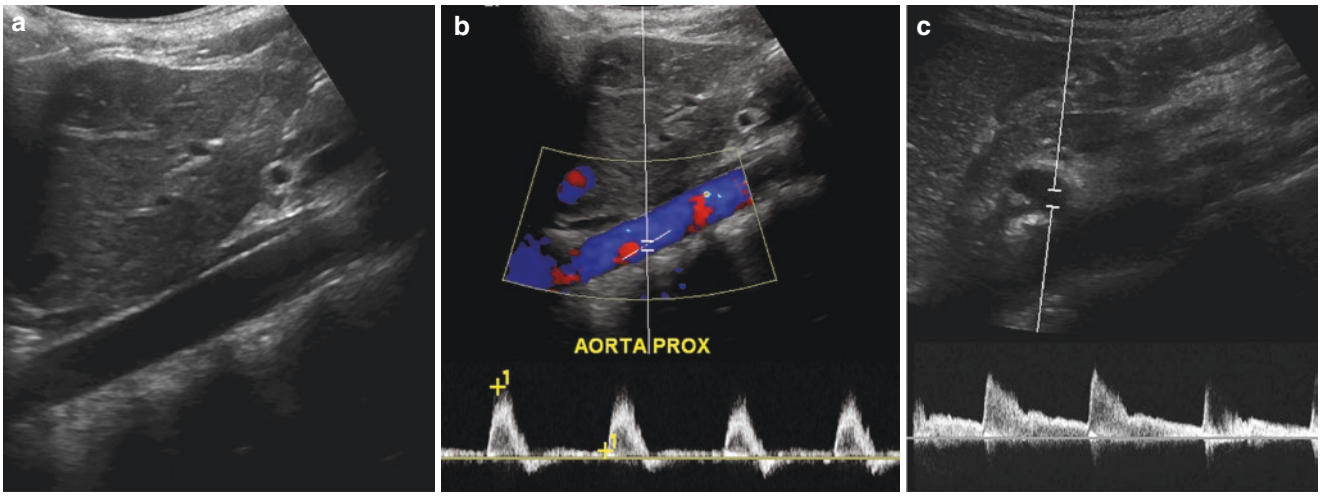

Fig. 19.37 Normal abdominal aorta in a 15-year-old female. (**a**) Sagittal grayscale ultrasound image depicts the echogenic walls of the aorta and the anechoic lumen. (**b**) Sagittal color Doppler ultrasound image with spectral analysis reveals a characteristic high-resistance triphasic waveform. (**c**) Spectral Doppler analysis of the celiac artery shows a normal biphasic, low-resistance waveform

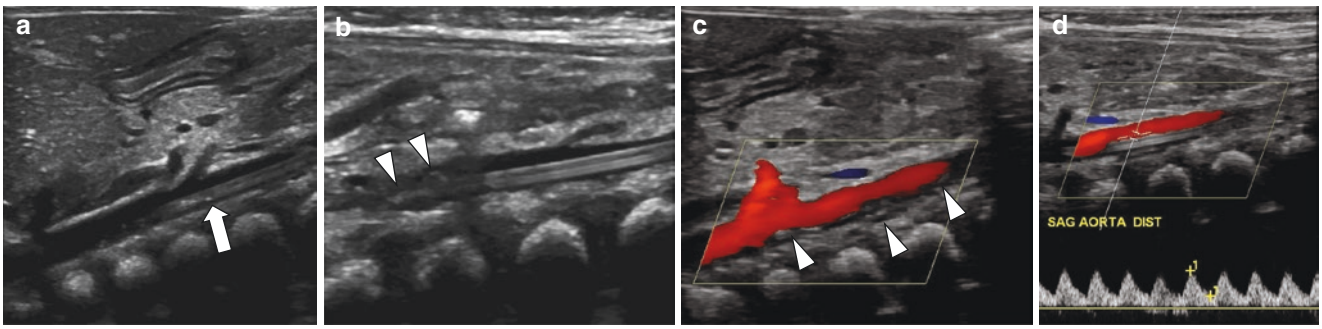

Fig. 19.38 Aortic thrombosis in an 8-day-old female with a right femoral arterial catheter. (**a**) Sagittal grayscale ultrasound image of the abdominal aorta reveals an intraluminal catheter (arrow). (**b**) Sagittal grayscale ultrasound image shows echogenic clot (arrowheads) on the distal catheter tip. (**c**) Sagittal color Doppler ultrasound image shows nonocclusive thrombus (arrowheads) along the posterior aortic wall. (**d**) Spectral Doppler ultrasound evaluation of the aorta distal to the thrombus shows low-velocity, low-resistance waveforms

thoracic aorta, with varying involvement of the renal and visceral branches. Mid-aortic syndrome is an important cause of renovascular hypertension in children and adolescents. Most patients present with symptoms of severe hypertension, absent femoral pulses, an abdominal bruit, and lower leg claudication. Children with long-standing refractory hypertension may develop encephalopathy and retinopathy.

Grayscale, color, and spectral Doppler ultrasound reveal narrowing of the abdominal aorta as well as variable narrowing of the major aortic branch vessels, especially the renal arteries (Fig. 19.39) [106]. Collateral vessels can also be identified. In the setting of Takayasu arteritis, arterial wall thickening can be present. Doppler spectral analysis shows elevated velocities at sites of stenosis with distal diminished flow velocities.

Management of mid-aortic syndrome is aimed at controlling arterial blood pressure, preventing long-term complications related to hypertension, and preserving end-organ function (including the heart and kidneys). Treatment can be pharmacological, endovascular, or surgical [104].

Aneurysm

Aortic aneurysms in infants are most often a complication umbilical arterial catheterization. The majority are mycotic in etiology and associated with bacteremia, especially *Staphylococcus aureus* and *S. albus* infection [107]. However, they can also be congenital and detected on prenatal ultrasound studies [108]. In older children, aortoiliac aneurysms are usually a manifestation of a connective tissue disorder such as Ehlers-Danlos syndrome or Marfan syndrome; inflammatory disorders such as Kawasaki disease and Takayasu arteritis; infection; or trauma [109]. In Marfan syndrome, there often is associated dilation of the aortic root. In Kawasaki disease, there may be multiple sites of aneu-

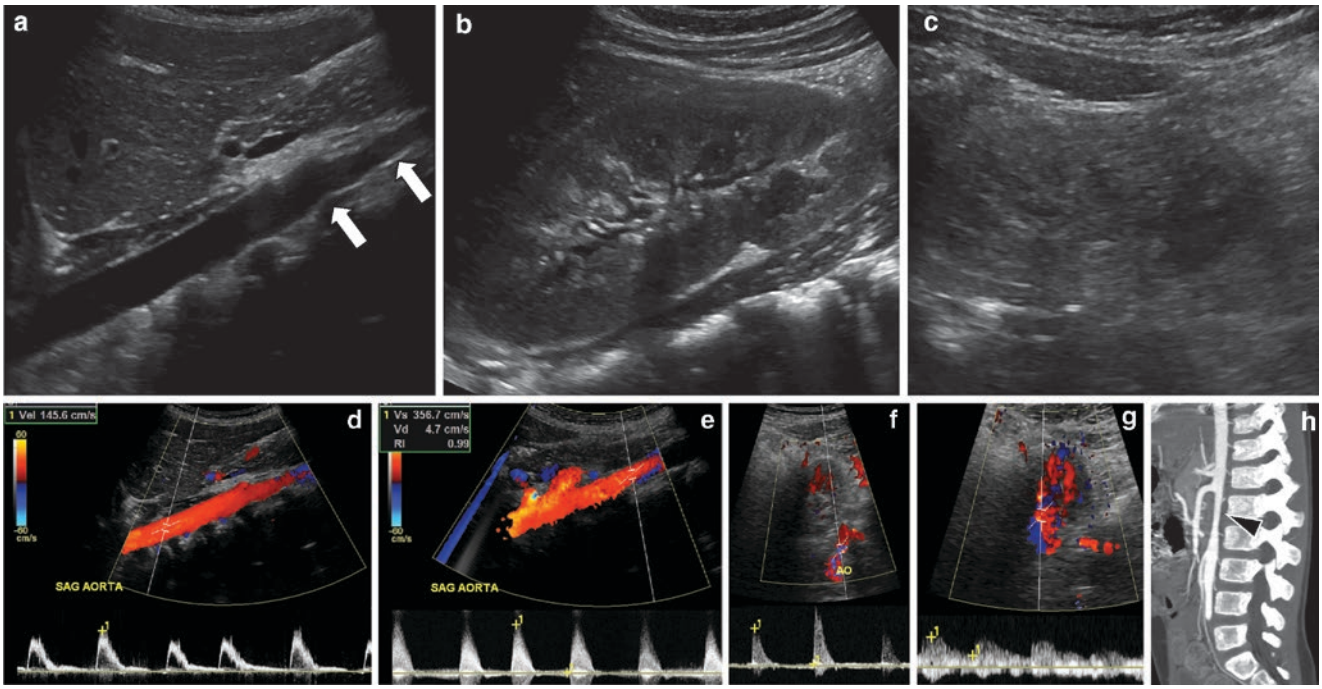

Fig. 19.39 Aortic stenosis in a 5-year-old male with mid-aortic syndrome. (**a**) Sagittal grayscale ultrasound image of the abdominal aorta reveals marked narrowing (arrows) in its midportion. (**b**) Sagittal grayscale ultrasound image of the normal right kidney. (**c**) Sagittal grayscale ultrasound image of the small left kidney demonstrates loss of normal corticomedullary differentiation. (**d**) Sagittal color Doppler ultrasound image with spectral analysis shows a proximal aortic velocity of 145.6 cm/sec. (**e**) Sagittal color Doppler ultrasound image with spectral analysis of the narrowed portion of the aorta shows an abnormally elevated velocity of 356.7 cm/sec. (**f**) Transverse color Doppler ultrasound image with spectral analysis of the left renal artery at its origin reveals an abnormal, high-resistance waveform due to stenosis. (**g**) Transverse color Doppler ultrasound image of the left main renal artery in the renal hilum shows an abnormal parvus-tardus waveform downstream from the stenotic arterial origin. (**h**) Sagittal contrast-enhanced maximum intensity projection (MIP) CT image shows the mid-abdominal aortic narrowing (arrowhead)

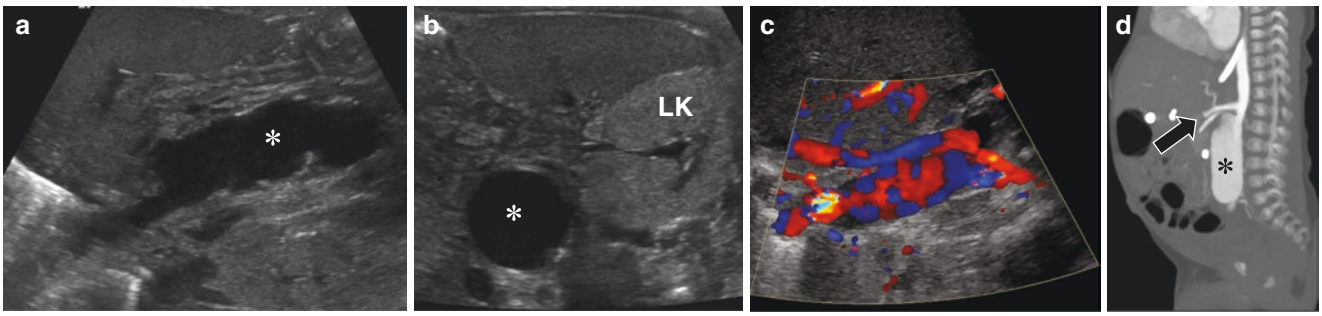

Fig. 19.40 Mycotic abdominal aortic aneurysm in a 4-month-old former 29-week gestational age infant with clinical course complicated by methicillin-sensitive *Staphylococcus aureus* bacteremia. (**a**) Sagittal grayscale ultrasound image reveals a markedly dilated aorta (asterisk) with an irregular contour. (**b**) Transverse grayscale ultrasound image demonstrates the widest portion of the aneurysm (asterisk) at the level of the left kidney (LK). (**c**) Sagittal color Doppler ultrasound image shows a swirling flow pattern within the aneurysm. (**d**) Sagittal MIP image from a contrast-enhanced CT shows superior displacement (arrow) of abdominal aortic branches by the aneurysm (asterisk)

rysm formation, including the coronary arteries; abdominal aorta; and iliac, femoral, and splanchnic arteries.

When an aneurysm is suspected, ultrasound images and measurements of the abdominal aorta are obtained in transverse and longitudinal planes (Fig. 19.40). Grayscale ultrasound will show focal or diffuse aortic dilation. Mural thrombus may also be present. The Doppler ultrasound findings will depend on the size of the aneurysmal neck, the amount of intraluminal thrombus, and the presence of calcification. The maximal aortic diameter is obtained perpendicular to the axis of the lumen of the aorta and measured from outer wall to outer wall. Longitudinal images are preferred for acquiring the most accurate measurements. Transverse imaging is important for identification of eccentrically located

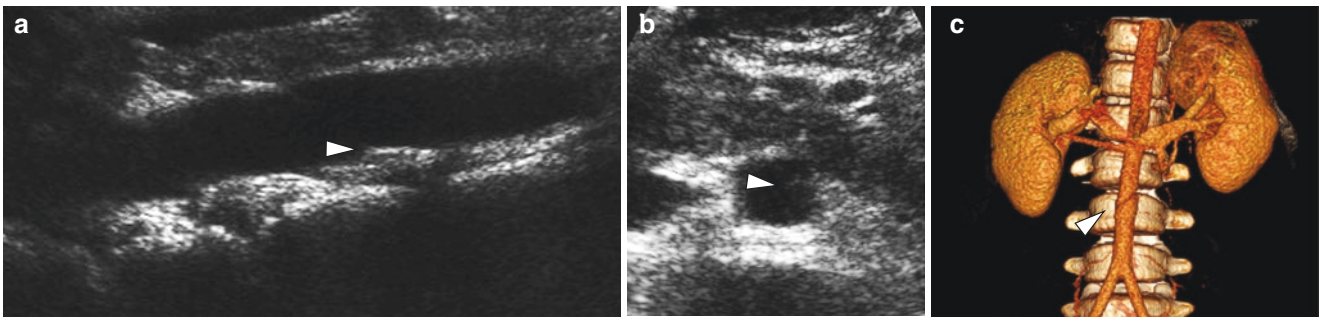

Fig. 19.41 Dissection of the abdominal aorta in a 9-year-old male after motor vehicle collision. Sagittal (**a**) and transverse (**b**) grayscale ultrasound images show a subtle irregularity (arrowheads) of the inner aortic wall consistent with an intimal flap. (**c**) Coronal 3D reconstructed image from a contrast-enhanced CT study confirms a dissection (arrowhead) of the infrarenal abdominal aorta

aneurysms. Normal age-related ultrasound measurements for the abdominal aorta in children can be consulted for reference purposes [110].

Treatment of aortic aneurysms in children varies according to the underlying cause [109]. Mycotic aneurysms are treated with antibiotics and surgical excision. With systemic inflammatory disorders, initial therapy is conservative and aimed at aneurysm prevention. Patients with Kawasaki disease receive anti-inflammatory medication in the acute phase, usually acetylsalicylic acid. If aneurysms subsequently develop, antithrombotic treatment is instituted to decrease the complication rate. Spontaneous aneurysmal rupture may occur that then requires surgical ligation or resection. Management of patients with Ehlers-Danlos syndrome is aimed at prevention of injury. Those with Marfan syndrome receive beta-blockers.

Dissection

Abdominal aortic dissection is very unusual in children. It occurs most frequently in the setting of Marfan syndrome, where it is nearly always associated with thoracic aortic dissection. Ultrasound does not generally play a role in the diagnosis which is usually made by CT. Occasionally an intimal flap may be identified by ultrasound (Fig. 19.41, Cineclip 19.4), usually during a study performed for follow-up evaluation of an aneurysm.

Inferior Vena Cava

Normal Development and Anatomy

The IVC is the main channel through which venous blood from the lower extremities and abdominal viscera returns to the right atrium.

Normal Development

The IVC and the azygos-hemiazygos venous systems arise during the 4th to 8th weeks of gestation through a complex pattern of development, anastomosis, and regression that involves the vitelline vein and the paired posterior cardinal, supracardinal, and subcardinal veins.

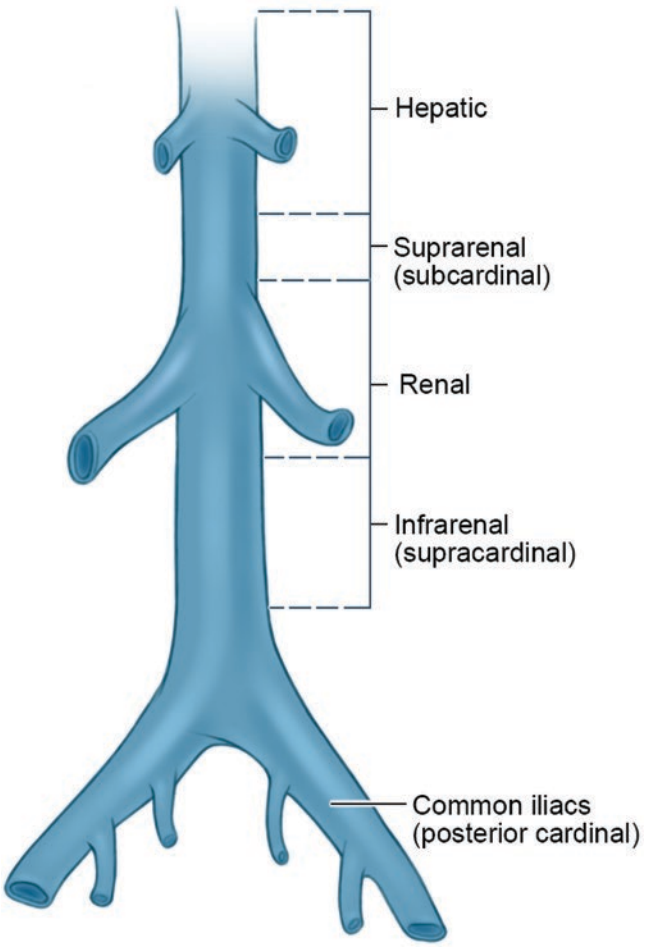

Fig. 19.42 Diagram of embryologic segments leading to formation of the inferior vena cava. (© Catherine Delphia 2020)

Normal Anatomy

The mature IVC has four segments: hepatic, suprarenal, renal, and infrarenal (Fig. 19.42) [111]. The vitelline vein contributes to the hepatic segment of the IVC. The suprarenal IVC is formed by a persistent portion of the right subcardinal vein. The renal segment of the IVC consists of the anastomosis between the right subcardinal and right

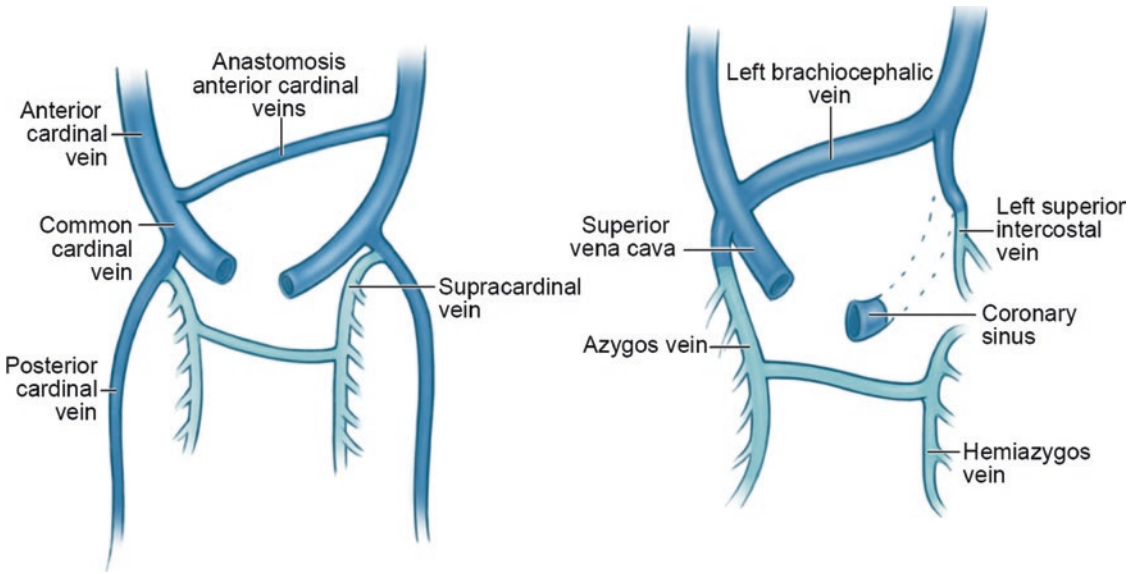

Fig. 19.43 Diagram of embryological vessels leading to the development of the azygos and hemiazygos venous systems. The supracardinal veins (left panel) ultimately develop into the azygos and hemiazygos veins (right panel). (© Catherine Delphia 2020)

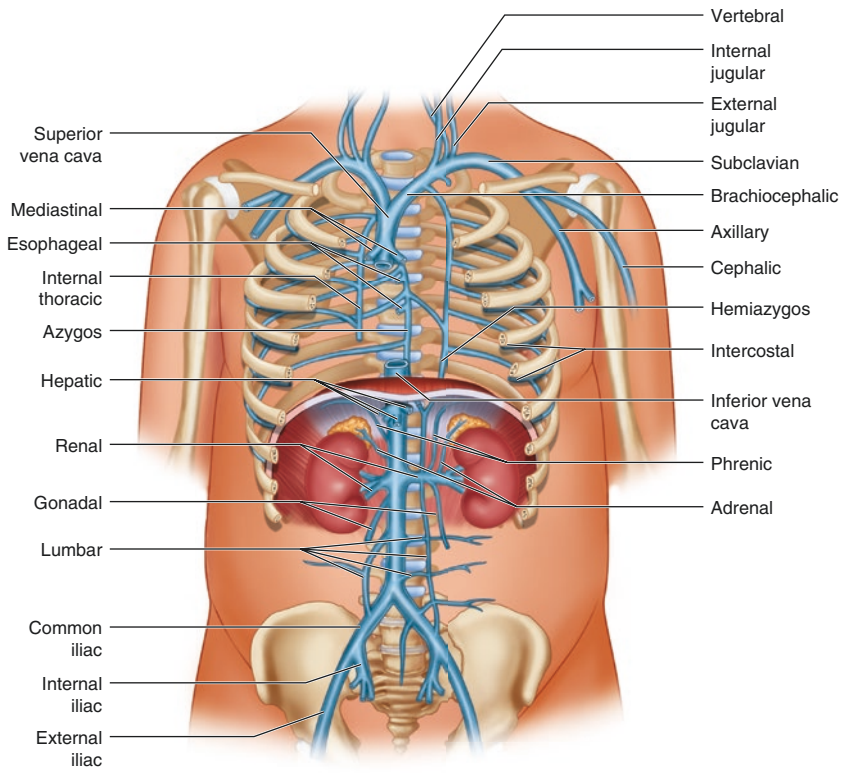

Fig. 19.44 Diagram of the major veins of the neck, chest, and abdomen

supracardinal veins. The infrarenal segment is derived from a persistent segment of the right supracardinal vein. The right posterior cardinal vein forms the distal-most IVC and its bifurcation into common iliac veins.

The embryonic veins also lead to the development of the azygos, hemiazygos, and common iliac veins. The azygos venous system arises from the supracardinal veins. The right supracardinal vein develops into the azygos vein, while the left supracardinal vein becomes the hemiazygos vein (Fig. 19.43).

The IVC arises at the confluence of the common iliac veins at the level of the fifth lumbar vertebra (Fig. 19.44). It runs to the right of the aorta and anterior to the vertebral bod-

ies. It extends through the diaphragm at the level of the eighth lumbar vertebra and after a short intrathoracic course drains into the right atrium.

On ultrasound evaluation, the IVC has an anechoic lumen. Its wall is thinner and less echogenic wall than the aorta, and its size and contour vary with changes in respiration and intra-abdominal pressure. With deep inspiration, there is a decrease in the diameter of the IVC, whereas the caliber of the IVC increases in expiration. The spectral Doppler waveform of the IVC varies according to location within the vessel. In the proximal IVC, a triphasic waveform is seen that reflects right atrial pulsatility and is similar to that within the hepatic veins. More distally, the waveform is less pulsatile and can be monophasic (Fig. 19.45) [3, 101].

In the setting of severe dehydration or hypovolemic shock, the IVC will appear collapsed with a relatively monophasic flow pattern. When right-sided heart pressures are elevated, the IVC will have an increased diameter, as in the setting of tricuspid insufficiency, right heart failure, or pericardial tamponade, and the spectral Doppler waveforms will appear exaggerated.

Congenital Anomalies

Congenital anomalies of the IVC are the result of abnormal development of the embryological vitelline, posterior cardinal, subcardinal, and supracardinal veins. They occur in about 4% of the population and are most often asymptomatic [111, 112].

Interruption of the IVC with Azygos Continuation

Interruption of the IVC below the liver with azygos or hemiazygos continuation is due to a failure of anastomosis of the embryonic hepatic and prerenal portions of the IVC. As a consequence, the suprarenal IVC drains either into the azygos vein and returns to the heart through the SVC or into the hemiazygos vein. The hepatic veins drain directly into the right atrium. This anomaly can occur as an isolated finding. However, it is frequently seen in patients with heterotaxy and complex congenital heart disease (i.e., the cardiosplenic syndromes) [113]. Although interruption of the IVC is much more common in the setting of polysplenia, it can also occur with asplenia [112].

Ultrasound features of interrupted IVC include absence of the intrahepatic portion of the IVC, drainage of the confluence of hepatic veins directly into the right atrium, and an enlarged right-sided azygos or left-sided hemiazygos vein. Unlike a normal IVC, an enlarged azygos vein will be located posterolateral to the aorta and dorsal to the right renal artery (Fig. 19.46).

There is no specific treatment for this anomaly. However, it is important to not mistake an enlarged azygos or hemiazygos vein identified on ultrasound examination for retrocrural adenopathy [111].

Retrocaval Ureter

Retrocaval ureter is a rare entity with a 3:1 male predominance. In the majority of cases, this anomaly is asymptom-

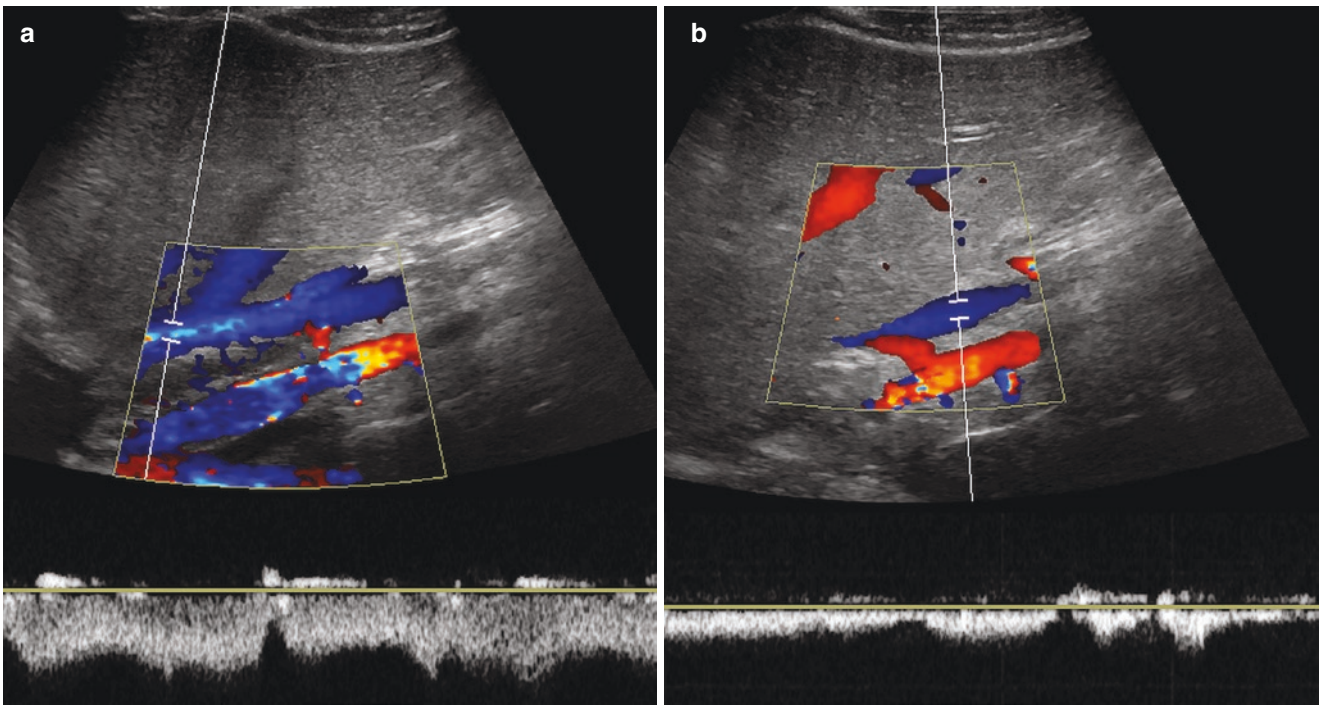

Fig. 19.45 Normal vena caval flow patterns. (**a**) Sagittal color Doppler ultrasound image with spectral analysis of the upper inferior vena cava (IVC) reveals a normal triphasic waveform. (**b**) Sagittal color Doppler ultrasound image of the mid-IVC demonstrates a less pulsatile waveform

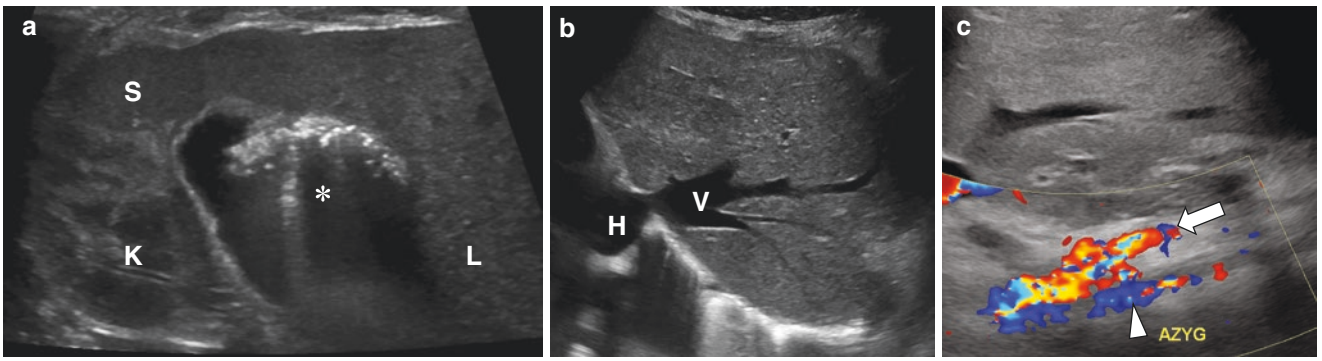

Fig. 19.46 Azygos continuation of the IVC in a 2-year-old female with heterotaxy. (**a**) Transverse grayscale ultrasound image of the upper abdomen reveals a left-sided liver (L), a right-sided spleen (S) and stomach (asterisk). *K*, Right kidney. (**b**) Sagittal grayscale ultrasound image shows the hepatic veins (V) draining directly into the heart (H). (**c**) Sagittal color Doppler ultrasound image shows a prominent azygos vein (arrowhead) posterior to the aorta (arrow). There is no intrahepatic IVC

atic. Symptomatic patients usually present with pain in the second to fourth decades of life. The infrarenal IVC usually develops from the embryological supracardinal vein. If instead it develops from the subcardinal vein, the ureter will pass posterior rather than anterior to the IVC. The aberrant course of the ureter is believed to result in obstruction. The ureter will then extend medially and anteriorly between the aorta and IVC to cross the right iliac vessels and enter the pelvis and bladder in the usual manner [114].

Two types of retrocaval ureter have been described. In the more common Type 1, the dilated ureter assumes a reversed-J or "fish hook" appearance. Ureteral obstruction develops at the edge of the iliopsoas at the site where the ureter turns cephalad before passing behind the IVC. In Type II, hydronephrosis is less severe, and the ureter passes horizontally behind the vena cava without an upward kink. Ureteral obstruction occurs at the lateral wall of the vena cava where the ureter is compressed behind the paravertebral muscles.
Retrocaval ureter is best depicted by cross-sectional imaging such as magnetic resonance urography (MRU) or CT. MRU or diuretic renography can assess the degree of functional obstruction. Ultrasound imaging will show dilation of the right collecting system and proximal ureter. Occasionally, the compressed retrocaval ureter may be identified. Ultrasound is useful for follow-up of children with known retrocaval ureter to assess for evidence of complications.

Treatment is needed only if there is significant obstruction, infection, urolithiasis, or increasing hydronephrosis. Surgery includes division of the retrocaval segment of ureter with excision of any stenotic segment and ureteropelvic or uretero-ureteric anastomosis anterior to the IVC.

Duplicated IVC

IVC duplication occurs when there is persistence of both the right and left supracardinal veins that form duplicated infrarenal IVC segments. The left infrarenal IVC will join the left renal vein and drains into a normal suprarenal IVC. Identification of a duplicated IVC has implications for patient treatment in the setting of deep vein thrombosis and recurrent emboli if placement of an infrarenal IVC filter is contemplated. If this anomaly is not recognized, recurrent pulmonary embolism can subsequently develop with potentially fatal consequences [111].

On ultrasound imaging, a left-sided IVC will drain the left renal vein and then cross the midline to join the right-sided IVC. A potential imaging pitfall is to mistake a left-sided IVC for an enlarged lymph node if the vessel is not followed along its course.

Left-Sided IVC

A left-sided IVC occurs when the right supracardinal vein regresses and there is abnormal persistence of the left supracardinal vein. As with a duplicated IVC, a left-sided IVC runs along the left side of the abdominal aorta, joins with the left renal vein, and empties into a normal right-sided suprarenal IVC (Fig. 19.47, Cineclip 19.5). Although a left-sided IVC is asymptomatic, if unrecognized it can lead to problems with central venous access during interventional procedures. A left-sided IVC may be confused with the abdominal aorta, limit access options for IVC filter placement, or complicate pulmonary thrombolysis procedures [111].

Thrombosis

IVC thrombosis occurs in the setting of both non-neoplastic and neoplastic disorders. Non-neoplastic or "bland" thrombus is the main cause of IVC obstruction, with its attendant risk of pulmonary embolism. Risk factors for IVC thrombosis include venous stasis, focal compression, hypercoagulability, malignancy, and IVC filters. Bland thrombus in the IVC may occur in isolation, but usually develops as an extension of

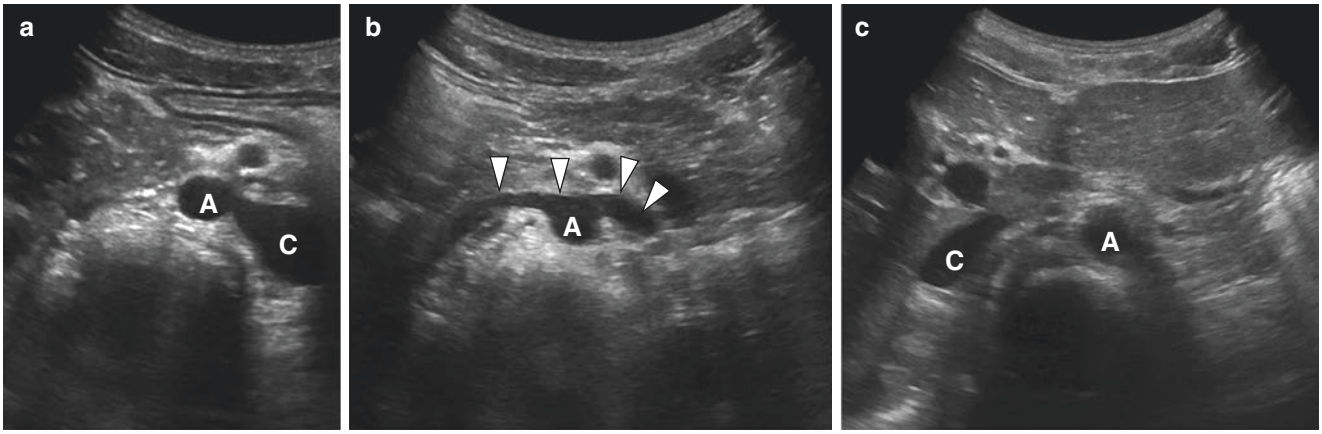

Fig. 19.47 Left-sided IVC in an 8-year-old female. (**a**) Transverse grayscale ultrasound image shows the infrarenal IVC (C) located on the left side of the abdomen. *A*, Aorta. (**b**) Transverse grayscale ultrasound image at the level of the renal veins shows the crossing of the IVC (arrowheads) from left to right, anterior to the aorta (A). (**c**) Transverse grayscale ultrasound image above the renal veins depicts the IVC (C) to the right of the midline. *A*, Aorta

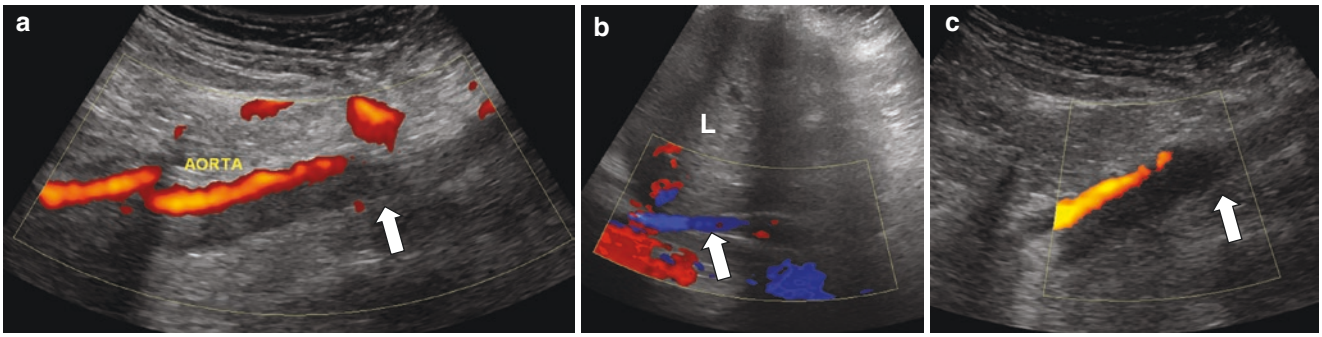

Fig. 19.48 Left lower extremity DVT extending from the popliteal vein to the low IVC in a 12-year-old female. (**a**) Sagittal power Doppler ultrasound image depicts extensive thrombosis (arrow) of the lower IVC. (**b**) Sagittal color Doppler ultrasound image reveals that the upper IVC (arrow) is patent. *L*, Liver. (**c**) Sagittal power Doppler ultrasound image shows complete thrombosis (arrow) of the left external iliac vein

thrombosed pelvic or lower extremity deep vein thrombosis (Fig. 19.48). Unlike tumor thrombus, bland thrombus does not expand the caval lumen and demonstrates no enhancement after IV contrast administration [115].

Neoplastic invasion of the IVC in children most often occurs in the setting of Wilms' tumor and is identified in approximately 4–8% of cases [116, 117]. Recognition of IVC tumor involvement is important as it may advance tumor staging, for example, from stage I to stage II, and necessitate an alteration in treatment approach. IVC extension of tumor is also associated with increased morbidity during nephrectomy. Other primary malignancies commonly associated with IVC invasion include renal cell carcinoma and hepatocellular carcinoma. Metastatic disease in the liver, kidneys, and adrenal glands can also involve the IVC via intravascular spread [111].

Both bland and malignant thrombi are echogenic and can partially or completely fill the caval lumen (Fig. 19.49). Bland thrombi are typically avascular on color and spectral Doppler imaging, while tumor thrombi may show internal vascularity as a result of neovascularization. When luminal occlusion is complete, flow will be absent in the IVC distal to the thrombus. With partial obstruction, there will be dampening of the spectral Doppler waveforms. Flow in collateral vessels can also be identified. IVC thrombi may completely resolve, leave a linear flap, or calcify. A calcified thrombus will be depicted as an echogenic, elongated intraluminal mass that may demonstrate posterior acoustic shadowing.

Anticoagulation is the mainstay of therapy for bland IVC thrombosis. Vena caval filters can be placed if anticoagulation therapy is contraindicated [115, 118]. The presence of

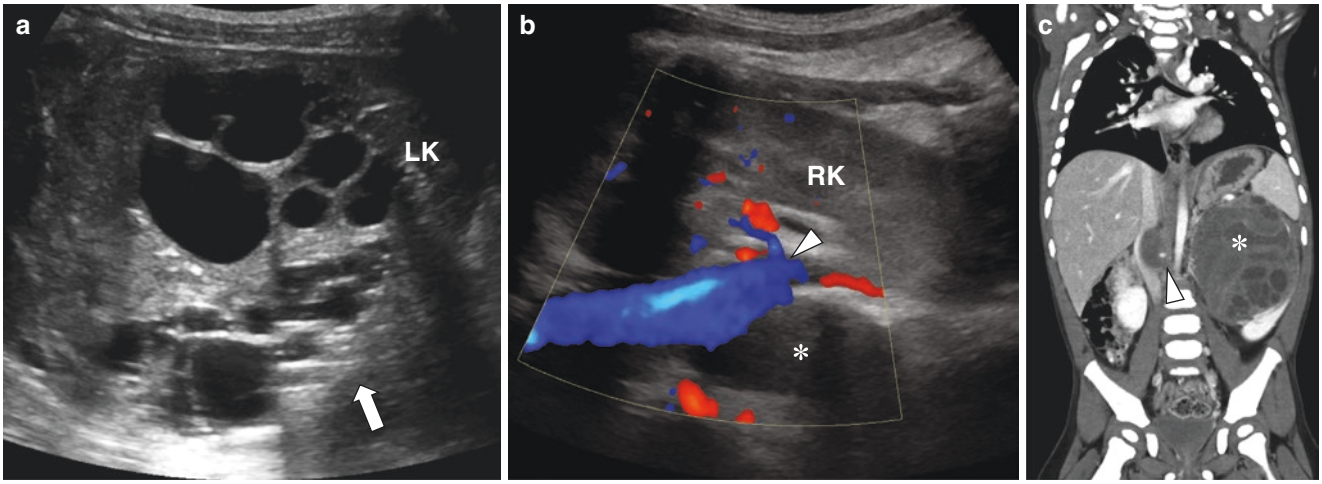

Fig. 19.49 IVC invasion in a 20-month-old male with Wilms' tumor. (**a**) Longitudinal grayscale ultrasound image reveals a large mass (arrow) replacing most of the left kidney (LK). (**b**) Coronal color Doppler ultrasound image of the right kidney (RK) shows a patent right renal vein (arrowhead) with expansile, echogenic tumor (asterisk) in the IVC. (**c**) Coronal contrast-enhanced CT image shows the large left renal mass (asterisk) and left renal vein tumor extending into (arrowhead) and distorting the IVC

tumor thrombosis significantly worsens prognosis and will have a significant impact on the approach to treatment which will vary according to tumor type [119].

May-Thurner Syndrome

Patients with May-Thurner syndrome, or iliac vein compression syndrome, are predisposed to iliofemoral thrombosis as a result of an anatomic variant where the right common iliac artery overlies and compresses the left common iliac vein against the lumbar spine [120]. The chronic compression leads to impaired venous return, and endothelial injury can lead to thrombosis with the potential for extensive DVT of the ipsilateral extremity. Patients who develop a left-sided DVT in the context of May-Thurner syndrome are typically young adults who will develop sudden swelling of the left lower extremity after surgery, during immobilization, or during pregnancy and the post-partum period. Adolescents can also be affected.

Although ultrasound is used to confirm the presence of acute DVT, it is not generally able to image the underlying venous stenosis and compression of the iliac vessels due to their deep location within the pelvis. Contrast venography is the reference standard imaging diagnostic procedure but is rarely performed. More often, the diagnosis is made by CT or MR imaging [120].

Patients generally respond poorly to anticoagulation therapy alone. Catheter-delivered thrombolytics and percutaneous mechanical thrombectomy, either with or without angioplasty and stent placement, are the standard of care for symptomatic patients with May-Thurner syndrome. Postoperative treatment includes anticoagulation for at least 3 months to prevent re-thrombosis. A retrievable IVC filter can also be considered for patients with a history of pulmonary embolism [121, 122].

References

1. Khalid N, Bordoni B. Embryology, great vessel. [Updated 2020 Jul 10]. In: StatPearls [Internet]. Treasure Island (FL): StatPearls Publishing; 2020 Jan-. Available from: https://www.ncbi.nlm.nih.gov/books/NBK545254/.
2. Weberruß H, Pirzer R, Böhm B, Elmenhorst J, Pozza RD, Netz H, et al. Increased intima-media thickness is not associated with stiffer arteries in children. Atherosclerosis. 2015;242(1):4855.
3. Chavhan GB, Parra DA, Mann A, Navarro OM. Normal Doppler spectral waveforms of major pediatric vessels: specific patterns. Radiographics. 2008;28(3):691–706.
4. Yazici B, Erdoğmuş B, Tugay A. Cerebral blood flow measurements of the extracranial carotid and vertebral arteries with Doppler ultrasonography in healthy adults. Diagn Interv Radiol. 2005;11(4):195–8.
5. Kehrer M, Goelz R, Schoning M. The development of haemodynamics in the extracranial cerebral arteries of healthy preterm and term neonates. Ultrasound Med Bio. 2004;30(3):283–7.
6. Patel N, McVeigh K, Sharma P, Parmer S. An impalement injury to the oropharynx in a paediatric patient – a case report. Br J Oral Maxillofac Surg. 2011;49(5):e12–3.
7. Randall DA, Kang DR. Current management of penetrating injuries of the soft palate. Otolaryngol Head Neck Surg. 2006;135(3):356–60.
8. Shannon E, Cohn D, Streifer M. Penetrating injuries of the parapharyngeal space. Arch Otolaryngol. 1972;96(3):256–9.
9. Russo RAG, Katsicas MM. Takayasu arteritis. Front Pediatr. 2018;6:265.
10. Schmidt W. Role of ultrasound in the understanding and management of vasculitis. Ther Adv Musculoskelet Dis. 2014;6(2):39–47.
11. Ma LY, Li CL, Ma LL, Cui XM, Dai XM, Sun Y, et al. Value of contrast-enhanced ultrasonography of the carotid artery for evaluating disease activity in Takayasu arteritis. Arthritis Res Ther. 2019;21(1):24.

12. Di Santo M, Stelmaszewski EV, Villa A. Takayasu arteritis in paediatrics. Cardiol Young. 2018;28(3):354–61.
13. Verlhac S, Balandra S, Cussenot I, Kasbi F, Vasile M, Kheniche A, et al. Extracranial carotid arteriopathy in stroke-free children with sickle cell anemia: detection by submandibular Doppler sonography. Pediatr Radiol. 2014;44(5):587–96.
14. Telfer PT, Evanson J, Butler P, Hemmaway C, Abdulla C, Gadong N, et al. Cervical carotid artery disease in sickle cell anemia: clinical and radiological features. Blood. 2011;118(23):6192–9.
15. Johnston KW, Rutherford RB, Tilson MD, Shah DM, Hollier L, Stanley JC. Suggested standards for reporting on arterial aneurysms. Subcommittee on Reporting Standards for Arterial Aneurysms, Ad Hoc Committee on Reporting Standards, Society for Vascular Surgery and North American Chapter, International Society for Cardiovascular Surgery. J Vasc Surg. 1991;13(3):452–8.
16. Wanhainen A, Bjorck M, Boman K, Rutegard J, Bergqvist D. Influence of diagnostic criteria on the prevalence of abdominal aortic aneurysm. J Vasc Surg. 2001;34(2):229–35.
17. Sosa PA, Matar P, Gross IT. Extracranial internal carotid aneurysm in a 10-year-old boy diagnosed via ultrasound. Pediatr Emerg Care. 2019;35(3):e49–52.
18. Edwards J, Carroll M, Wooster M, Shames M. True extracranial carotid artery aneurysm in a child. J Vasc Surg Cases. 2015;1(2):110–2.
19. Pourhassan S, Grotemeyer D, Fokou M, Heinen W, Balzer K, Ramp U, et al. Extracranial carotid arteries aneurysms in children: single-center experiences in 4 patients and review of the literature. J Pediatr Surg. 2007;42(11):1961–8.
20. Fullerton HJ, Johnston SC, Smith WS. Arterial dissection and stroke in children. Neurology. 2001;57(7):1155–60.
21. Stence NV, Fenton LZ, Goldenberg NA, Armstrong-Wells J, Bernard TJ. Craniocervical arterial dissection in children: diagnosis and treatment. Curr Treat Options Neurol. 2011;13(6):636–48.
22. Hejrati N, Ebel F, Guzman R, Soleman J. Posttraumatic cerebrovascular injuries in children. A systematic review. Childs Nerv Syst. 2020;36(2):251–62.
23. Silverboard G, Tart R. Cerebrovascular arterial dissection in children and young adults. Semin Pediatr Neurol. 2000;7(4):289–300.
24. Wang J, Lee YZ, Cheng Y, Zheng Y, Gao J, Tang X, et al. Sonographic characterization of arterial dissections in Takayasu arteritis. J Ultrasound Med. 2016;35(6):1177–91.
25. Eksioglu AS, Tasci Yildiz Y, Senel S. Normal sizes of internal jugular veins in children/adolescents aged birth to 18 years at rest and during the Valsalva maneuver. Eur J Radiol. 2014;83(4):673–9.
26. Klem C. Head and neck anatomy and ultrasound correlation. Otolaryngol Clin N Am. 2010;43(6):1161–9.
27. Laganà MM, Pelizzari L, Scaccianoce E, Dipasquale O, Ricci C, Baglio F, et al. Assessment of internal jugular vein size in healthy subjects with magnetic resonance and semiautomatic processing. Behav Neurol. 2016;2016:9717210.
28. Lichtenstein D, Saïfi R, Augarde R, Prin S, Schmitt JM, Page B, et al. The internal jugular veins are asymmetric. Usefulness of ultrasound before catheterization. Intensive Care Med. 2001;27(1):301–5.
29. Contrera KJ, Aygun N, Ward BK, Gooi Z, Richmon JD. Internal jugular vein duplication and fenestration: case series and literature review. Laryngoscope. 2016;126(7):1585–8.
30. Bansal AG, Oudsema R, Masseaux JA, Rosenberg HK. US of pediatric superficial masses of the head and neck. Radiographics. 2018;38(4):1239–63.
31. Bindal SK, Vasisth GO, Chibber P. Phlebectasia of internal jugular vein. J Surg Tech Case Rep. 2012;4(2):103–5.
32. Jianhong L, Xuewu J, Tingze H. Surgical treatment of jugular vein phlebectasia in children. Am J Surg. 2006;192(3):286–90.
33. Latham GJ, Thompson DR. Thrombotic complications in children from short-term percutaneous central venous catheters: what can we do? Paediatr Anaesth. 2014;24(9):902–11.
34. Derderian SC, Good R, Vuille-Dit-Bille RN, Carpenter T, Bensard DD. Central venous lines in critically ill children: thrombosis but not infection is site dependent. J Pediatr Surg. 2019;54(9):1740–3.
35. Andrew M, David M, Adams M, Ali K, Anderson R, Barnard D, et al. Venous thromboembolic complications (VTE) in children: first analyses of the Canadian Registry of VTE. Blood. 1994;83(5):1251–7.
36. Monagle P, Adams M, Mahoney M, Ali K, Barnard D, Bernstein M, et al. Outcome of pediatric thromboembolic disease: a report from the Canadian Childhood Thrombophilia Registry. Pediatr Res. 2000;47(6):763–6.
37. Journeycake JM, Buchanan GR. Catheter-related deep venous thrombosis and other catheter complications in children with cancer. J Clin Oncol. 2006;24(28):4575–80.
38. Van TT, Cox LM, Cox ME, Dien BJ. Prevalence of Fusobacterium necrophorum in children presenting with pharyngitis. J Clin Microbiol. 2017;55(4):1147–53.
39. Albertyn LE, Alcock MK. Diagnosis of internal jugular vein thrombosis. Radiology. 1987;162(2):505–8.
40. Kuppalli K, Livorsi D, Talati NJ, Osborn M. Lemierre's syndrome due to Fusobacterium necrophorum. Lancet Infect Dis. 2012;12(10):808–15.
41. Torres C, Hogan M, Patro S, Chakraborty S, Nguyen T, Thornhill R, et al. Extracranial venous abnormalities: a true pathological finding in patients with multiple sclerosis or an anatomical variant? Eur Radiol. 2017;27(1):239–46.
42. Kloppenburg GT, de Vries JP, Schuurman JP, Koelemij R, Wille J. Current perspectives on management of congenital jugular vein aneurysms. Vasc Endovasc Surg. 2011;45(3):237–40.
43. Calligaro KD, Ahmad S, Dandora R, Dougherty MJ, Savarese RP, Doerr KJ, et al. Venous aneurysms: surgical indications and review of the literature. Surgery. 1995;117(1):1–6.
44. American College of Radiology (ACR), American Institute of Ultrasound in Medicine (AIUM), Society of Pediatric Radiology (SPR), Society of Radiologists in Ultrasound (SRU): ACR-AIUM-SPR-SRU practice parameter for the performance of peripheral venous ultrasound examination. Available from https://www.acr.org/-/media/ACR/Files/Practice-Parameters/US-PeriphVenous.pdf
45. Staub D, Partovi S, Imfeld S, Uthoff H, Baldi T, Aschwanden M, Jaeger K. Novel applications of contrast-enhanced ultrasound imaging in vascular medicine. Vasa. 2013;42(1):17–31.
46. Moore KL, Persaud TVN, Torchia MG. Cardiovascular system. In: Moore KL, Persaud TVN, Torchia MG, editors. The developing human: clinically oriented embryology. 11th ed. Edinburgh. Elsevier; 2020.
47. Kusztal M, Weyde W, Letachowicz K, Gołebiowski T, Letachowicz W. Anatomical vascular variations and practical implications for access creation on the upper limb. J Vasc Access. 2014;15(Suppl 7):S70–5.
48. Abou-Foul AK, Borumandi F. Anatomical variants of lower limb vasculature and implications for free fibula flap: systematic review and critical analysis. Microsurgery. 2016;36(2):165–72.
49. Eliason JL, Coleman DM, Gumushian A, Stanley JC. Arterial reconstructions for chronic lower extremity ischemia in preadolescent and adolescent children. J Vasc Surg. 2018;67(4):1207–16.
50. Wang SK, Lemmon GW, Drucker NA, Motaganahalli RL, Dalsing MC, Gutwein AR, et al. Results of nonoperative management of acute limb ischemia in infants. J Vasc Surg. 2018;67(5):1480–3.
51. Jager KA, Phillips DJ, Martin RL, Hanson C, Roederer GO, Langlois YE, et al. Noninvasive mapping of lower limb arterial lesions. Ultrasound Med Biol. 1985;11(3):515–21.
52. Khan SZ, Khan MA, Bradley B, Dayal R, McKinsey JF, Morrissey NJ. Utility of duplex ultrasound in detecting and grading de novo femoropopliteal lesion. J Vasc Surg. 2011;54(4):1067–73.
53. Price VE, Chan AK. Arterial thrombosis in children. Expert Rev Cardiovasc Ther. 2008;6(3):419–28.

54. Moneta GL, Yeager RA, Antonovic R, Hall LD, Caster JD, Cummings CA, et al. Accuracy of lower extremity arterial duplex mapping. J Vasc Surg. 1992;15(2):275–8.
55. Hatsukami TS, Primozich JF, Zierler RE, Harley JD, Strandness DE Jr. Color Doppler imaging of infrainguinal arterial occlusive disease. J Vasc Surg. 1992;16(4):527–31.
56. Mustapha JA, Saab F, Diaz-Sandoval L, Karenko B, McGoff T, Heaney C, et al. Comparison between angiographic and arterial duplex ultrasound assessment of tibial arteries in patients with peripheral arterial disease: on behalf of the Joint Endovascular and Non-Invasive Assessment of LImb Perfusion (JENALI) Group. J Invasive Cardiol. 2013;25(11):606–11.
57. Lim S, Javorski MJ, Halandras PM, Kuo PC, Aulivola B, Crisostomo P. Epidemiology, treatment, and outcomes of acute limb ischemia in the pediatric population. J Vasc Surg. 2018;68(1):182–8.
58. Sadat U, Hayes PD, Varty K. Acute limb ischemia in pediatric population secondary to peripheral vascular cannulation: literature review and recommendations. Vasc Endovasc Surg. 2015;49(5–6):1427.
59. Davis FM, Eliason JL, Ganesh SK, Blatt NB, Stanley JC, Coleman DM. Pediatric nonaortic arterial aneurysms. J Vasc Surg. 2016;63(2):466–76. e1
60. Sivaharan A, Elsaid T, Stansby G. Acute leg ischaemia in a child due to a thrombosed popliteal aneurysm. EJVES Short Rep. 2018;42:1–3.
61. Wilson WR, Bower TC, Creager MA, Amin-Hanjani S, O'Gara PT, Lockhart PB, et al. Vascular graft infections, mycotic aneurysms, and endovascular infections: a scientific statement from the American Heart Association. Circulation. 2016;134(20):e412–60.
62. Sörelius K, Mani K, Björck M, Nyman R, Wanhainen A. Endovascular repair of mycotic aortic aneurysms. J Vasc Surg. 2009;50(2):269–74.
63. Mansour MA, Gorsuch JM. Diagnosis and management of pseudoaneurysms. Perspect Vasc Surg Endovasc Ther. 2007;19(1):58–64.
64. Hall HA, Minc S, Babrowski T. Peripheral artery aneurysm. Surg Clin North Am. 2013;93(4):911–23.
65. Ford EG, Stanley P, Tolo V, Woolley MM. Peripheral congenital arteriovenous fistulae: observe, operate, or obturate? J Pediatr Surg. 1992;27(6):714–9.
66. Li JC, Cai S, Jiang YX, Dai Q, Zhang JX, Wang YQ. Diagnostic criteria for locating acquired arteriovenous fistulas with color Doppler sonography. J Clin Ultrasound. 2002;30(6):336–42.
67. González SB, Busquets JC, Figueiras RG, Martin CV, Pose CS, de Alegria AM, Mourenza JA. Imaging arteriovenous fistulas. AJR Am J Roentgenol. 2009;193(5):1425–33.
68. Gooding GA, Hightower DR, Moore EH, Dillon WP, Lipton MJ. Obstruction of the superior vena cava or subclavian veins: sonographic diagnosis. Radiology. 1986;159(3):663–5.
69. Needleman L, Cronan JJ, Lilly MP, Merli GJ, Adhikari S, Hertzberg BS, et al. Ultrasound for lower extremity deep venous thrombosis: multidisciplinary recommendation from the Society of Radiologists in Ultrasound consensus conference. Circulation. 2018;137(14):1505–15.
70. Bundens WP, Bergan JJ, Halasz NA, Murray J, Drehobl M. The superficial femoral vein. A potentially lethal misnomer. JAMA. 1995;274(16):1296–8.
71. Lin EP, Bhatt S, Rubens D, Dogra VS. The importance of monophasic Doppler waveforms in the common femoral vein: a retrospective study. J Ultrasound Med. 2007;26(7):885–91.
72. Lockhart ME, Sheldon HI, Robbin ML. Augmentation in lower extremity sonography for the detection of deep venous thrombosis. AJR Am J Roentgenol. 2005;184(2):419–22.
73. Noren A, Ottosson E, Sjunnesson M, Rosfors S. A detailed analysis of equivocal duplex findings in patients with suspected deep venous thrombosis. J Ultrasound Med. 2002;21(12):1375–83.
74. Miller N, Obrand D, Tousignant L, Gascon I, Rossignol M. Venous duplex scanning for unilateral symptoms: when do we need a contralateral evaluation? Eur J Vasc Endovasc Surg. 1998;15(1):18–23.
75. Naidich JB, Torre JR, Pellerito JS, Smalberg IS, Kase DJ, Crystal KS. Suspected deep venous thrombosis: is US of both legs necessary? [comment]. Radiology. 1996;200(2):429–31.
76. Stevens SM, Elliott CG, Chan KJ, Egger MJ, Ahmed KM. Withholding anticoagulation after a negative result on duplex ultrasonography for suspected symptomatic deep venous thrombosis. Ann Intern Med. 2004;140(12):985–91.
77. Weber TM, Lockhart ME, Robbin ML. Upper extremity venous Doppler ultrasound. Radiol Clin North Am. 2007;45(3):513–24.
78. Goldfisher R. Lower-extremity venous ultrasound – past, present and future. Pediatr Radiol. 2017;47(9):1209–13.
79. Hamper UM, DeJong MR, Scoutt LM. Ultrasound evaluation of the lower extremity veins. Radiol Clin North Am. 2007;45(3):525–47.
80. Lee BB. Venous embryology: the key to understanding anomalous venous conditions. Phlebolymphology. 2012;19(4):170–81.
81. Casella IB, Presti C, Yamazaki Y, Vassoler AA, Furuya LA, Sabbag CD. A duplex scan-based morphologic study of the femoral vein: incidence and patterns of duplication. Vasc Med. 2010;15(3):197–203.
82. Sadowska A, Spodnik JH, Wójcik S. Variations in popliteal fossa venous anatomy: implications for diagnosis of deep-vein thrombosis. Folia Morphol (Warsz). 2013;72(1):51–6.
83. Quinlan DJ, Alikhan R, Gishen P, Sidhu PS. Variations in lower limb venous anatomy: implications for US diagnosis of deep vein thrombosis. Radiology. 2003;228(2):443–8.
84. Screaton NJ, Gillard JH, Berman LH, Kemp PM. Duplicated superficial femoral veins: a source of error in the sonographic investigation of deep vein thrombosis. Radiology. 1998;206(2):397–401.
85. Park ES, Choi HS, Lee KS, Kim SW, Lee JM. Venous thromboembolism in children and young adults in Korea: analysis of the Korean Health Insurance Review and Assessment Service Database. J Korean Med Sci. 2019;34(49):e316.
86. Heit JA. Epidemiology of venous thromboembolism. Nat Rev Cardiol. 2015;12(8):464–74.
87. Sandoval JA, Sheehan MP, Stonerock CE, Shafique S, Rescorla FJ, Dalsing MC. Incidence, risk factors, and treatment patterns for deep venous thrombosis in hospitalized children: an increasing population at risk. J Vasc Surg. 2008;47(4):837–43.
88. Bates SM, Jaeschke R, Stevens SM, Goodacre S, Wells PS, Stevenson MD, et al. Diagnosis of DVT: antithrombotic therapy and prevention of thrombosis, 9th ed: American College of Chest Physicians Evidence-Based Clinical Practice Guidelines. Chest. 2012;141(2 Suppl):e351S–418S.
89. Ageno W, Squizzato A, Wells PS, Büller HR, Johnson G. The diagnosis of symptomatic recurrent pulmonary embolism and deep vein thrombosis: guidance from the SSC of the ISTH. J Thromb Haemost. 2013;11(8):1597–602.
90. Wilbur J, Shian B. Diagnosis of deep venous thrombosis and pulmonary embolism. Am Fam Physician. 2012;86(10):913–9.
91. Wells PS. Integrated strategies for the diagnosis of venous thromboembolism. J Thromb Haemost. 2007;5(Suppl 1):41–50.
92. Le Gal G, Carrier M, Rodger M. Clinical decision rules in venous thromboembolism. Best Pract Res Clin Haematol. 2012;25(3):303–17.
93. Qaseem A, Snow V, Barry P, Hornbake ER, Rodnick JE, Tobolic T, et al. Current diagnosis of venous thromboembolism in primary care: a clinical practice guideline from the American Academy of Family Physicians and the American College of Physicians. Ann Fam Med. 2007;5(1):57–62.
94. Segal JB, Eng J, Tamariz LJ, Bass EB. Review of the evidence on diagnosis of deep venous thrombosis and pulmonary embolism. Ann Fam Med. 2007;5(1):63–73.
95. Wells PS, Anderson DR, Rodger M, Forgie M, Kearon C, Dreyer J, et al. Evaluation of D-dimer in the diagnosis of suspected deep-vein thrombosis. N Engl J Med. 2003;349(13):1227–35.
96. Chin EE, Zimmerman PT, Grant EG. Sonographic evaluation of upper extremity deep venous thrombosis. J Ultrasound Med. 2005;24(6):829–38.
97. Malec L, Young G. Treatment of venous thromboembolism in pediatric patients. Front Pediatr. 2017;5:26.
98. Monagle P, Chan AK, Goldenberg NA, Ichord RN, Journeycake JM, Nowak-Göttl U, et al. Antithrombotic therapy in neonates and children: antithrombotic therapy and prevention of thrombosis, 9th

ed: American College of Chest Physicians Evidence-Based Clinical Practice Guidelines. Chest. 2012;141(2 Suppl):e737S–801S.
99. Hardman RL. Management of chronic deep vein thrombosis in women. Semin Intervent Radiol. 2018;35(1):3–8.
100. Lin PH, Chaikof EL. Embryology, anatomy, and surgical exposure of the great abdominal vessels. Surg Clin North Am. 2000;80(1):417–33.
101. Coley BD. Pediatric applications of abdominal vascular Doppler imaging: part I. Pediatr Radiol. 2004;34(10):757–71.
102. Nagel K, Tuckuviene R, Paes B, Chan AK. Neonatal aortic thrombosis: a comprehensive review. Klin Padiatr. 2010;222(3):134–9.
103. Dieffenbach BV, Nath BD, Tracy ET, Kim HB. Management of symptomatic neonatal aortic thrombosis: when is surgery indicated? J Pediatr Surg Case Rep. 2019;47:101247.
104. Porras D, Stein DR, Ferguson MA, Chaudry G, Alomari A, Vakili K, et al. Midaortic syndrome: 30 years of experience with medical, endovascular and surgical management. Pediatr Nephrol. 2013;28(10):2023–33.
105. Rumman RK, Nickel C, Matsuda-Abedini M, Lorenzo AJ, Langlois V, Radhakrishnan S, et al. Disease beyond the arch: a systematic review of middle aortic syndrome in childhood. Am J Hypertens. 2015;28(7):833–46.
106. Yan L, Li HY, Ye XJ, Xu RQ, Chen XY. Doppler ultrasonographic and clinical features of middle aortic syndrome. J Clin Ultrasound. 2019;47(1):22–6.
107. Mendeloff J, Stallion A, Hutton M, Goldstone J. Aortic aneurysm resulting from umbilical artery catheterization: case report, literature review, and management algorithm. J Vasc Surg. 2001;33(2):419–24.
108. Kim JI, Lee W, Kim SJ, Seo JW, Chung JW, Park JH. Primary congenital abdominal aortic aneurysm: a case report with perinatal serial follow-up imaging. Pediatr Radiol. 2008;38(11):1249–52.
109. Restrepo R, Ranson M, Chait PG, Connolly BL, Temple MJ, Amaral J, et al. Extracranial aneurysms in children: practical classification and correlative imaging. AJR Am J Roentgenol. 2003;181(3):867–78.
110. Munk A, Darge K, Wiesel M, Troeger J. Diameter of the infrarenal aorta and the iliac arteries in children: ultrasound measurements. Transplantation. 2002;73(4):631–5.
111. Smillie RP, Shetty M, Boyer AC, Madrazo B, Jafri SZ. Imaging evaluation of the inferior vena cava. Radiographics. 2015;35(2):578–92.
112. Oliveira JD, Martins I. Congenital systemic venous return anomalies to the right atrium review. Insights Imaging. 2019;10(1):115.
113. Bartram U, Wirbelauer J, Speer CP. Heterotaxy syndrome – asplenia and polysplenia as indicators of visceral malposition and complex congenital heart disease. Biol Neonate. 2005;88(4):278–90.
114. Soundappan SV, Barker AP. Retrocaval ureter in children: a report of two cases. Pediatr Surg Int. 2004;20(2):158–60.
115. Kandpal H, Sharma R, Gamangatti S, Srivastava DN, Vashisht S. Imaging the inferior vena cava: a road less traveled. Radiographics. 2008;28(3):669–89.
116. Khanna G, Rosen N, Anderson JR, Ehrlich PF, Dome JS, Gow KW, et al. Evaluation of diagnostic performance of CT for detection of tumor thrombus in children with Wilms tumor: a report from the Children's Oncology Group. Pediatr Blood Cancer. 2012;58(4):551–5.
117. Zhang L, Yang G, Shen W, Qi J. Spectrum of the inferior vena cava: MDCT findings. Abdom Imaging. 2007;32(4):495–503.
118. Sheth S, Fishman EK. Imaging of the inferior vena cava with MDCT. AJR Am J Roentgenol. 2007;189(5):1243–51.
119. Quencer KB, Friedman T, Sheth R, Oklu R. Tumor thrombus: incidence, imaging, prognosis and treatment. Cardiovasc Diagn Ther. 2017;7(Suppl 3):S165–77.
120. Harbin MM, Lutsey PL. May-Thurner syndrome: history of understanding and need for defining population prevalence. J Thromb Haemost. 2020;18(3):534–42.
121. Xue GH, Huang XZ, Ye M, Liang W, Zhang H, Zhang JW, et al. Catheter-directed thrombolysis and stenting in the treatment of iliac vein compression syndrome with acute iliofemoral deep vein thrombosis: outcome and follow-up. Ann Vasc Surg. 2014;28(4):957–63.
122. Carroll S, Moll S. Inferior vena cava filters, May-Thurner syndrome, and vein stents. Circulation. 2016;133:e383–7.